SEL-65-109

THERMAL BEHAVIOR OF THE IONOSPHERE AND OBSERVATIONS OF THE EXOSPHERE AND THE IONOSPHERE BY MEANS OF DISTANT EARTH SATELLITES

by

A. V. da Rosa

December 1965

Technical Report No. 2

Prepared under
National Aeronautics and Space Administration
Contract NASr-136

Radioscience Laboratory
Stanford Electronics Laboratories
Stanford University Stanford, California

ABSTRACT

A theoretical study of the time-dependent thermal behavior of the ionospheric electron gas is made, leading to the following conclusions:

1. Very substantial heating occurs in the ionosphere before there is any perceptible increase in ionization.
2. The electron temperature reaches a peak some time after sunrise but much before heat production becomes maximum.
3. At a given phase of the solar cycle summer temperatures are higher than winter temperatures. Summer temperatures at solar cycle minimum may be higher than winter temperatures at solar cycle maximum.
4. At sufficiently small solar zenithal angles a maximum appears in the temperature profile at some 300 km height, heat flowing both upward and downward from this peak.

A second topic treated deals with the results from the radio-beacon experiment aboard EGO. Profiles of local electron concentration in the exosphere at heights between 6000 and 30,000 km were obtained. In addition, the examination of early morning data showed marked rearrangements in the ionized layer taking place between one half and one and one half hours after sunrise. This rearrangement can be interpreted as an upward flux of ionization from the ionosphere into the exosphere, and lasted about 20 minutes in the passages observed. The flux attained the value of 1.5×10^{9} electrons cm^{-2} sec^{-1} on one of the days measured.

The final topic consists of a statistical investigation of the behavior of the nighttime columnar content of the ionosphere. It was observed that at Stanford the majority of nights exhibited an unchanging content while at Hawaii the content tended to decay. It was also found that the average K_p of non-decaying nights at Stanford was much lower than the K_p of decaying nights. These results are interpreted as supporting the theory of an exosphere fed nocturnal F-layer.

ACKNOWLEDGEMENT

Guidance and advice received from Professor Owen K. Garriott for the completion of this work is very gratefully acknowledged. Also appreciated are the helpful discussions with Professor Robert A. Helliwell and with Jacyntho J. Angerami. The data collection owes much to the efforts of Stanley C. Hall and the reduction to Mrs. Ulla Lundquist. The ionograms used in this work were kindly furnished by Mrs. Joyce Getty of the Stanford Research Institute. Thanks also go to Fred L. Smith, III, who supplied the data for the last chapter of this work.

The radio-beacon transmitter aboard the EGO satellite was developed under the responsability of Messrs. Robert S. Lawrence and Edward Schiffmacher of the National Bureau of Standards, Boulder, Colorado.

The work was financed by Contract NASr-136 with the National Aeronautics and Space Administration.

CONTENTS

TABLES

ILLUSTRATIONS

ILLUSTRATIONS (cont)

ILLUSTRATIONS (cont)

I. INTRODUCTION

The transition period between night and day, in the ionosphere, is marked by profound changes in the ion concentration and electron temperature. The theoretical behavior of the former, during these hours, has been treated by several authors as, for instance Rishbeth [1961], but it appears that no models for the corresponding temperature variations of the plasma have so far been considered. Since experimental results hint at drastic temperature changes at dawn, and since these temperature variations have strong influence on the distribution of the ionization, it becomes important, for the proper interpretation of experimental data related to this period of time, to investigate theoretically the effect of solar rays on the heating of the electron gas.

Although, as stated above, the transient heating of the ionosphere has not yet been examined, the thermal behavior of the upper atmosphere has, in general, been the subject of several theoretical investigations supported by many experimental measurements. Originally the attention of most authors was directed towards the time variations of the neutral atmosphere; more recently several articles treating the steady state midday plasma temperature have appeared. The present work extends these studies to the solution of the time-dependent problem.

Lowan [1955] studied the cooling of the upper atmosphere after sunset by solving a simplified heat conduction equation in which the conductivity, λ, was assumed to be height-independent, and all the heat transfer was solely by conduction. Boundary and initial conditions used were the temperatures given by the Rocket Panel.

Harris and Priester [1962], in a classical article, made a much more extensive study of the time variations of the

thermospheric thermal structure, covering the full 24-hour period. In addition to heat conduction (including a temperature dependent conductivity), the authors also considered cooling by infrared radiation of atomic oxygen and the effect of the gain and loss of heat due to the work of the expanding and contracting air, against gravity. This convective influence was found to be small, causing a decrease of less than 5% in the mean diurnal temperatures. Harris and Priester found that, by using as sole heating source the solar extreme ultra violet (euv), they were unable to match the diurnal density variation of the empirical Bonn Observatory model of 1961 [Martin, et al, 1961]. The theoretical curves peaked at 1700 LMT while the real maximum was observed to occur at 1400 LMT. To obtain a better agreement between theory and experiment, an additional "ad hoc" heating source, of roughly the same total energy as the euv, had to be assumed, having a peak at 0900 LMT. The calculated tables of atmospheric temperatures and densities and of the concentration of the various neutral particle species, for every hour of the day and for the altitude range between 120 and 2000 km, have been widely used as models of the atmosphere by different investigators.

The thermal properties of the ionospheric plasma were investigated by Hanson and Johnson [1961] and by Hanson [1962] who showed that, at midday, the electron temperature would substantially exceed that of the neutral gas at altitudes near the peak of production. Hanson estimated the heat input function and solved the steady state heat flow equation taking into account only the heat losses of the electron gas through coupling with ions and neutrals, i.e., ignoring the thermal conductivity of the electrons.

Dalgarno, et al, [1963], in a much quoted paper, carried out essentially the same analysis, but included considerably more detail in the production and loss mechanism.

It should be pointed out here that although Hanson and Dalgarno obtained very useful results, the fact that electron conductivity was neglected leads to two important difficulties. Firstly, the predicted temperature above the production peak is much lower than the generally observed value. In fact, the theory calls for a sharp decrease in electron temperature above the peak while in practice a nearly height-independent temperature is measured. Secondly, an unstable situation may result if the electron concentration is too small. This can be seen if the production term is equated to the dominant loss term (the one due to ions) as the above authors do. One obtains:

$$\frac{Q}{C} = \frac{n}{268} \frac{(T_e - T_n)}{T_e^{3/2}}$$

where Q is the heat energy released per cubic centimeter per second,

C is the heat capcity per cubic centimeter; for electrons it is equal to $\frac{3}{2}$ kn (where k is Boltzmann's constant),

n is the electron or ion concentration, and

T_e and T_i are, respectively, the electron and ion temperatures.

This can be written

$$\frac{Q}{n^2} \propto \frac{T_e - T_i}{T_e^{3/2}}$$

For a given T_i and sufficiently large Q/n^2 no value of T_e will balance the equation, meaning that this particular cooling mechanism is inadequate and the temperature will rise until heat conductivity, which grows with increasing temperature, limits it. Neglecting the conductivity leads thus to an unacceptable conclusion, a situation termed "runaway electron temperature condition" by Hanson and Johnson [1961].

More recently Geisler and Bowhill [1965] took the investigation one important step further by not only perfecting the heat production function (including the non local production of heat by fast photo-electrons generated far away from the heated point) but also by including the important effect of the thermal conductivity in the electron gas. This inclusion considerably complicates the mathematical problem transforming the heat flow equation from an ordinary first order differential equation into a second order partial differential equation. The steady state solution obtained fits the experimental observation much more closely.

A time dependent solution of the electron gas temperature including both the losses by coolant gases and heat transfer by conduction is presented in Chapter III, thereby allowing the investigation of the thermal behavior of the ionospheres during moments like sunrise and sunset when the rapid changes in temperature might invalidate the steady state solution.

Another topic dealt with in this report has to do with artificial satellites which have certainly proven their great usefulness as tools for ionospheric research. Their flexibility in this work stems not only from the wide range of equipment that can be installed aboard, but also from the large variety of orbits in which a satellite can be placed. The majority of ionospheric studies by means of satellites has been carried out by using devices put into roughly circular orbits between 300 and 1000 km above sea level. Garriott and Little [1960] pointed out the advantages of using geostationary satellites for the measurements of some ionospheric properties. As yet, however, no vehicle specifically designed for research has been launched in such an orbit, but the existence of synchronous communications satellites has provided the opportunity to carry out some of the investigations envisaged in the above mentioned article. By using the 136 Mc carrier of a telemetry transmitter aboard Syncom III, Garriott,

Smith, and Yuen [1965] have made extensive observations of the behavior of the columnar electron content through the measurement of the Faraday rotation angle of the incoming signal. From the rise of the content at dawn, the above authors have deduced the value of the integrated production rate of electron-ion pairs.

Several satellites have been placed in highly eccentric orbits, carrying aboard plasma probes, magnetometers and other measuring devices. The first vehicle equipped with a radio beacon designed for propagation experiments, to be placed in an orbit which takes it out to several earth radii from the surface, is EGO (OGO-A). When such radio beacons radiate two harmonically related frequencies, it is possible to measure columnar electron content not only by the Faraday-rotation-angle method, as in the case of Syncom III, but also by the differential-Doppler-frequency method. The latter yields the columnar content up to the satellite, while the former, being weighted by the geomagnetic field strength, "sees" only the lower levels of ionization. The difference between these two measurements serves as an estimate of the columnar content of the exosphere up to the satellite.

Changes in this "exospheric columnar content" yield information about true temporal variations of the exospheric ionization, about local electron concentration in the exosphere and about horizontal gradients of ionization in that region. In the EGO experiment these effects are apt to be mixed together and it is not always possible to separate them. The observation of the temporal variations led to the detection of a hitherto unreported phenomenon: a large upward flux of ionization from the ionosphere to the exosphere, which occurs some time after sunrise. This phenomenon can be investigated more effectively by the use of a radio-beacon transmitter with two harmonically related frequencies, as the one on EGO, placed aboard a geostationary satellite. Such

an experiment would not only provide a means of measuring the temporal variations in the exosphere, undisturbed by the effects of the motion of the satellite with respect to the observer, but would also allow daily observations in contrast with the infrequent ones that can be made with EGO.

Local concentration measurements depend on the radial velocity of the satellite and can be made only in the region of high concentration within the plasmapause. It is important, therefore, that the satellite orbit be of low inclination so that a substantial part of its path near perigee is within this region. Future measurements of exospheric concentration profiles by the radio propagation method would profit from the use of equatorial (zero inclination) satellites placed in highly eccentric orbits. Under such conditions the useful path length would be at a maximum and, at least for observing stations near the equator, the problems due to satellite motion perpendicular to the line of sight, would be minimized.

II. PRELIMINARIES

A. THE SATELLITE

The S-49 satellite, also known as EGO (Eccentric Geophysical Observatory) or OGO-A, was launched on 5 September 1964 and carries aboard, among other experiments, a pair of radio beacons operating at harmonically related frequencies (40.01 and 360.09 Mc), which are modulated by 20- and 200-kc signals. The various spectral components have the output powers shown below.

Frequency (Mc)		Output Power (mw)
40	Carrier	230
	Each 200-kc sideband	230
	Each 20-kc sideband	55
360	Carrier	125
	Each 200-kc sideband	20
	Each 20-kc sideband	12.5

The 40-Mc transmitting antenna is a simple dipole (gain: 2 db); the 360-Mc antenna is a yagi (gain: 8 db). The orbit of the satellite is highly eccentric: apogee is at nearly 149,000 km, while perigee (which occurs at about 20° S geographic latitude) has been steadily increasing in height, at a rate of some 5,000 km/year. On 28 February 1965, it was at slightly more than 3,000-km altitude. The period of the orbit is very close to 64 hours. The inclination of the orbit, unlike that of less-eccentric sztellites, is also growing. The rate is about 18 deg/year; at the above date, it had reached a value of 39.1 deg.

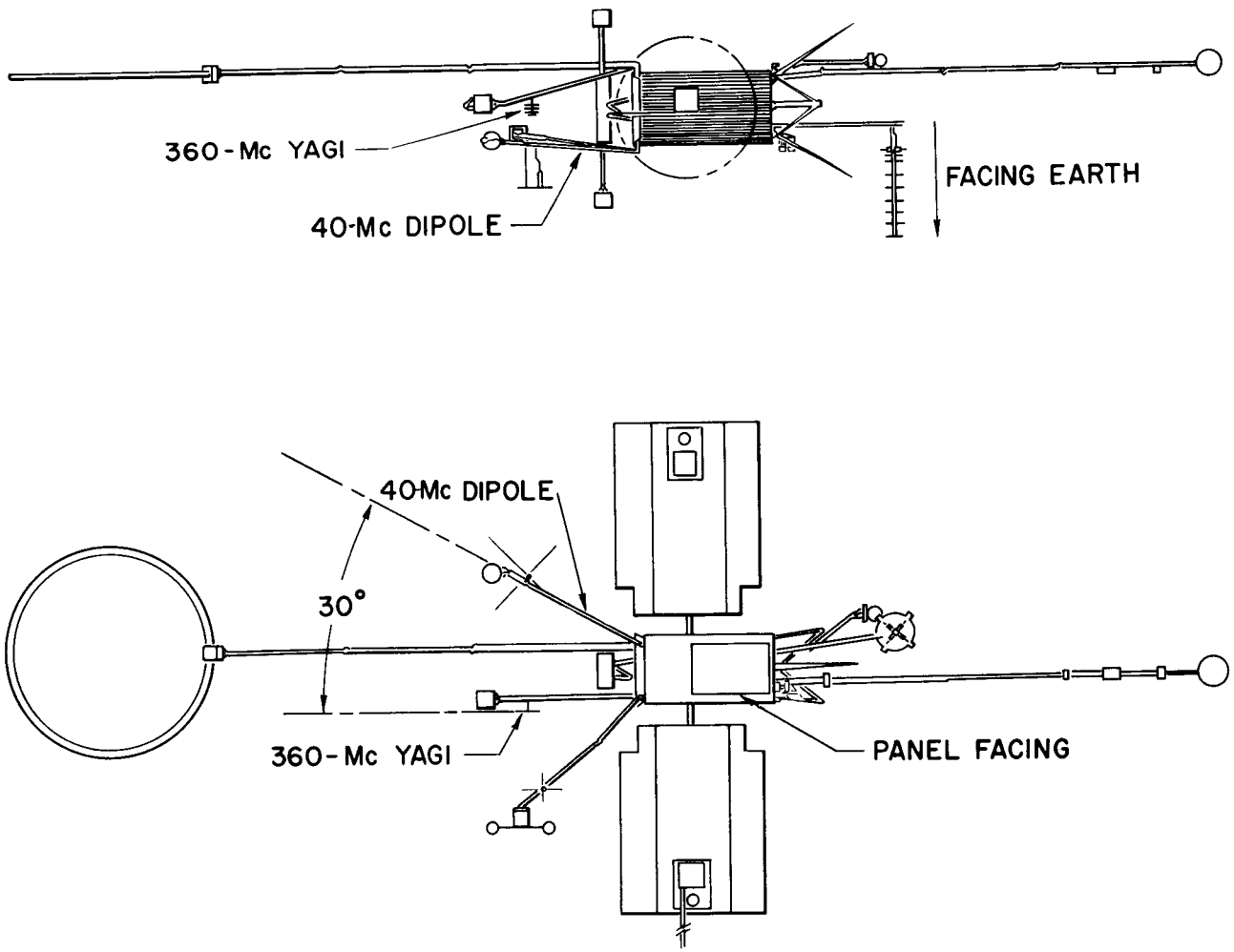

FIG. 1. GENERAL CONFIGURATION OF THE EGO SHOWING THE POSITION OF THE TWO RADIO-BEACON ANTENNAS.

It was planned to have an earth-stabilized satellite, but difficulties that appeared immediately after launch caused the satellite to spin at a rate of 5 rpm, introducing some unexpected complications in the radio-beacon experiment. The spin-axis orientation is not known precisely. Values of 42.5 deg in right ascension and -9 deg in declination, suggested by some independent measurements, were used in interpreting the data.

Figure 1 shows the general configuration of the satellite.

B. GENERAL DISCUSSION OF THE ANALYSIS

The radio-beacon experiment aboard the EGO satellite was designed with the objective of investigating the exosphere by studying the behavior of the columnar electron content between ground and satellite as the latter rises from perigee in its very eccentric orbit. Since this involves looking at a tenuous exosphere through a much denser ionosphere, it became immediately apparent that simple assumptions about the latter, such as time invariance and horizontal stratification, would lead to errors that would completely mask the effects sought. To avoid this difficulty, it was decided to make simultaneous measurements of the differential-Doppler frequency and the Faraday-rotation angle. The former can be translated into columnar content from ground to transmitter while the latter, being weighted by the geomagnetic field, yields columnar content determined mainly by the ionization below, say, 1000 km. The difference between the contents thus obtained can be attributed to the columnar content of the exosphere up to satellite height and should be fairly independent of the variations in the lower ionosphere.

Both the differential-Doppler-frequency and the Faraday-rotation-angle methods require independent measurement of an absolute reference value--in the Doppler method because of an unknown integration constant and in the Faraday method because of the uncertainty in the number of half rotations.

The absolute reference for Doppler is derived from group-delay measurements. Unfortunately, instrumentation difficulties have caused us to place little reliance on the absolute values thus obtained. It appears, however, that there is no fundamental difficulty in the method and it can probably be made to yield useful results. Many conclusions can be drawn from the EGO radio-beacon data even when these absolute values are unknown, because they do not affect the shape of the columnar-content-vs-time curve.

The measurement of the absolute reference level for the Faraday-rotation-angle columnar-content curve is more critical because here the slope of the curve is dependent on the level, which is derived from the differential-Faraday-rotation-angle between the two 200-kc sidebands of the 40-Mc signal. This latter measurement leads to a wide scatter of points but, with suitable averaging process, it is believed that errors of less than ±10 per cent can be attained. Our confidence in this accuracy is bolstered by comparisons with simultaneous measurements made with Syncom III and S-66 satellites (Garriott, Smith and Yuen [1965]).

Curves of columnar-content-vs-time are shown in Fig. 14. The Doppler and Faraday results are obtained independently and it can be seen that the irregularities in the ionosphere are faithfully reproduced in both traces. For the present investigation it is the difference between the two slant-content curves that is of interest. Figure 15 shows this difference for the days represented in the preceding figure. Because of the difficulties mentioned before with the group-delay measurements, it was impossible to assign a correct value to the magnitude of the difference; the shape of the curve gives, however, useful information.

The amplitude fluctuations of the 360-Mc carrier, being relatively unaffected by the Faraday effect, are used to measure the spin rate of the satellite. The differential-Faraday data are obtained by scaling the time difference

between the lower- and upper-sideband minima and comparing this with the period between two consecutive minima of one of the sidebands.

The Faraday-rotation angle is obtained by scaling the time of occurrence of every tenth minimum to the nearest 0.1 sec, and comparing the average interval between two minima with the spin period of the satellite. The differential-Doppler frequency is scaled by a simple cycle count. Group-delay data are collected by annotating the phase-meter readings. In general, all data were scaled at 1-min intervals.

C. EQUIPMENT

To make full use of the radio-beacon aboard EGO it is necessary to receive the following signals:

a. The carriers at 40 and 360 Mc for differential-Doppler-frequency measurements.

b. The 20- or 200-kc modulations on both the 40- and 360-Mc signals, for group delay measurements.

c. Either the carrier or one of the 200-kc sidebands of the 40-Mc signal for the Faraday-rotation-angle measurement.

d. One pair of signals at 40 Mc. This may be the carrier and one of the sidebands or else the two sidebands. The latter combination is preferable due to the larger frequency spacing and the consequent improvement in data scaling precision.

Due to the small power radiated by the spacecraft, it became important that antennas of considerable gain be used. Two independent arrays of four yagis mounted on the corners of a square, constituted the 40-Mc antenna. At each corner two six-element yagis were located perpendicularly to each other and interconnected with the parallel yagis in the remaining corners. In this fashion, two mutually perpendicular, linearly polarized arrays, furnishing each a 13 db gain, could be used either individually as linear elements for the

Faraday-rotation-angle measurement, or combined to form a circularly polarized system (with choice of right or left polarization) for the differential-Doppler receivers. The use of this latter type of antenna eliminates the Faraday nulls that would otherwise tend to unlock the receivers. The 360-Mc signal was picked up by four right circular helical antennas giving a 22 db gain. The whole ensemble was provided with an alt-azimuth mounting on a pedestal so as to permit tracking the satellite. Azimuth and elevation information was transmitted to the receiving site by means of selsyn indicators.

The expected signal-to-noise ratio with the satellite at apogee was about 12 db for the 360-Mc carrier and its 200-kc sidebands, 14 db for the 40-Mc carrier and 17 db for the 200-kc sidebands of the latter. These ratios were based on sky noise temperature of 850 and 15,000 degrees Kelvin, for the 360- and 40-Mc signals, respectively. Because of the unexpected spinning of the satellite, considerable signal strength was lost through transmitting antenna misorientation, making it impossible to realize the expected signal-to-noise ratios. Continuous lock with the satellite near apogee could not be maintained and the useful range for data acquisition remained limited to 70,000 km.

The receiving equipment was built especially for this experiment by Smyth Research Associates (SRA). For the reception of the Doppler information two phase lock receivers were employed. Their voltage controlled oscillators (vco) locked on the two incoming carriers and their signal was fed to a pair of phase comparators, the output of which was recorded on a Sanborn graphic recorder. One of the phase comparators received the signal directly from the vco's, while the other had one of the voltages retarded by 90 degrees. This arrangement permits the determination of which is the higher of the two frequencies being compared. Comparison was made at 40 Mc. Two synchronous demodulators in

each Doppler receiver recovered the modulation envelope superimposed on the carriers. The two audio tones--one from each receiver--were fed to a phasemeter and the reading monitored visually. To insure an adequate signal-to-noise ratio the audio tones had to be passed through a narrow band tracking filter. The selectivity of the loop filter for the differential Doppler measurement was set at 5 cps for the 40-Mc receiver and 15 cps for the 360-Mc one.

For the Faraday-rotation-angle measurement two additional phase lock receivers were used. The injection voltage for the first mixer in these receivers was derived from the 40-Mc Doppler receiver vco thus not only providing a signal during the Faraday minima, but also removing all the Doppler shift due to the satellite motion. The resulting 20.5-Mc intermediate frequency signal was then applied to two independent phase-lock systems capable of tuning to the carrier or either of the 200-kc sidebands. Loop filter selectivity was set at 45 cps. The amplitude of the signal, obtained from a demodulator constituted the useful output and was recorded on the same Sanborn chart as the differential-Doppler beat.

Provisions existed for the recording of the amplitude of the 40- and 360-Mc carrier amplitude from the Doppler receivers.

D. THE DATA

The raw data input for the EGO propagation experiment consists of

a. The amplitude trace of one of the 40-Mc signals received with a linear antenna and containing the fades or minima caused by the spinning of the satellite modified by the Faraday effect. From this information and from an absolute reference obtained from item b, the columnar electron content below the exosphere is obtained.

b. A second trace similar to the one mentioned in a, but at a slightly different frequency. From the difference between the Faraday effect on the two signals, the absolute values of the columnar content are determined.

c. A trace of the beat between the 40- and 360-Mc signals (the latter having had its frequency divided by 9). This trace allows the determination of the time variation of the columnar content up to satellite. An integration of these results yields the shape of the content-vs-time curve and the knowledge of an absolute reference value--that could be obtained from item d--would permit the correct drawing of such a curve. As explained previously, it proved impossible to obtain the reference value and, therefore, the knowledge of the absolute value of the exosphere content is lacking. Nevertheless the important time variations of this content are still very useful.

d. A tabulation of the phase-angles-vs-time obtained from the group delay experiment. This part did not work reliably.

A detailed study of the processing of the raw data to obtain the various columnar-contents-vs-time curves has been described by da Rosa [1965]. The effects of the satellite spin on the measurements is profound and in the paper referred to, this is thoroughly examined.

For each EGO run, the data, in its final processed form ready for analysis, consists of curves in which the columnar contents measured by the two techniques described and the so-called exosphere columnar content are plotted versus time, at one-minute intervals. Such curves, most of which were taken at Stanford, cover from 2 to 5 hours and, through a peculiarity of the satellite period, all fall around one of three times of the day: early morning, midday, and early evening. Sunrise was observed in the first group while sunset occurred in the last. Exosphere columnar content is defined here as the difference between the columnar contents obtained from Doppler and from Faraday (see Chapter IV).

If there were no temporal changes in the exosphere and if the satellite moved radially out, one would expect that, as the observer to spacecraft distance progressively increased, the columnar content of the exosphere would appear to grow. The growth rate would yield information about local

electron concentration from which exosphere concentration profiles could be constructed. Such a simple model is frequently not valid, not only due to substantial time changes in the ionization at high altitudes, but also due to the fact that the satellite's motion perpendicular to the ray path (particularly large at the beginning of the run) combined with horizontal gradients in the exosphere will influence the observed columnar content. When there is reason to believe that one of the three factors that cause columnar content changes, largely outweighs the other two, it is possible to obtain certain results of interest. Thus for instance, one may argue that during the night there is probably little temporal variation at these latitudes. On the other hand, during the outbound runs, there is a relatively long period when the spacecraft seems almost geostationary and when, consequently, horizontal gradients are not very important. Also, when the satellite is far out, its radial velocity is sufficiently small and the local density presumably low enough so that the receding motion has an insignificant effect on the content-vs-time curve.

It had been planned to carry out prolonged observations of EGO near its apogee by using three widely-spaced stations capable of providing continuous coverage. Such stations located at Stanford, Athens and Kyoto were all implemented but the project suffered due to the inability of tracking the satellite above 70,000 km. It is hoped that with OGO-B this kind of observation can be made, and that the resulting small changes in distance and in apparent position of the beacon will reduce some of the present difficulties in data interpretation.

All the Syncom III data were obtained either from Garriott, Smith and Yuen [1965] or from unpublished information kindly furnished by Fred L. Smith, III, one of the coauthors of the article mentioned above. The method employed to reduce the

raw data to columnar-content-vs-time curves is described in that article.

III. THE THEORETICAL TIME-DEPENDENT THERMAL BEHAVIOR OF THE IONOSPHERIC ELECTRON GAS

In this chapter the temperature variation of the ionospheric electron gas during the dawn hours will be investigated theoretically. The solution of this problem is of importance if an understanding of the behavior of the early morning ionosphere (studied in the next chapter) is to be gained. A time-dependent heat flow equation is established and its numerical solution is obtained.

A. ELECTRON GAS HEATING AND COOLING MECHANISMS IN THE IONOSPHERE

Undoubtedly, the main cause of upper atmosphere heating is the solar extreme ultraviolet radiation (euv) notwithstanding the fact that other sources such as hydromagnetic wave dissipation, electric fields and particle precipitation, may also play an important role.

In order to be able to examine how the temperature of the ionosphere reacts to the sunrise, simplified models will be considered, in which the only heat source is the euv. It is assumed that all the heat input is via the electron gas--direct heating of neutrals and ions being taken as negligible. Heating of the electron gas results from the thermalization of fast electrons created in the ionization of neutral gases by photon absorption or by collision with the fast electrons themselves. At low altitudes where the mean free path of a fast electron is small compared with a scale height, this thermalization occurs in the immediate vicinity of the point where the electron was ejected from its parent atom (local heating). Only part of the energy of the photo-electron appears as heat of the electron gas, the remainder being used in inelastic collisions, the products of which do not yield their internal energy in the region or at the moment of interest.

The form of the heating function, Q(z), i.e., the amount of heat released per unit time per unit volume, has been worked out by several of the authors mentioned in the introduction, especially by Geisler and Bowhill [1965] who included the "non local heating."

In the present work the Geisler and Bowhill production function has been adopted, with a modification to include the influence of the solar zenithal angle. Strictly speaking, the isotropic pitch angle distribution of the ejected photo-electrons, used in the model above, should be replaced by the more complex expression given by Mariani [1965] due to the assymetry between the magnetic field and the direction of the solar radiation, that exists at dawn. This would alter somewhat the value of the production function at high altitudes, but would have only a small effect on the electron temperature profile. The solar zenithal angle was introduced by applying the Chapman function correction to the Chapman -β-like distribution of heat input below 300 km.

Thus

$$Q(z) = Q_m \exp\left(1 - \frac{z - z_m}{H} - Ch(\chi)e^{-\frac{z - z_m}{H}}\right)$$

where Q_m is the value of Q at the peak of heat production for overhead sun, which occurs at z_m;

H is the scale height of atomic oxygen;

χ is the solar zenithal angle; and

$Ch(\chi)$ is the Chapman function.

The adopted values of z_m and H were respectively 180 km and 53 km. Q_m was taken as 7000 ev per cubic centimeter per second for the solar minimum conditions and was scaled up in proportion to the increase in 10.7 cm solar flux, for other periods.

For altitudes above 300 km, the formula below was used.

$$Q(z) = Q_0 \left[1 + \frac{2}{3}(1-M^2)^{1/2}\left(\frac{1}{4M^2} - \frac{5}{8}\right) + \frac{M^2}{4}\log\left|1 + \frac{(1-M^2)^{1/2}}{M}\right|\right]$$

where $M^2 \equiv \exp\,[\,-(z - 300)\,/\,2H\,]$

These expressions were taken directly from the Geisler and Bowhill work mentioned.

Q_0 is the value of Q determined from the Chapman formula applicable to heights below 300 km.

Figure 2 shows the shape of the production function at solar minimum, for two different values of χ .

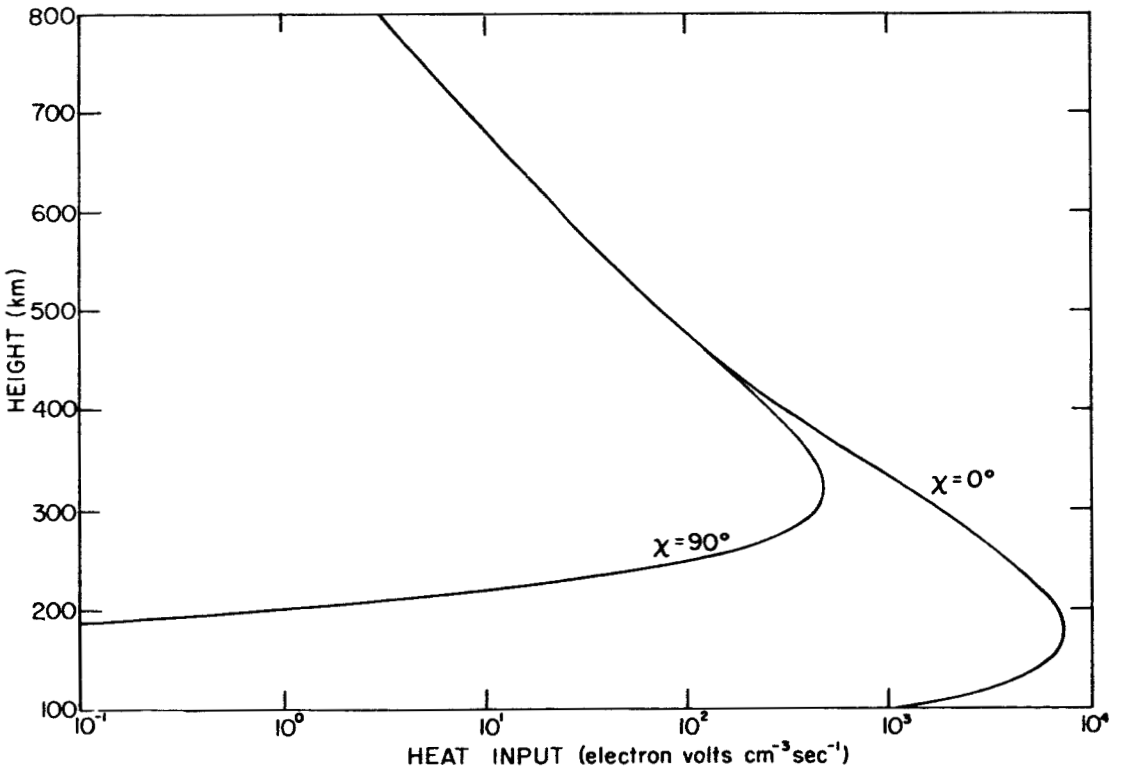

FIG. 2. SOLAR-CYCLE-MINIMUM HEAT INPUT TO THE ELECTRON GAS (AFTER GEISLER AND BOWHILL [1965]). A Chapman function dependence on the solar zenithal angle, χ , was introduced. Isotropic ejection of fast electrons is assumed.

Ions and neutrals act as coolants of the electron gas during the day and, if no other source is present, as heat sources, at night. The heat exchange mechanism is very complicated and an excellent treatment of this problem can be found in Dalgarno, et al, [1963]. A good summary description of the phenomenon can also be found in Geisler and Bowhill [1965] so that it is unnecessary to repeat it here.

The calculation of the thermal response of the atmospheric electron gas to the effect of the rising sun involves the solution of the time dependent heat flow equation containing terms representing the cooling of the gas through heat coupling to other particle species and through the conduction in the electron gas itself. The equation is a nonlinear, parabolic partial differential equation of second order in the space dimension. Since no horizontal variations in temperature are considered, only one single space dimension--height--is considered. The solution of the equation requires the choice of one initial and two boundary conditions.

The initial condition is the temperature profile that exists at the end of the night just prior to the first heating due to the solar euv. The large thermal sluggishness of the neutral atmosphere and the existence of a nighttime heating source in the Harris and Priester model, are responsible for the existence of steep temperature height-gradients even in the predawn period. If it is assumed that there are no sources capable of heating the electron gas in the absence of the sun, then due to the small heat capacity of this gas compared to the rest of the atmosphere, the electron temperature will fall quickly to that of the neutrals. The existence of the steep gradients mentioned will cause considerable heat flow downward. Under the assumption above, this heat must come from the neutrals by direct coupling and this, in turn, requires that the electrons become cooler than the neutrals.

The temperature difference will depend inversely on the efficiency of the heat transfer mechanism which will grow with the increasing ratio of neutral to electron concentration, i.e., with diminishing heights.

One boundary condition chosen is that the electron temperature is always equal to that of the neutral gases at 120 km. This is admittedly arbitrary because no accurate simultaneous measurements of the two temperatures involved are available. The fairly high neutral density seems to justify in part this assumption.

There is a choice of the type of upper boundary condition that can be used: one can stipulate a given temperature, a given temperature gradient or a given heat flux, depending on the physical situation being investigated.

B. THE TIME-DEPENDENT HEAT FLOW EQUATION

Consider a unit volume cell of a gas consisting of a mixture of various species of particles. Consider in particular the thermal behavior of species "1" when heat energy input to the gas is entirely by way of this species. As argued previously, this is the case of the higher atmosphere where, as a good first approximation, all the heat input is via the electron gas. Let the heat energy input per unit volume per unit time be designated by Q, measured in electron volts per cm^3 per second.

If there were no mechanism for heat loss, species "1" would show a steady raise in temperature given by

$$C_1 \frac{dT_1}{dt} = Q$$

where C_1 is the heat capacity of gas "1", in electron volts per degree Kelvin per cubic centimeter. Since to each degree of freedom there is associated an energy of $\frac{1}{2}kT$ it follows that, for electrons which have only the three (translational) degrees of freedom, $C = \frac{3}{2}kn$, where n is the concentration

(number of particles per cubic centimeter) and k is Boltzmann's constant. Both Q and C may be time dependent, and, in the atmosphere are certainly height dependent.

Species "1" inside the cell will exchange part of its thermal energy with the surroundings by two processes.

1. Heat Transfer

As soon as the temperature of species "1" exceeds that of the rest of the gas, some of its energy will be communicated to the other species. The amount of heat energy loss per unit volume will, clearly, be proportional to the temperature difference between species "1" and species "i" and to the concentration of the latter.

Let L be the energy lost per unit time per unit volume by species "1" through this process

$$L = A\ (T_1 - T_i)\ n_i$$

where A is a parameter which depends on the temperature and on the species involved and which will be examined more closely further on. The total heat energy transferred, per unit time and unit volume, from gas 1 to the remaining gases in the mixture is the sum of the values of L, represented here by the symbol ΣL.

The coolant gases, by removing heat from the electrons, will themselves heat up. Due to the large heat capacity of the neutrals, they will respond only slowly, showing a small rate of temperature increase. To compute the behavior of a simplified ionosphere model the temperature of the neutrals can be taken, as a first approximation as constant--if the time span during which the electron temperature is being examined is sufficiently short--or else the temperature changes of neutrals can be programmed to follow the Harris and Priester model.

The temperature of the ions at low altitudes, say below some 500 km, is close to that of the neutrals due to

the good inter-species coupling. At higher altitudes the electron-ion coupling begins to be more and more important until, in the neighborhood of 1000 km, it is the dominant factor in heat removal by the cooling fluid. Since the rate of heat transfer from the ions to the neutral gas can be mathematically described, the ion temperature can be computed from the available data by balancing heat input to the ion gas from the electron gas and heat output from the ion gas to the neutral atmosphere. It should be noted that heat conduction by ions is not important because the conductivity is proportional to the inverse of the square root of the mass of the charged particle. Hence the predominant ion gas, O^+, has a conductivity almost 200 times lower than that of the electron gas.

In the present work the ion temperature is handled in the somewhat arbitrary fashion described in the last section of this chapter. The inclusion of the exact ion temperature would require the solution of a pair of simultaneous differential equations at each height step, while the simplifying assumption adopted, reduced this to the solution of a single equation at each step. The resulting errors are small, especially in view of the fact that at high altitudes electron temperature is mainly determined by the conductivity of the electron gas and not greatly influenced by inter-species heat exchanges.

2. Conduction

If the temperature throughout the gas is not uniform, then heat will flow from the hotter to the cooler point. The heat flux density will be proportional to the temperature gradient and to the heat conductivity, λ . In one dimension

$$\text{heat flux density} = \lambda \frac{\partial T_i}{\partial z} \text{ electron volts cm}^{-2} \text{ sec}^{-1}$$

If the gradient is uniform, just as much heat flows in as out of the cell, and no energy is deposited in it. The energy change in the cell is

$$Q_{cond.} = \frac{\partial}{\partial z} \left(\lambda \frac{\partial T_1}{\partial z} \right)$$

The conductivity λ is a function of T_1 and, therefore, of z. For neutrals $\lambda \propto T^{1/2}$ but for electrons the dependence is much stronger, as $\lambda = BT^{5/2}$. The value of B will be derived in the next section.

Taking both heat exchange mechanisms into account, one obtains a time dependent heat flow equation which, for the electron gas, is

$$\frac{\partial T_e}{\partial t} = \frac{1}{C_e} \left[B \frac{\partial}{\partial z} \left(T_e^{5/2} \frac{\partial T_e}{\partial z} \right) + Q - \Sigma L \right]$$

C. NUMERICAL VALUE OF VARIOUS PARAMETERS

In the preceding section, the thermal conductivity of the electron gas was assumed to be $\lambda = BT^{5/2}$. To determine the value of B we refer to Spitzer [1962] who states that this conductivity, in a Lorentz gas, is

$$\lambda_L = 1.95 \times 10^{-12} \frac{T_e^{5/2}}{\ln\Lambda} \frac{\text{cal}}{\text{sec deg cm}}$$

The value of $\ln\Lambda$ is a slow function of T_e and of the electron concentration. The table below is taken from Spitzer.

TABLE 1. VALUES OF $\ln\Lambda$

T_e	Electron Concentration		
	10^0	10^3	10^6
10^2	16.3	12.8	9.4
10^3	19.7	16.3	12.8
10^4	23.2	19.7	16.3

Since T_e in the ionosphere is of the order of 1000° K and N_e is between 10^3 and 10^6 electrons cm^{-3}, a reasonable value of $\ln\Lambda$ is 15. Thus

$$\lambda_L = 1.3 \times 10^{-13} T_e^{5/2}$$

The ratio of the conductivities of an actual gas to that of a Lorentz gas is, for electrons, 0.225, hence

$$\lambda = 2.9 \times 10^{-14} T_e^{5/2} \qquad \frac{\text{cal}}{\text{sec deg cm}}$$

or

$$\lambda = 7.7 \times 10^{5} T_e^{5/2} \qquad \frac{\text{e.v.}}{\text{sec deg cm}}$$

whence

$$B = 7.7 \times 10^{5} \qquad \frac{\text{e.v.}}{\text{sec deg}^{7/2} \text{ cm}}$$

The values of the various constants, all designated A, relating heat loss to the coolant gases to the product of coolant concentration and temperature difference, have been amply discussed by Hanson, Dalgarno, and by Geisler and Bowhill.

Hanson and Johnson [1961] calculated the value for A for the electron gas to oxygen-ion coupling and found

$$A = \frac{C_e}{268\ T_e^{3/2}}$$

where T_e is the electron temperature and C_e is the heat capacity of the gas in electron volts per cubic centimeter per degree Kelvin.

For losses to molecular oxygen, Hanson [1962] finds

$$A = 4.0 \times 10^{-14} T_e - 8.0 \times 10^{-12}$$

For losses to molecular nitrogen, Geisler and Bowhill [1965] adopt the formula below extracted from Dalgarno, et al, [1963] and from Dalgarno and Moffett [1962]:

$$A = 7.6 \times 10^{-16} T_e + [1.2 \times 10^{-11} - 5.6 \times 10^{-15} T_N]$$

where T_N is the temperature of the neutrals.

D. NUMERICAL SOLUTION OF THE TIME-DEPENDENT HEAT FLOW EQUATION

The heat flow equation developed in Section B can be written

$$\frac{\partial T}{\partial t} = U(z,t,T) \frac{\partial^2 T}{\partial z^2} + V(z,t,T) \left(\frac{\partial T}{\partial z}\right)^2 + W(z,t,T)$$

where

$$U \equiv \frac{B}{C_e} T^{5/2}$$

$$V \equiv \frac{5}{2} \frac{B}{C_e} T^{3/2}$$

$$W \equiv \frac{1}{C_e} (Q - \Sigma L)$$

The partial differential equation above can be substituted by the corresponding difference equation

$$\frac{T_{i,j+1} - T_{i,j}}{\Delta t} = U_{i,j} \frac{T_{i+1,j} - 2T_{i,j} + T_{i-1,j}}{(\Delta z)^2} +$$

$$+ V_{i,j} \left(\frac{T_{i+1,j} - T_{i,j}}{\Delta z}\right)^2 + W_{i,j}$$

where i is the order of the height step, Δz;

j is the order of the time step, Δt;

$U_{i,j}$ stands for $U(i\Delta z, j\Delta t)$ and so on.

Here the unknown, $T_{i,j+1}$, is an explicit function of known parameters.

It is very important to realize that as $\Delta z, \Delta t \to 0$, the solution of the difference equation does <u>not</u> necessarily converge to the solution of the differential equation. If

there is no convergence--the values of T may oscillate wildly with each time step--the equation is said to be unstable.

The exact condition of stability is not known to this author, but is, probably

$$\max (U_{i,j}) \frac{\Delta t}{(\Delta z)^2} < \frac{1}{2}$$

and additional constraints related to $V_{i,j}$ and $W_{i,j}$. This imposes an extremely stringent restriction on the sizes of the steps Δz, Δt, i.e., the mesh sizes in the z, t plane that can be used, making it in fact, impossible to solve the physical problem on hand by the above scheme. That it is so can be seen from the evaluation of the maximum time step allowed. Consider as an example, the situation when the electron concentration is as low as 10^4 cm^{-3} and the temperature is 1000° K. These are values that can occur easily, at heights of 1000 km. Under such conditions

$$U = \frac{7.7 \times 10^5 \ T^{5/2}}{1.29 \times 10^{-4} \ n}$$

Here we expressed the heat capacity of the electron gas, $\frac{3}{2}kn$, in electron volts and as a function of the concentration n. Introducing the chosen values of concentration and temperature, we obtain

$$U \approx 2 \times 10^{13}$$

Even using fairly large height steps of 20 km, the maximum time step will be 0.1 seconds. Since the time intervals of interest are of the order of one hour, 40,000 iterations would be necessary. This is not only quite expensive in terms of computer time, but also would certainly become meaningless due to the accumulated truncation and round-off errors.

To circumvent these difficulties, it is possible to use implicit difference equations, the general scheme being the expression of the space derivatives not in terms of the values of the dependent variable at the last computed time step alone, but also (or exclusively) in terms of the values at the next (future) step. Thus, the second derivative could be represented by

$$\frac{1}{(\Delta z)^2}\left[\alpha\,(T_{i+1,j+1} - 2T_{i,j+1} + T_{i-1,j+1}) + (1-\alpha)\,(T_{i+1,j} - 2T_{i,j} + T_{i-1,j})\right]$$

where α is a constant. When $\alpha = \frac{1}{2}$ the scheme is known as the Crank and Nicholson scheme and when $\alpha = 1$, it is the Laasonen scheme. (See Crank and Nicholson [1947] and Laasonen [1949].) The former leads to truncation error, $e = 0\,[(\Delta t)^2] + 0\,[(\Delta x)^2]$ while the latter has the disadvantage of larger error, $e = 0\,[(\Delta t)] + 0\,[(\Delta x)^2]$. Many other schemes, some with smaller errors, are possible. Since we are not interested in extreme precision and considering that the extension of the high accuracy schemes to complicated non linear problems can lead to serious difficulties, we will adopt the simpler Laasonen method.

We will find separately the implicit expressions for the conduction and for the loss terms of the heat flow difference equations corresponding to the differential equation below

$$\partial T = \frac{B}{C}\,\partial t\,\frac{\partial}{\partial z}\left(T^{5/2}\,\frac{\partial T}{\partial t}\right) - \partial t\,\frac{\Sigma L}{C} + \partial t\,\frac{Q}{C}$$

conduction term — loss term — production term

and then will solve the complete equation.

1. The Conduction Term

The conduction term $\partial t\,\frac{B}{C}\,\frac{\partial}{\partial z}\,(T^{5/2}\,\frac{\partial T}{\partial z})$ can be substituted by a corresponding difference expression

$$\Delta z \; \mu_i \left[\left(T^{5/2} \frac{\partial T}{\partial z} \right)_{i+\frac{1}{2}} - \left(T^{5/2} \frac{\partial T}{\partial z} \right)_{i-\frac{1}{2}} \right]$$

where

$$\mu_i \equiv \frac{\Delta t}{(\Delta z)^2} \frac{B}{C}$$

Here we took the values of the variable $T^{5/2} \frac{\partial T}{\partial z}$, half way between mesh points. Expanding, we obtain

$$\mu_i \left[\left(T^{5/2} \right)_{i+\frac{i}{2}} (T_{i+1} - T_i) - \left(T^{5/2} \right)_{i-\frac{1}{2}} (T_i - T_{i-1}) \right]$$

and if we approximate $\left(T^{5/2} \right)_{i+\frac{1}{2}} \approx \left(\frac{T_{i+1} + T_i}{2} \right)^{5/2}$ and the same for $\left(T^{5/2} \right)_{i-\frac{1}{2}}$ then the conduction term becomes

$$\mu_i \left[\left(\frac{T_{i+1} + T_i}{2} \right)^{5/2} (T_{i+1} - T_i) - \left(\frac{T_i + T_{i-1}}{2} \right)^{5/2} (T_i - T_{i-1}) \right]$$

If we evaluate this term at step j and introduce it into the complete difference equation, then we will encounter the instability problem mentioned previously. To apply an implicit scheme all T must be evaluated at step $j+1$ and are therefore unknown. For brevity, let $x_i \equiv T_{i,j+1}$ and $T_i \equiv T_{i,j}$.

The conduction term contains the unknown x_i raised to the 5/2 power and this makes it impossible to solve the algebraic equations to explicitate x_i, because a system of N simultaneous equations of degree $\frac{5}{2}(N-1)$ results.

For this reason it becomes essential to linearize the term by using a truncated Taylor series. Thus

$$\left(\frac{x_{i+1} + x_i}{2} \right)^{5/2} \approx \left(\frac{T_{i+1} + T_i}{2} \right)^{5/2} +$$

$$+ \frac{5}{2} \left(\frac{T_{i+1} + T_i}{2} \right)^{3/2} \left(\frac{x_{i+1} + x_i - T_{i+1} - T_i}{2} \right)$$

and similarly for the other factor. Using this approximation:

$$\mu_i \Bigg\{ \left(\frac{T_{i+1} + T_i}{2}\right)^{5/2} (x_{i+1} - x_i) + \frac{5}{4} \left(\frac{T_{i+1} + T_i}{2}\right)^{3/2} [x_{i+1}^2 - x_1^2 - (T_{i+1} + T_i)(x_{i+1} - x_i)]$$

$$- \left(\frac{T_i + T_{i-1}}{2}\right)^{5/2} (x_i - x_{i-1}) - \frac{5}{4} \left(\frac{T_i + T_{i-1}}{2}\right)^{3/2} [x_i^2 - X_{i-1}^2 - (T_i + T_{i-1})(x_i - x_{i-1})] \Bigg\}$$

We now introduce new symbols for simplification

$$\zeta_i \equiv \mu_i \left(\frac{T_{i+1} + T_i}{2}\right)^{5/2}$$

$$\eta_i \equiv \frac{5}{4} \mu_i \left(\frac{T_{i+1} + T_i}{2}\right)^{3/2}$$

$$\Theta_i \equiv - \mu_i \left(\frac{T_i + T_{i-1}}{2}\right)^{5/2}$$

$$\varepsilon_i \equiv - \frac{5}{4} \mu_i \left(\frac{T_i + T_{i-1}}{2}\right)^{3/2}$$

The conduction term is now

$$\zeta_i (x_{i+1} - x_i) + \eta_i [x_{i+1}^2 - x_i^2 - (T_{i+1} + T_i)(x_{i+1} - x_i)]$$

$$+ \Theta_i (x_i - x_{i-1}) + \varepsilon_i [x_i^2 - x_{i-1}^2 - (T_i + T_{i-1})(x_i - x_{i-1})]$$

The presence of the x_i^2 terms requires further linearization and we write

$$x_i^2 \approx 2T_i x_i - T_i^2$$

so that the conduction term becomes

$$\zeta_i (x_{i+1} - x_i) + \eta_i [2T_{i+1}x_{i+1} - T_{i+1}^2 - 2T_i x_i + T_1^2$$

$$- T_{i+1}x_{i+1} + T_{i+1}x_i - T_i x_{i+1} + T_i x_i] + \Theta_i (x_i - x_{i-1})$$

$$+ \tau_i [2T_i x_i - T_i^2 - 2T_{i-1}x_{i-1} + T_{i-1}^2 - T_i x_i - T_{i-1}x_i$$

$$+ T_i x_{i-1} + T_{i-1}x_{x-1}] = [- \Theta_i + \tau_i (T_i - T_{i-1})] x_{i-1}$$

$$+ [\Theta_i - \zeta_i + \eta_i (T_{i+1} - T_i) + \tau_i (T_i - T_{i-1})] x_i$$

$$+ [\zeta_i + \eta_i (T_{i+1} - T_i)] x_{i+1} + \eta_i (T_i^2 - T_{i+1}^2)$$

$$+ \tau_i (T_{i-1}^2 - T_i^2)$$

2. The Loss Term

In addition to the conduction term, the expression for the time derivative of the electron temperature contains the terms

$$W(z,t,T) \equiv \frac{Q}{C_e} - \frac{\Sigma L}{C_e}$$

the latter, called here the "loss term" involves the dependent variable, T, in a variety of power from $T^{-3/2}$ to T^2. When writing a difference equation, it is necessary to include these functions of T in an implicit fashion to insure stability.

Taking into account cooling by N_2, O_2, O and O^+, but neglecting the effect of He, we can write

$$-\frac{\Sigma L}{C_e} = -(T_i - T_N)\left[\frac{N_i}{268}\, T_i^{-3/2} + 1.1 \times 10^{-14}\, N(O)_i \right.$$

$$\times T_i^{1/2} + (7.6 \times 10^{-16} \times T_i + 1.2 \times 10^{-11} - 5.6 \times 10^{-15}$$

$$\left. \times T_{N_i})\, N(N2)_i + (4 \times 10^{-14} \times T_i - 8 \times 10^{-12}) \times N(O2)_i \right]$$

$$= -(T_i - T_N)\left[\alpha_i T_i^{-3/2} + \beta_i T_i^{1/2} + \gamma_i T_i + \delta_i\right]$$

where

$$\alpha_i \equiv \frac{N_i}{268} \qquad \beta_i \equiv 1.1 \times 10^{-14} N(O)_i$$

$$\gamma_i \equiv 4 \times 10^{-14} \times N(O_2) + 7.6 \times 10^{-16} N(N_2)_i$$

$$\delta_i \equiv (1.2 \times 10^{-11} - 5.6 \times 10^{-15}\, T_{N_i})\, N(N_2)_i$$

$$- 8 \times 10^{-12}\, N(O_2)_i$$

and T_{N_i} is the temperature of the neutrals. Hence

$$-\frac{\Sigma L}{C_e} = \alpha_i T_{N_i} T_i^{-3/2} - \alpha_i T_i^{-1/2} + \beta_i T_{N_i} T_i^{1/2} - \beta_i T_i^{3/2}$$

$$+ \gamma_i T_{N_i} T_i - \gamma_i T_i^2 + \delta_i T_{N_i} - \delta_i T_i = \alpha_i T_{N_i} T_i^{-3/2}$$

$$- \alpha_i T_i^{-1/2} + \beta_i T_{N_i} T_i^{1/2} + (\gamma_i T_{N_i} - \delta_i)\, T_i - \beta_i T_i^{3/2}$$

$$- \gamma_i T_i^2 + \delta_i T_{N_i}$$

Using the implicit scheme, all T_i are considered at a time step $j+1$ and by again writing $x_i \equiv T_{i,j+1}$;

$T_i \equiv T_{i,j}$ and linearizing, we obtain

$$-\frac{\Sigma L}{C_e} = \alpha_i T_{N_i}\left[T_i^{-3/2} - \frac{3}{2}\,T_i^{-5/2}(x_i - T_i)\right] - \alpha_i\left[T_i^{-1/2} -\right.$$

$$\left. - \frac{1}{2}\,T_i^{-3/2}(x_i - T_i)\right] + \beta_i T_{N_i}\left[T_i^{1/2} + \frac{1}{2}\,T_i^{-1/2}(x_i - T_i)\right] -$$

$$- \beta_i\left[T_i^{3/2} + \frac{3}{2}\,T_i^{1/2}(x_i - T_i)\right] + (\gamma_i T_{N_i} - \delta_i)\,x_i -$$

$$- \gamma_i\left[T_i^{2} + 2\,T_i(x_i - T_i)\right] + \delta_i T_{N_i} \quad =$$

$$= \left(-\frac{3}{2}\,\alpha_i T_{N_i} T_i^{-5/2} + \frac{1}{2}\,\alpha_i T_i^{-3/2} + \frac{1}{2}\,\beta_i T_{N_i} T_i^{-1/2} -\right.$$

$$\left. - \frac{3}{2}\,\beta_i T_i^{1/2} + \gamma_i T_{N_i} - \delta_i - 2\,\gamma_i T_i\right)\,x_i \quad +$$

$$+ \frac{\alpha_i}{2}\left(5\,T_{N_i} T_i^{-3/2} - 3\,T_i^{-1/2}\right) + \frac{\beta_i}{2}\left(T_{N_i} T_i^{1/2} + T_i^{3/2}\right) +$$

$$+ \gamma_i T_i^{2} + \delta_i T_{N_i}$$

or

$$-\frac{\Sigma L}{C_e} \equiv A_i + B_i\,x_i$$

and

$$W = \frac{Q}{C} + A_i + B_i\,x_i$$

3. The Complete Equation

Combining the conduction and the loss terms with a production term, we can write the complete implicit difference equation describing the heat flow in the ionospheric electron gas.

$$x_i = T_i + \left[-\Theta_i + \varepsilon_i(T_i - T_{i-1})\right] x_{i-1} + \left[\Theta_i - \zeta_i + \eta_i(T_{i+1} - T_i) + \right.$$

$$\left. + \varepsilon_i(T_i - T_{i-1})\right] x_i + \left[\zeta_i + \eta_i(T_{i+1} - T_i)\right] x_{i+1} +$$

$$+ \eta_i(T_i^2 - T_{i+1}^2) + \varepsilon_i(T_{i-1}^2 - T_i^2) + \Delta t \left(\frac{Q}{C} + A_i + B_i x_i\right)$$

Collecting terms

$$e_i x_{i-1} + b_i x_i + a_i x_{i+1} = c_i \qquad i = 1, 2, \ldots N-1$$

where

$$a_i = \zeta_i + \eta_i(T_{i+1} - T_i)$$

$$e_i = -\Theta_i + \varepsilon_i(T_i - T_{i-1})$$

$$b_i = \Delta t\, B_i - 1 + \Theta_i - \zeta_i + \eta_i(T_{i+1} - T_i) + \varepsilon_i(T_i - T_{i-1})$$

$$c_i = -T_i - \Delta t\left(\frac{Q}{C} + A_i\right) - \eta_i(T_i^2 - T_{i+1}^2) - \varepsilon_i(T_{i-1}^2 - T_i^2)$$

Invoking the boundary conditions

$$x_o = T_{o,j} = \text{constant}$$

and

$$\frac{\partial T}{\partial z}(z_{max}, t) \rightarrow T_{N,j} = T_{N-1,j} \rightarrow x_N - x_{N-1}$$

or

$$x_N = \text{constant}$$

There can be a choice of the type of upper boundary condition adopted.

We have now a system of N-1 equations and N-1 unknowns.

$$\begin{aligned} e_1x_0 + b_1x_1 + a_1x_2 &= C_1 \\ e_2x_1 + b_2x_2 + a_2x_3 &= C_2 \\ e_3x_2 + b_3x_3 + a_3x_4 &= C_3 \\ &\cdots\cdots\cdots\cdots \\ e_{N-1}x_{N-2} + b_{N-1}x_{N-1} + a_{N-1}x_N &= C_{N-1} \end{aligned}$$

Starting from the bottom, each x_i can be determined from the knowledge of x_{i+1}.

$$x_1 = -\frac{a_1}{b_1}x_2 + \frac{c_1 - e_1 x_0}{b_1} \equiv C_1 x_2 + D_1$$

$$C_1 = -\frac{a_1}{b_1}$$

$$D_1 = \frac{c_1 - e_1 x_0}{b_1}$$

$$x_2 = -\frac{a_2}{b_2}x_3 + \frac{c_2 - e_2 x_1}{b_2}$$

$$b_2x_2 = -a_2x_3 + c_2 - e_2C_1x_2 - e_2D_1$$

$$x_2 = -\frac{a_2}{b_2 + e_2C_1}x_3 + \frac{c_2 - e_2D_1}{b_2 + e_2C_1} \equiv C_2 x_3 + D_2$$

In general

$$x_i = C_i x_{i+1} + D_i$$

$$C_i = \frac{-a_i}{b_i + e_i C_{i-1}}$$

$$D_i = \frac{c_i - e_i D_{i-1}}{b_i + e_i C_{i-1}}$$

If the upper boundary condition fixed a value for x_N then clearly x_{N-1} can be easily found and so on down to x_1. If the upper boundary condition was a zero derivative, then the last equation for x yields a relation between x_{N-1} and x_N:

$$x_{N-1} = C_{N-1}\, x_N + D_{N-1}$$

but according to this boundary condition

$$x_{N-1} = x_N = \frac{D_{N-1}}{1 - C_{N-1}}$$

Finally, if the upper boundary condition is a given upward or downward flux of heat, G_p, then we have

$$\frac{\partial T}{\partial z} = \frac{G_p}{\lambda} = \frac{G_p}{B\, T_e^{5/2}}$$

or

$$x_N - x_{N-1} = \frac{\Delta z\, G_p}{B\, x_N^{5/2}}$$

and

$$x_{N-1} = C_{N-1} x_N + D_{N-1}$$

In the above equation a downward flux of heat corresponds to $G_p > 0$. Combining the two equations

$$(1 - C_{N-1})\, x_N^{7/2} - D_{N-1}\, x_N^{5/2} - \frac{\Delta z\, G_p}{B} = 0$$

This allows the calculation of x_N and consequently of x_{N-1}.

Since x_N and x_{N-1} are known, all other x_i can be found, yielding the temperature profile at time $(j+1)\Delta t$ as a function of the profile at the preceding time step, $j\Delta t$. The problem is thereby solved because the first profile is the given initial condition.

E. STEADY-STATE SOLUTION OF THE HEAT FLOW EQUATION

In order to obtain a partial check on the accuracy of the solution of the time-dependent heat flow equation, one can compare the end value thus obtained with a directly calculated steady-state result.

1. Analytical Solution

Due to the complicated form of the loss term, an analytical solution can be obtained only for the lossless case. The simple case of no production can be handled very easily. The steady-state heat flow equation becomes

$$\frac{\partial}{\partial z}\left(\lambda \frac{\partial T}{\partial z}\right) = C \frac{\partial T}{\partial t} = 0$$

$$\frac{dT}{dz}\frac{d\lambda}{dz} + \lambda \frac{d^2T}{dz^2} = 0$$

but $\lambda = B\, T^{5/2}$, hence

$$\frac{dT}{dz}\frac{d}{dz}\left(T^{5/2}\right) + T^{5/2}\frac{d^2T}{dz^2} = \frac{5}{2}\, T^{3/2}\left(\frac{dT}{dz}\right)^2 + T^{5/2}\frac{d^2T}{dz^2} = 0$$

or

$$\frac{d^2T}{dz^2} + \frac{5}{2}\, T^{-1}\left(\frac{dT}{dz}\right)^2 = 0$$

The solution is found in Kampke [1959], number 6.51, and is

$$T = (C_1 z + C_2)^{2/7}$$

As boundary conditions choose

$$T = T_o \quad \text{at } z = z_o$$

and

$$T = T_m \quad \text{at } z = z_m$$

Introducing these conditions into the equation above

$$C_1 = \frac{T_o^{7/2} - T_m^{7/2}}{z_o - z_m}$$

$$C_2 = \frac{z_o T_m^{7/2} - z_m T_o^{7/2}}{z_o - z_m}$$

This analytical solution was used as a first check on the numerical steady-state solution described below.

2. Numerical Solution

The numerical solution of the full steady-state equation (including production and loss) was obtained by Geisler and Bowhill [1965] using the integro-differential form of the steady-state heat flow equation given below.

$$\lambda \frac{dT}{dz} = \int_z^\infty dz' \, (Q - \Sigma L)$$

One of the boundary conditions is built-in in this equation, i.e., the upper boundary condition is fixed as a

zero derivative of temperature with height. A slightly more general solution can be obtained -- giving freedom of the type of upper boundary condition adopted -- by integrating the complete differential equation using the popular eigen-value approach described by Rishbeth and Barron [1960] in connection with ionospheric diffusion.

The differential equation and its corresponding difference equation are

$$\frac{d^2T}{dz^2} + \frac{5}{2} T^{-1} \left(\frac{dT}{dz}\right)^2 + \frac{C}{B} T^{-5/2} W(z,t,T) = 0$$

$$\frac{T_{i+1} - 2 T_i + T_{i-1}}{(\Delta z)^2} + \frac{5}{2} \frac{1}{T_i} \frac{(T_{i+1} - T_i)^2}{(\Delta z)^2} + \frac{C}{B} \frac{1}{T_i^{5/2}} W_i = 0$$

$$i = 0, 1, \ldots N$$

Solving for T_{i-1}

$$T_{i-1} = 2 T_i - T_{i+1} - \frac{5}{2} \frac{(T_{i+1} - T_i)^2}{T_i} - \frac{C}{B} \frac{(\Delta z)^2}{T_i^{5/2}} W_i$$

Thus the value of T at the level i-1 can be calculated from the knowledge of T at the two levels immediately above. The upper boundary condition may be either

$$T_N = T_m$$

(where T_m is a chosen value of temperature), or

$$T_{N-1} = T_N$$

The downward integration is made, in either case, by assuming an arbitrary but reasonable value for T_{N-1}. One has then both T_N and T_{N-1}. As the integration proceeds, the temperature may become negative or it may become excessive as a result of the incorrectly assumed T_{N-1}. When this happens, the computer starts the integration again with an altered value of T_{N-1}. This is repeated automatically until the value of T_o -- the lower boundary condition -- falls within the chosen tolerance. The whole operation is quite fast; as an example, using a Burroughs B-5500, it took 14 seconds to find the correct temperature profile when the lower boundary was set at 355 ± 1 degrees and the starting value of T_{N-1} was set at 1200 degrees. The computer tried out various values for this latter temperature and found 1098 degrees to be correct.

Fig. 3 compares the analytical with the numerical solution for the lossless case. It can be seen that with a 20 km height step the agreement is acceptable and with a 5 km height step it is excellent.

F. RESULTS

Before examining the results of the theoretical study presented here, the limitations of the models used and the basic assumptions employed should be reviewed.

The boundary conditions were

a. At 120 km the electron and neutral temperatures are equal, i.e., perfect thermal contact between plasma and the rest of the atmosphere is assumed.

b. At 1000 km the electron temperature is height independent. This is equivalent to saying that no appreciable heat sources exist at that height. The production function, Q, at 1000 km is, in fact, four orders of magnitude lower than at the $\chi = 0$ production peak and makes, therefore, an insignificant contribution to the local heating. Neutrals

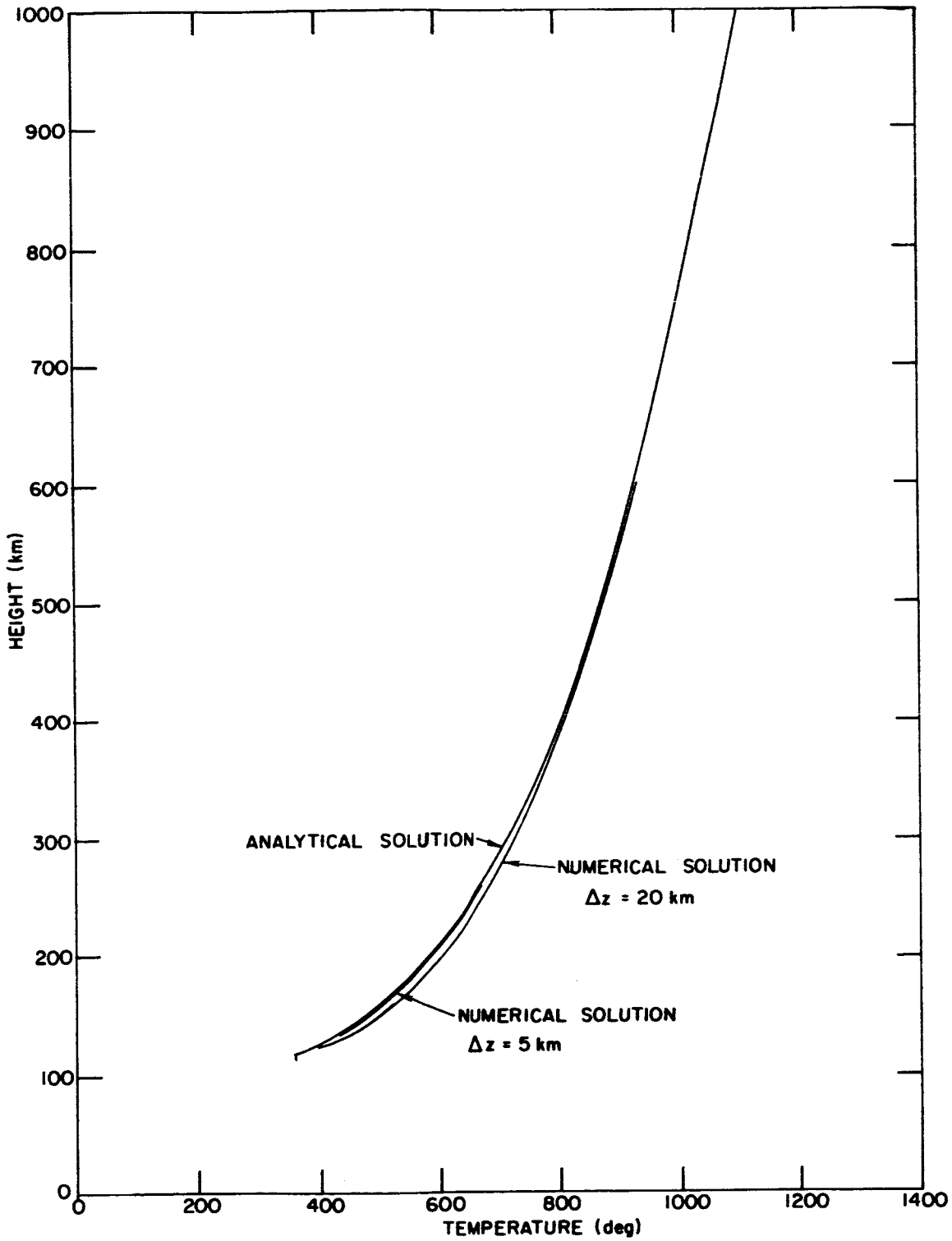

FIG. 3. COMPARISON OF THE SOLUTIONS OF THE STEADY-STATE HEAT CONDUCTION EQUATION (NO PRODUCTION, NO LOSSES). The numerical solution with height steps of 5 km is practically indistinguishable from the exact analytical solution. Height steps of 20 km cause a slight loss of accuracy.

exist at these heights in concentrations that are many orders of magnitude below that around 200 km, and have consequently a negligible cooling action. Heat conduction to or from the protonosphere would result in a temperature gradient different from zero but this effect is not understood well enough to be included in this analysis, however one nighttime temperature profile (Fig. 6a) was calculated using as an upper boundary condition a fixed downward heat flux from the protonosphere.

The heat input function adopted was that of Geisler and Bowhill [1965] modified to include a Chapman function dependence on the solar zenithal angle. The value of the heat function was made proportional to the 10.7 cm solar flux to accomodate solar cycle variations. The "non-local" heating effect depends on the choice of pitch angle distribution of the ejected photo-electrons; the isotropic distribution used by Geisler and Bowhill was maintained in spite of the large angle between solar direction and the magnetic field. The use of the correct distribution given by Mariani [1964] has probably only a second order effect on the final electron temperature.

The solar zenithal angle was assumed to vary linearly with time at the rate of -3.2×10^{-3} degrees sec^{-1}.

To obtain the concentration of the neutral species, the temperatures for each height step obtained from the Harris and Priester [1962] model and the reference concentrations at 120 km were read by the computer and from these data the height-dependent concentration for N_2, O_2 and O were calculated using a diffusive equilibrium formula. The existence of H and He was ignored. All calculations were made assuming that the neutral temperature did not change with time.

Ion temperatures, as explained before, were not calculated directly because this would slow down the computer by at least one order of magnitude. An estimate of ion temperature was obtained by taking $T_i = T_n$ in all altitudes below

500 km, $T_i = T_e$ at all altitudes above 800 km and by interpolating between these values in the range between 500 and 800 km. The steady-state ion temperature distribution lends some support to this scheme.

The transient thermal behavior of the electron gas depends critically on its heat capacity and hence, on the electron concentration profile. The models chosen here are necessarily arbitrary and this may be the main source of any discrepancy between theoretical and observed results. The steady state nighttime concentration profiles used at the begining of each integration have the general shape of a Chapman-α layer modified both on the bottom and on the top. At the bottom the Chapman layer would give an unrealistically low electron concentration, so the distribution between 120 and 160 km was altered to yield a concentration of 1000 electrons cm^{-3} at the lower height and a linearly increasing concentration up to 160 km where the Chapman distribution takes over. From a chosen height (600 km in most cases) diffusive equilibrium distribution of hydrogen ions starts. The peak height of the Chapman layer was taken as 250 km. The scale height used was variable depending on the average ion-electron temperature at each altitude.

EGO radio-propagation measurements have shown that first noticeable increase of columnar electron content in the early morning, occurs at a solar zenithal angle of about 95 degrees. From that moment on, on many days, both the content and the value of the electron concentration at the F2 peak, as seen by ground-based ionosondes, may be approximated by a linear increase with time. On other days the behavior is quite different and much more complicated and is considered "anomalous" as far as the present investigation is concerned.

For the models used, the electron concentration at the F2 peak was taken as constant while the solar zenithal angle exceeded 95 degrees. At smaller angles, the concentration

was made to increase linearly with time. To be able to choose representative values of the initial concentration and its rate of increase, ionosonde data, recorded at Washington, D.C., and published by the CRPL, were examined. The period from mid-1953 to the begining of 1959 was chosen because it covers both sunspot minimum and maximum conditions. Fig. 4 shows the average monthly value of the F2-peak electron con-

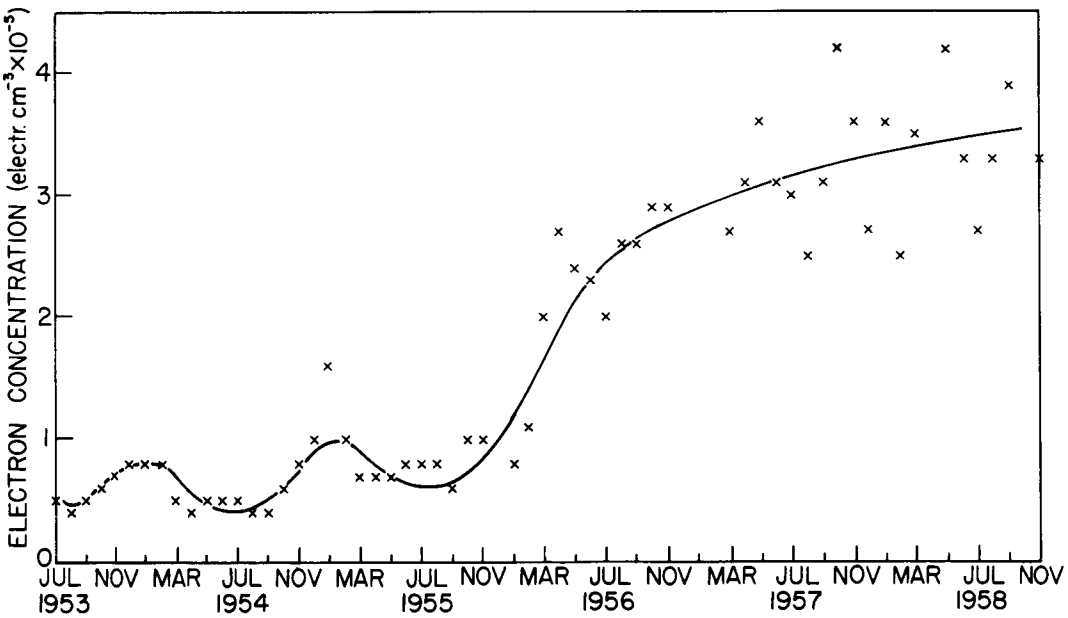

FIG. 4. THE MONTHLY AVERAGE OF THE PREDAWN F2-PEAK ELECTRON CONCENTRATION AT WASHINGTON, D. C.

centration just prior to the first sunrise effect. It can be seen that, if Washington, D.C., is considered as representative of mid-latitude conditions, then at these latitudes the predawn concentrations are small at the solar cycle minimum and exhibit a 2:1 seasonal variation. At solar maximum this seasonal variation seems largely to disappear, while the con-

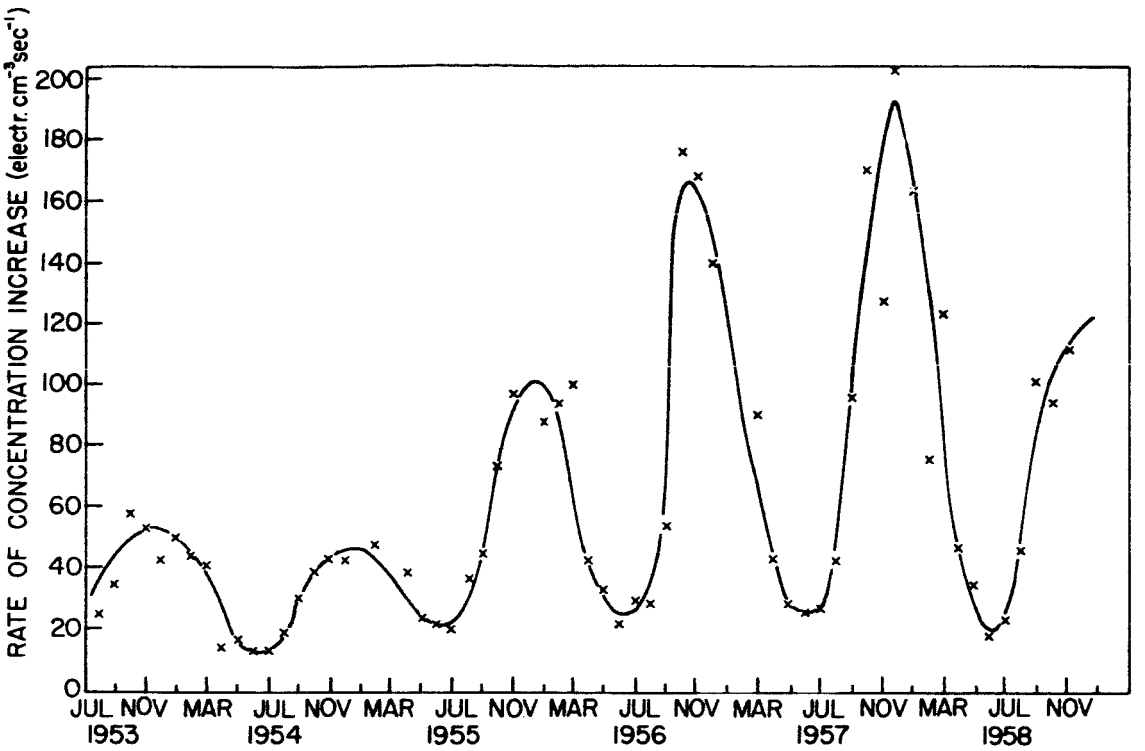

FIG. 5. STRONG SEASONAL AND SOLAR CYCLE INFLUENCE IS EVIDENT IN THE RATE OF F2-PEAK ELECTRON CONCENTRATION BUILDUP, JUST AFTER DAWN.

centrations are much greater. Fig. 5 indicates the very strong solar cycle and seasonal dependence of the rate of concentration buildup near sunrise. The seasonal effect is clearly related to the "winter anomaly". Since the midlatitude value of $N_{max}F2$ at night does not show much of a seasonal variation while the midday value is much larger in winter than in summer, it follows that the winter electron concentration increase rate must be much larger than the summer one.

Based on an inspection of the figures mentioned above, four models were selected as indicated in Table 2.

The initial temperatures prior to the impingement of the first solar rays were obtained by introducing an arbitrary initial distribution, setting $Q = 0$ and allowing the computer to calculate the temperatures long enough, so that a

TABLE 2. PROPERTIES OF THE IONOSPHERE MODELS IN THE EXAMPLES

	Predawn Electr. Conc. (F2 maximum) El $cm^{-3} \times 10^{-5}$	Rate of Conc. Incr. (F2 maximum) El. $cm^{-3} sec^{-1}$
Sunspot Minimum		
Summer	0.4	13
Winter	0.8	45
Sunspot Maximum		
Summer	3.0	25
Winter	3.0	180

steady-state profile was obtained. Due to the small heat capacity of the nighttime electron gas, it takes less than 20 minutes of real time for the temperature profile, assumed initially to be equal to that of the neutral gases, to reach its final value. Since the typical time step used in the computation was one hundred seconds, the total of 12 steps allowed before the sun was "turned on" was more than ample.

One immediate conclusion is that for the models with no nighttime heat source the electron temperature must be lower than that of the neutrals as it was explained in section B of this Chapter. Geisler and Bowhill had arrived at this result previously. Fig. 6 compares the temperature profiles of neutrals and electrons for two different phases of the solar cycle, when no nocturnal heat source for the electrons is assumed. The temperature is, however, very sensitive to the presence of small nighttime sources.

To the knowledge of this author there exist no simultaneous measurements of neutral and electron temperatures at night, but published values of electron-to-ion temperature ratios are available and these appear to be always equal or larger than unity. (See Evans and Loewenthal [1964].) Since

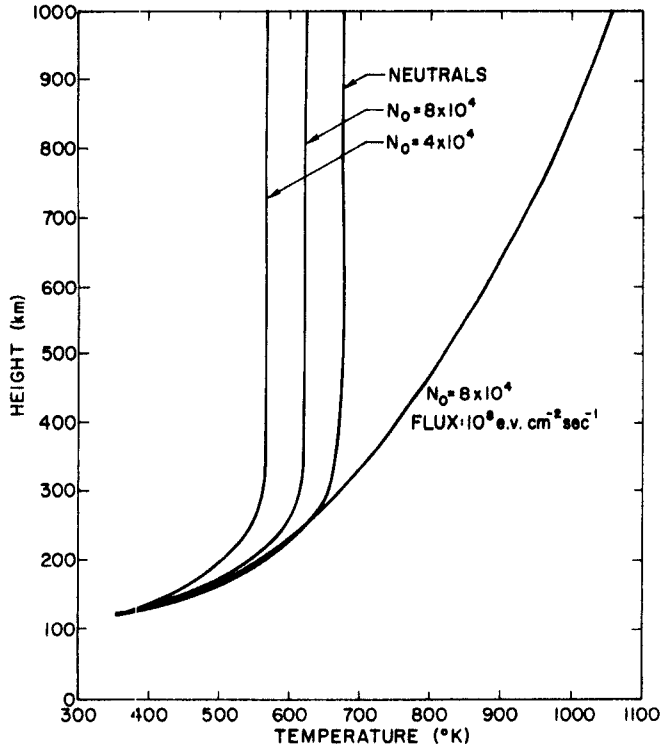

a. For solar cycle minimum conditions

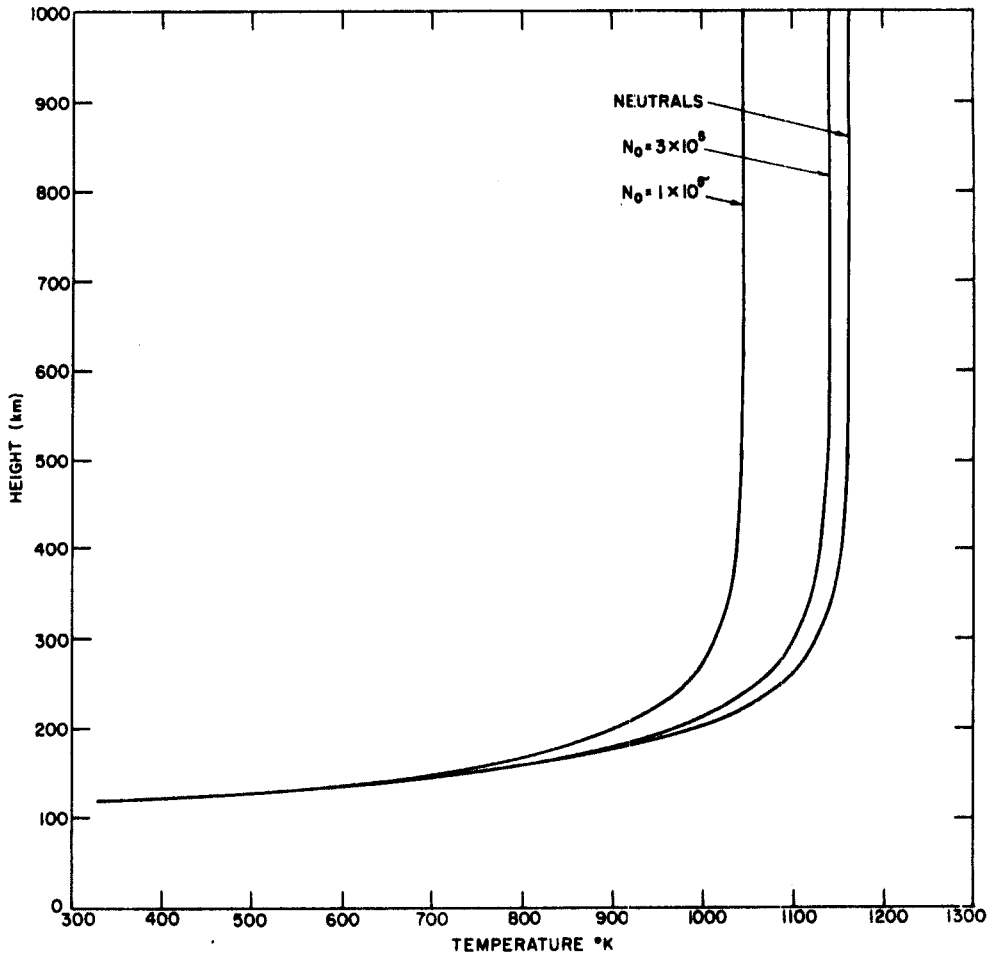

b. For solar cycle maximum conditions

FIG. 6. NIGHTTIME STEADY-STATE ELECTRON TEMPERATURE.

it would be difficult to imagine a situation in which electrons are colder than neutrals while ions are hotter, one must conclude that there is a nocturnal source of energy that selectively heats the electrons. Such selectivity seems to exclude the effect of hydromagnetic waves associated with geomagnetic disturbances. Electric fields cannot be ruled out as a cause of the phenomenon, but the most plausible explanation is the heating through downward conduction of the thermal energy stored in the protonosphere as suggested by Geisler and Bowhill. They estimated that, at midlatitudes, a downward flux of heat from the protonosphere of the order of 10^8 ev $cm^{-2}sec^{-1}$ can be maintained throughout the night. Such a heat flux will greatly alter the temperature profile as can be seen in Fig. 6a. It is interesting, however, to observe that at lower altitudes, as previously pointed out by Geisler and Bowhill, the electron temperature is slightly lower than that of the neutrals.

Before turning our attention to the early morning effects, it should be remembered that, just as it has, so far, been impossible to produce a comprehensive theory capable of predicting or explaining the detailed behavior of the electron concentration in the F-layer, so also one cannot, at this stage, hope to take into account all the complexly interrelated factors and produce a theory that goes beyond a first approximation of the time variation of the ionospheric thermal structure. Thus, the results presented here give but a very general picture of what happens to the electron temperature when the sun rises. The changes in temperature depend critically on the electron concentration, the distribution of which depends again on the temperature. In the present analysis part of this interaction is included: the scale height of the ionization is made dependent on the calculated temperature. The concentration at the peak of the layer is, however, made to vary in a prescribed manner instead

of allowing production, losses and diffusion to determine the whole profile. This latter course of action would be extremely difficult, and would involve many areas that are as yet insufficiently known.

Figure 7 shows the thermal history of the electron gas at different heights and for different combinations of initial peak concentration, concentration build up rate and solar cycle phase. It is immediately obvious from the inspection of these figures that frequently a peak in temperature is reached, sometime after sunrise but much before the production reaches its maximum. This peak is the result of the competing influence of increasing heat production and increasing heat capacity of the electron gas due to the growing concentration.

Experimental diurnal curves of electron temperature are not abundant, but those that are available tend to confirm the existence of this morning peak. See Figs. 8 through 11. These experimental curves are obtained either by incoherent back-scatter radar or by direct measurements by means of plasma probes mounted on satellites. The former technique is limited in the maximum height of observation by the power available and, in time resolution, by the long integration time necessary. It also depends on assumptions made regarding the ion composition of the atmosphere. Evans and Loewenthal [1964] and Evans [1965] present results from the Millstone Hill Radar Observatory in which the time resolution is 1 hour and the maximum height observed was 750 km. Carlson [1965] shows measurements made at the Arecibo Ionospheric Observatory with time resolution ranging from 15 to 60 minutes and maximum height of 450 km.

Diurnal electron temperature curves derived from satellite measurements are composite curves of many passes and from them it is difficult to eliminate seasonal effects as well as day-to-day variations. Measurements made at

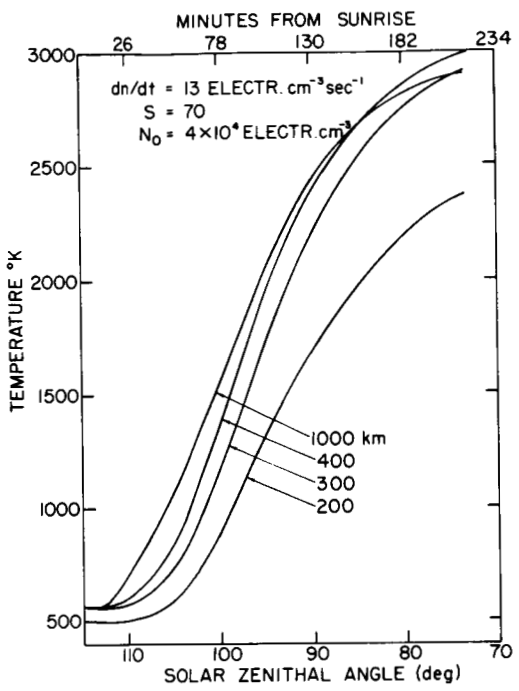

a. Summer, during solar cycle minimum

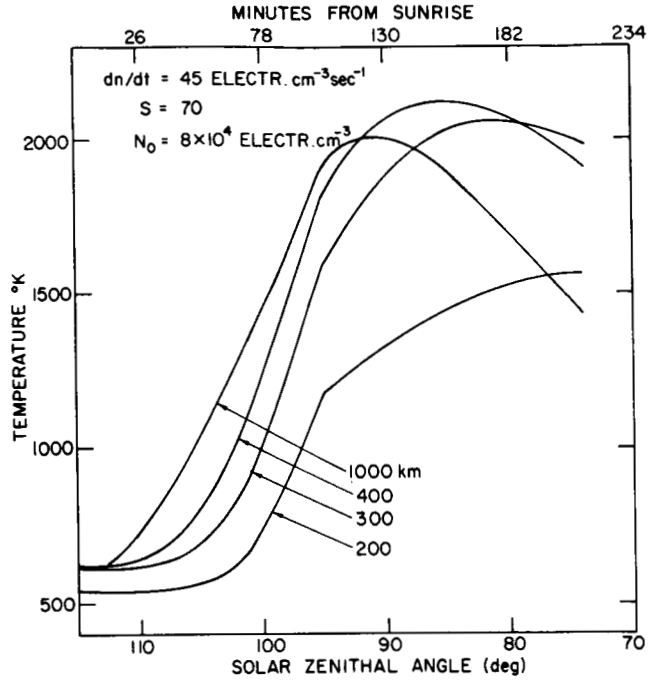

b. Winter, during solar cycle minimum

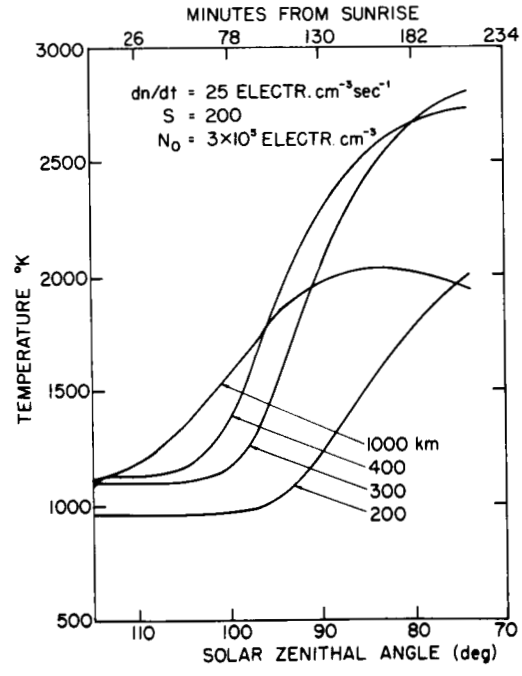

c. Summer, during solar cycle maximum

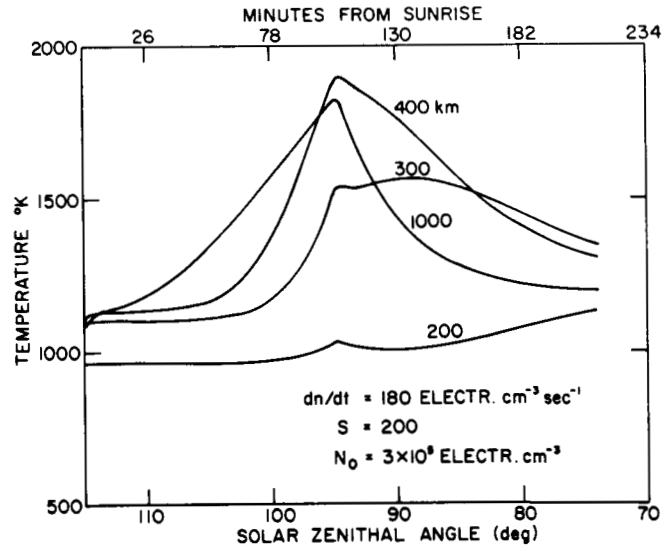

d. Winter, during solar cycle maximum

FIG. 7. THERMAL HISTORY OF THE ELECTRON GAS AT SUNRISE. (N_0 and dn/dt refer to the F2-peak.)

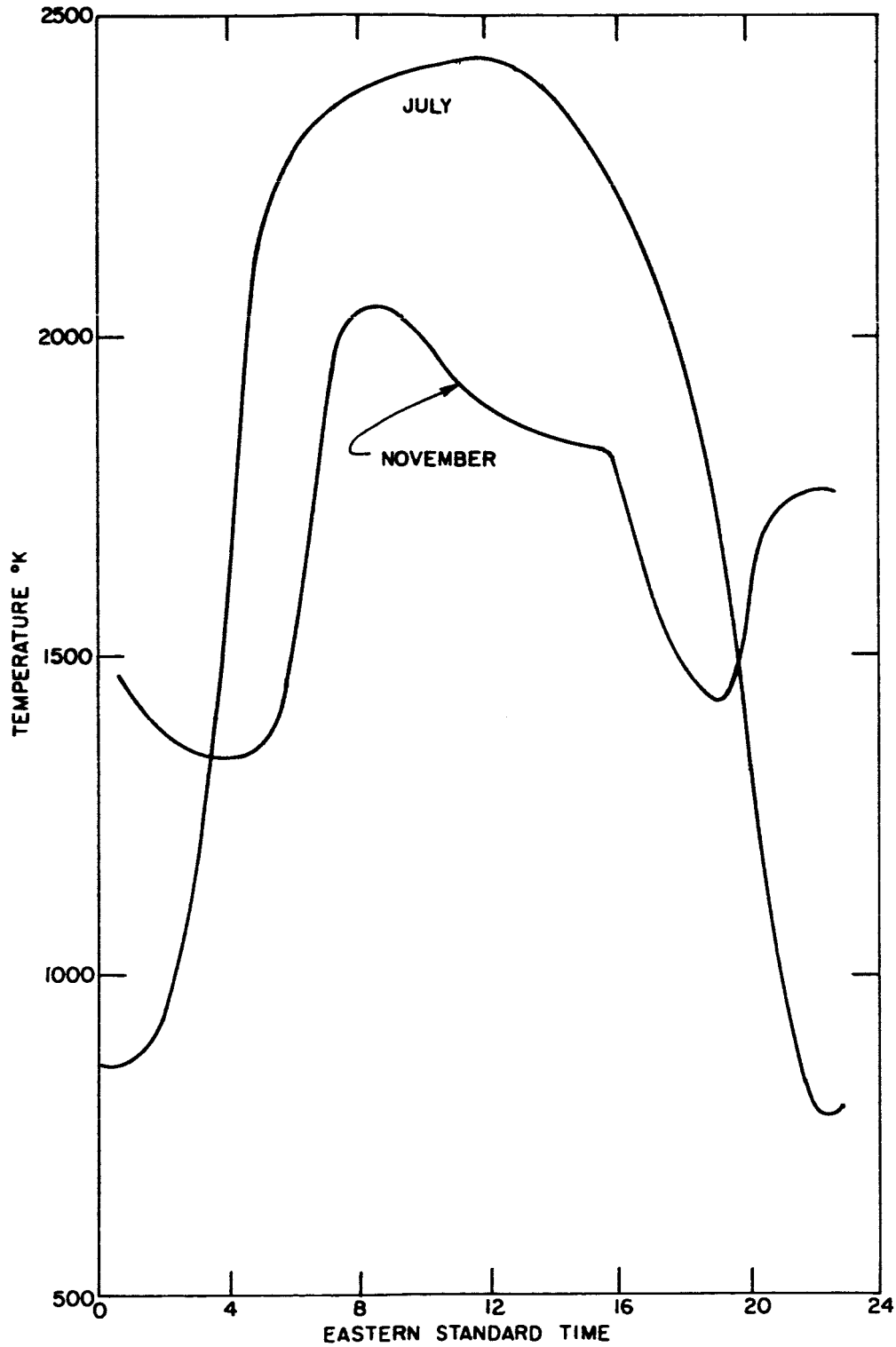

FIG. 8. BEHAVIOR OF THE ELECTRON TEMPERATURE AT 350 KM IN SUMMER AND IN WINTER OF 1963 OVER THE MILLSTONE RADAR OBSERVATORY. From Evans [1965].

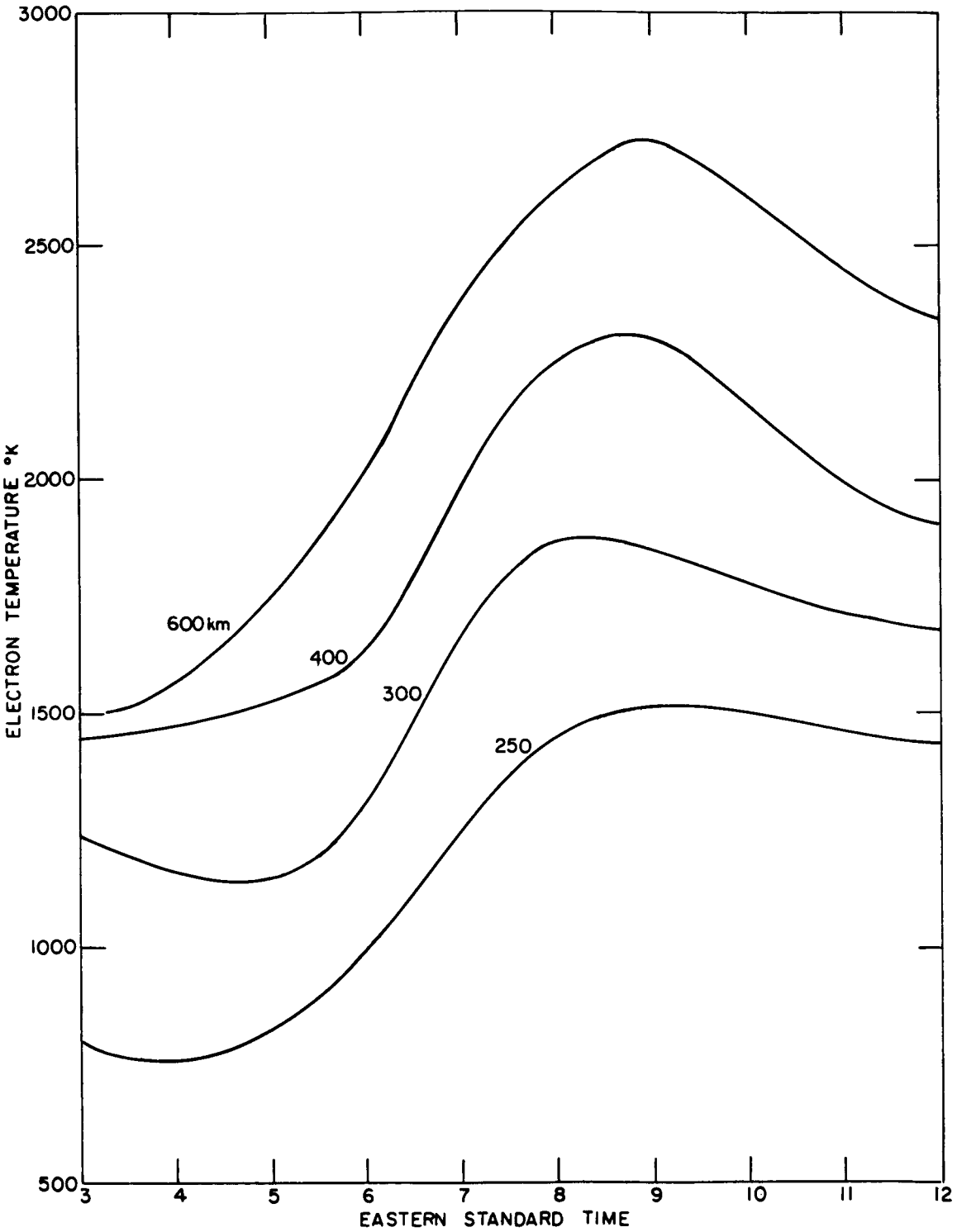

FIG. 9. AVERAGE ELECTRON TEMPERATURE DURING NOVEMBER 1963 OVER THE MILLSTONE RADAR OBSERVATORY. This figure was obtained by scaling the plot of isothermals presented in Fig. 6 of the article by Evans [1965] and is therefore of reduced accuracy.

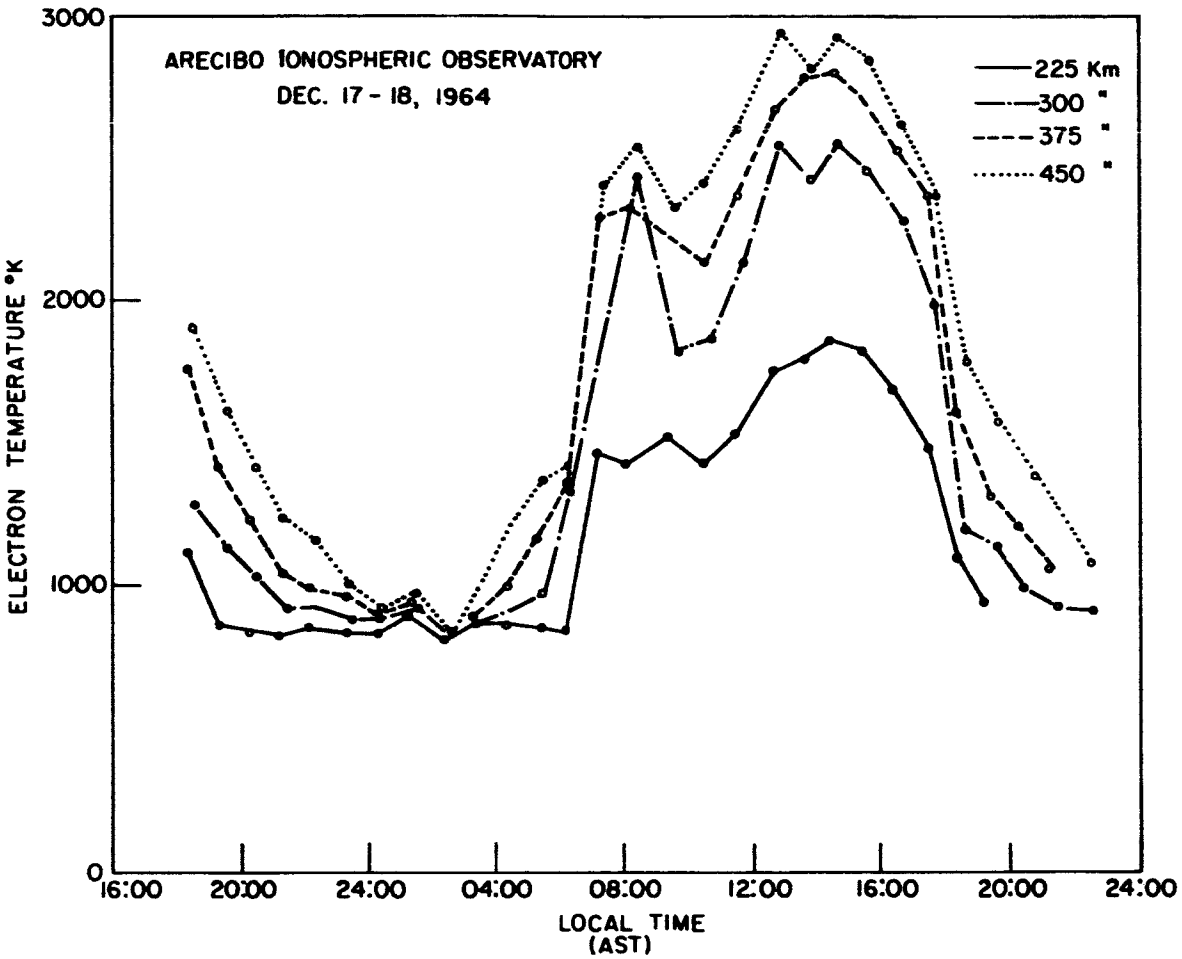

FIG. 10. ELECTRON TEMPERATURE ABOVE THE ARECIBO IONOSPHERIC OBSERVATORY ON 17-18 DECEMBER 1964. From Carlson [1965].

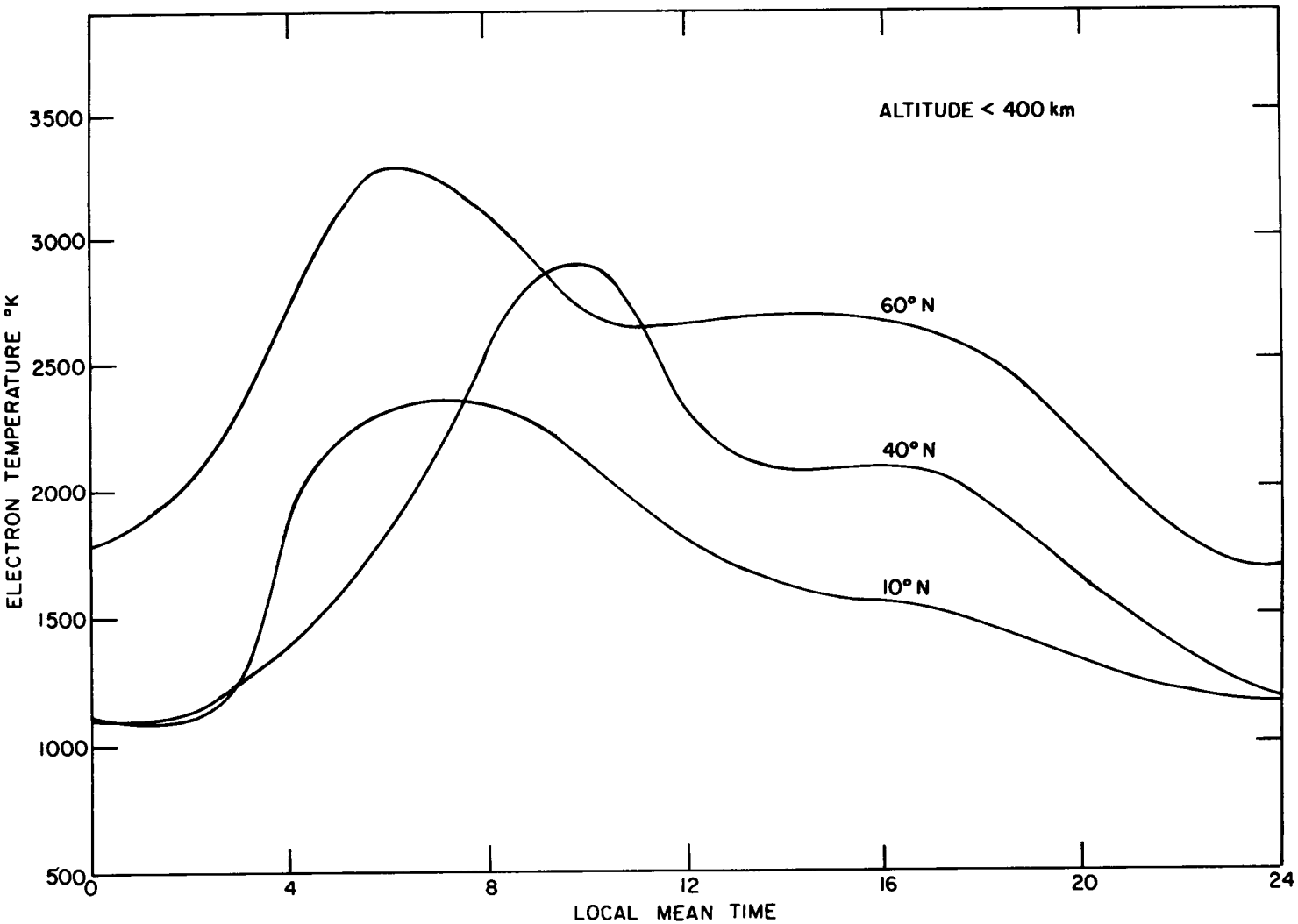

FIG. 11. AVERAGE ELECTRON TEMPERATURE AT THREE DIFFERENT LATITUDES OBTAINED FROM LANGMUIR PROBES MOUNTED ON EXPLORER XVII. From Spencer, et al [1964].

different heights and places are also apt to be mixed together. Spencer, et al [1964] present such curves which are reproduced in Fig. 11.

Since the peak owes its existence to the opposing effects of growing production and concentration, it is easy to understand why Fig. 7 shows that

a) The peak is more pronounced the higher the altitude observed because of the smaller heat production at these larger elevations. Figure 9 which was scaled from an isothermal map presented by Evans [1965] and Fig. 10 from Carlson [1965] confirm, at least partially, this conclusion for it can be seen that the peak is small at the lower altitudes. In the latter figure, the peak at the highest observed altitude (450 km) is not as pronounced as at 375 km. This is probably a real effect associated with causes that have not been included in the theoretical study. On this particular day the electron concentration itself showed a peak at around 0800 LMT so that the assumption of a linear increase of concentration with time, used in the theory, is violated.

b) The peak is more pronounced under conditions of low production (solar cycle minimum) or of high concentration build up rates (winter). There are no direct observations of electron temperatures other than in the solar minimum period of 1963 through 1965. Slab thickness measurements (ratio of total columnar content to F2-peak concentration) can be interpreted in terms of electron gas temperature (see for example, Bhonsle, da Rosa and Garriott [1965]) and the results confirm both the seasonal and solar cycle variations while the results displayed in Fig. 8 support the conclusions about the seasonal variations of the peak.

As expected, Fig. 7 shows that the temperature of the electron gas at high elevations starts rising much earlier than at the lower levels where the sun rays reach later in the morning. Carlson's results in Fig. 10 bear this out in

part, although the very early rise of temperature at 450 km is probably due to influx of hot electrons from the magnetic conjugate points as that author suggests.

Figure 12 shows a sequence of temperature profiles calculated for different solar zenithal angles.

Very early in the morning all the heating occurs at high altitudes where the sun is shining. Due to the low local electron concentration and the resulting small heat capacity, the temperature at these heights is raised considerably in spite of the fact that the total ionization of the atmosphere has changed very little. Figure 13 indicates the lowest height illuminated at a given solar zenithal angle and from it one can see that at $\chi = 110^{o}$ the levels above 400 km are in sun light, noticeable heating occurring there, and some heat being conducted to lower altitudes.

As the sun climbs higher, production grows and the production peak sinks to lower heights. The temperature rise may be very large in the summer, especially at the maximum of the solar activity cycle due to a combination of intense radiation and slow concentration build up. See Figs. 12a and 12c. During the winter the fast increase in the electron concentration prevents the temperature from reaching high values (Figs. 12b and 12d). As far as maximum temperatures are concerned, the seasonal effect dominates the solar cycle variations. For the models used, the higher heat capacity of the denser ionosphere at solar cycle maximum more than compensates the increased euv flux, resulting in lower temperatures than that of corresponding season during solar cycle minimum.

Irrespective of season or solar cycle phase, the temperature profile shows no appreciable "bulge" until the solar zenithal angle reaches a value of between 90 to 95 degrees. From there on a pronounced maximum appears in most cases as the heat released near 300 km is too much to be

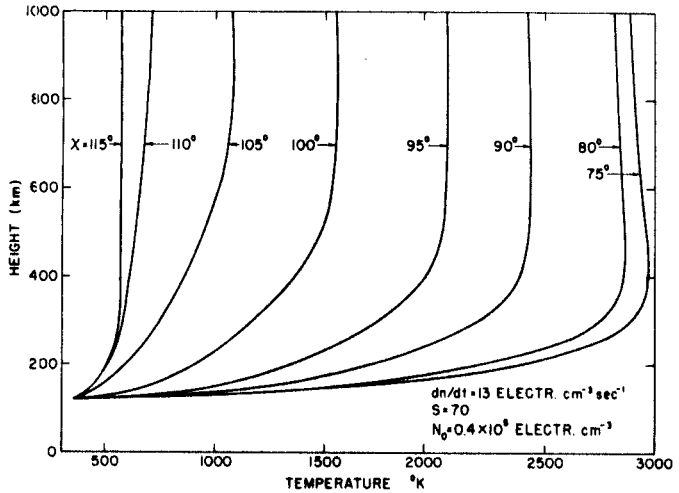

a. Summer, during solar cycle minimum.

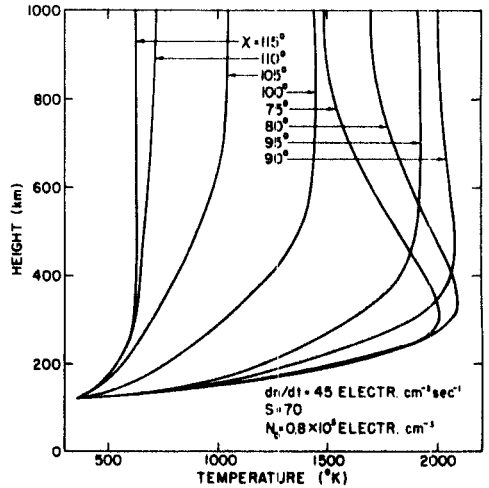

b. Winter, during solar cycle minimum.

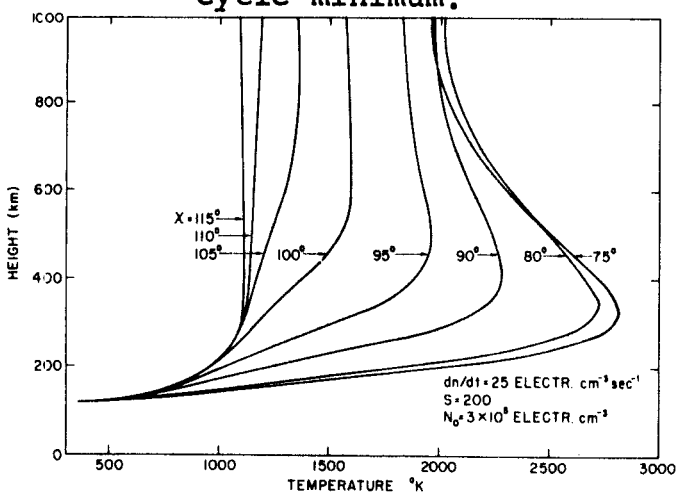

c. Summer, during solar cycle maximum.

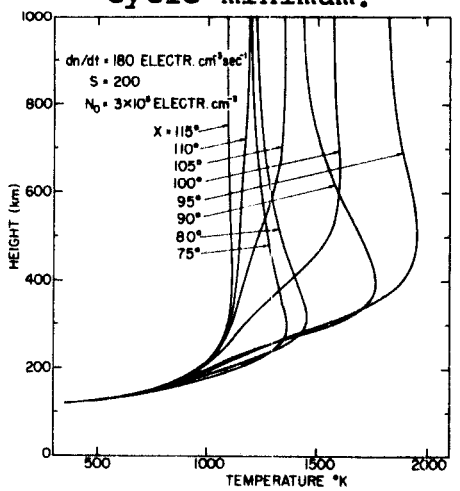

d. Winter, during solar cycle maximum.

FIG. 12. PROFILES OF ELECTRON TEMPERATURE AT VARIOUS TIMES AFTER SUNRISE. (N_0 and dn/dt refer to the F2-peak)

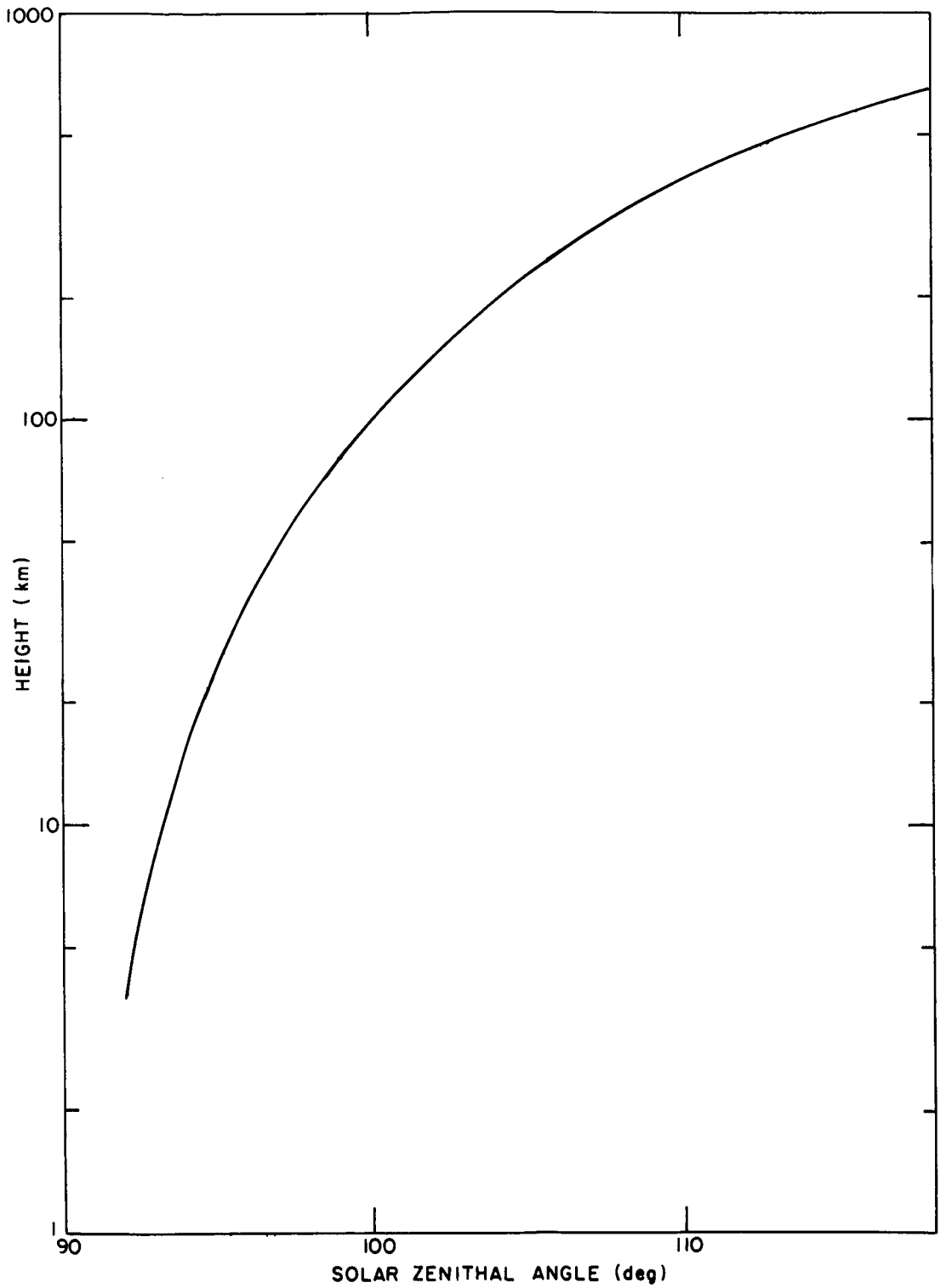

FIG. 13. LOWEST HEIGHT ILLUMINATED AT A GIVEN SOLAR ZENITHAL ANGLE.

disposed of locally or to be conducted downward. Another heat sink is necessary and it is the region above 300 km. Under these conditions substantial heat flows both up and down from the peak. In a more realistic model in which the constraint of zero slope for the temperature-vs-height curve at 1000 km is not imposed, part of this heat will flow into the protonosphere and be stored there for eventual release at night.

IV. IONOSPHERE AND EXOSPHERE OBSERVATIONS WITH THE EGO SATELLITE

A. FACTORS AFFECTING THE COLUMNAR CONTENT OF THE IONOSPHERE

The columnar content of the ionosphere, being in a large measure determined by the F-layer, reflects the well-known day-to-day variability of the latter. The large number of factors, ranging from the solar wind velocity to the tropospheric weather, that can be plausibly linked to changes in columnar content, interact in such a complex way as to render nearly impossible the establishment of a typical model for the detailed behavior of the ionized layers of the atmosphere. The best that one can hope to do is to describe and -- when possible -- explain the most frequently occuring "anomalies" in the diurnal changes of the ionosphere. "Anomalies" are here loosely defined as any deviation from the admittedly simplified picture of an electron content that is related in an uncomplicated way to the solar zenithal angle. (Clearly, under such definition, the existence of substantial ionization late at night is a profound anomaly.)

Although this work is concerned mainly with a description of the late night - early morning behavior of the columnar electron content, it is of interest to examine, in a general fashion, the various factors that may influence the F-layer.

The ionospheric structure is a result of the interplay of the production, loss and plasma transport processes. Since the electron concentration is much higher in the F-region than in any other region of the ionosphere, the columnar content of the ionosphere is principally determined by the F-region concentrations. In this region the principal production process is the photoionization of atomic oxygen by the available extreme ultraviolet radiation from the sun. The nitrogen molecule, that is also an abundant constituent, especial-

ly in the lower levels of the region under discussion, tends to contribute more towards the heat input than to the observable ionization, in part because of the rapid dissotiative recombination of N_2^+ with an electron and in part due to the relatively short lifetime of NO^+ (as compared with O^+) in the F-region. The NO^+ is the result of the reaction

$$N_2^+ + O \rightarrow NO^+ + N$$

that, according to Ferguson et al. [1965], is the most important of the several chemical reactions that eliminate the ionized nitrogen molecule from the ionosphere.

The amount of ionization depends not only on the energy flux received from the sun, but also on the ratio of molecular nitrogen to atomic oxygen in the atmosphere, a ratio that is a function of the turbopause height which, in turn, may depend on tropospheric weather.

The production of electrons by photoionization may thus be related to the -- so far -- highly unpredictable weather in the lower atmosphere and to the somewhat variable euv output from the sun. Bourdeau, Chandra and Neupert [1964] presented curves of the daily average value of the euv flux between 170 and 370 A measured from OSO data, corresponding to the period of March to May, 1962, inclusive. It can be seen that the flux varied between 0.35 and 0.59 ergs cm^{-2} sec^{-1} during this period. The good correlation found between euv flux and 10.7 cm flux values showed that the latter (which can be observed from the surface of earth in contrast with the former that must be measured outside the atmosphere) is a useful index of the euv radiation intensity. This is to be expected since both are coronal radiations and may respond in a similar way to changing conditions in that region of the sun.

Not too much is known about a possible additional source

of ionization in midlatitudes, such as the precipitation of high energy particles. This may be an important process in the auroral zone, but it is not clear what role it plays closer to the equator. At any rate, such a process would seem to be dependent on the conditions of the outer magnetosphere and the solar wind and would therefore only contribute to an even more erratic behavior of the ionosphere.

Just as the production processes cannot be relied upon to repeat themselves exactly from day to day, so also is the case of the losses of ionization which depend on the chemical composition of the atmosphere (hence on turbopause height) and, perhaps, on the temperature of the various constituents. Since the loss of ionization is a function of the concentration of the gas that causes the attachment or recombination of electrons and ions, and since this concentration is a strong function of height, it can be easily seen that any force that causes the ionization to move up or down can have a very strong influence on the loss rate. Gravity is an important downward force but it is certainly not time dependent. Diffusion being temperature dependent will have effects that vary from day to day. A third important force is the presence of an electrostatic field which could dramatically change the loss rate by lifting or lowering the layer. Such a field, be it produced by dynamo action or by some other process, could in all probability be quite different from one day to the next.

The temperature, besides being capable of influencing the various chemical reaction rates and altering the loss process as explained above, will have a marked effect in determining the vertical distribution of ionization especially in the regions of the ionosphere where diffusion is the dominant process. The main heating process is the absorption of euv radiation in the atmosphere, either through photodissociation below some 120 km or photoionization above that level. Given

the variability of the euv radiation from the sun, it is obvious that the temperature of the ionosphere cannot be expected to be the same every day. In addition there is another source of thermospheric heating. Snyder, Neugebauer and Rao [1963] have shown that a strong correlation exists between the solar wind velocity and the geomagnetic index, K_p. Jacchia and Slowey [1963, 1964] measured the neutral temperature increase associated with geomagnetic disturbances. Evans [1965], by means of incoherent backscatter experiments observed the heating of the ionospheric plasma during magnetically disturbed days. From all the above results, it is clear that the temperature of the ionosphere, and hence its columnar content, can be influenced by the solar wind velocity which can exhibit large variations from day to day as the sun rotates and the source of the plasma stream that is affecting the earth changes.

B. OBSERVATIONS OF THE EARLY MORNING IONOSPHERE

Fig. 14 displays columnar ionospheric contents during the late night and early morning, as a function of time, observed by the Doppler and the Faraday techniques using signals from the radio-beacons aboard EGO. The methods by which the raw data were reduced were described by da Rosa [1965]. The difference between the Doppler and the Faraday contents, dubbed "relative exospheric columnar content", plotted versus the solar zenithal angle, is shown in Fig. 15. It should be pointed out here that the absolute value of this difference is arbitrary and that, notwithstanding the expression "exospheric content", the quantity plotted may also be a measure of rearrangements in the lower ionosphere which do not affect the exosphere itself. This point will be discussed later. The contents were computed for each 1 minute interval and provide therefore excellent time resolution.

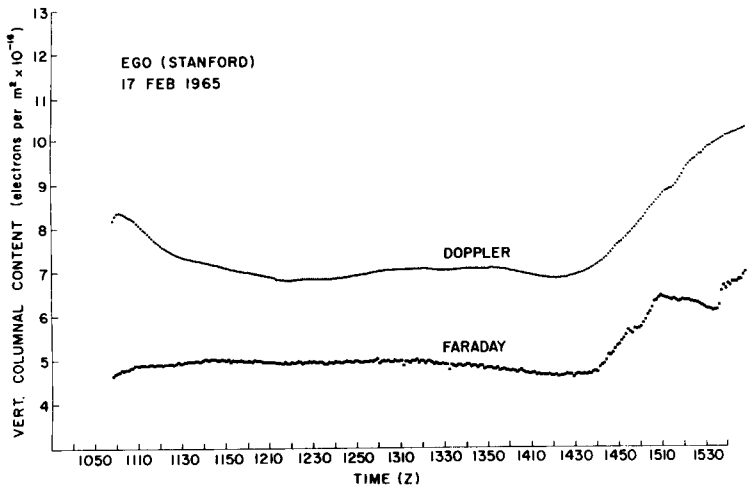
EGO (STANFORD)
17 FEB 1965
DOPPLER
FARADAY
VERT. COLUMNAL CONTENT (electrons per m² x 10⁻¹⁶)
TIME (Z)

(a)

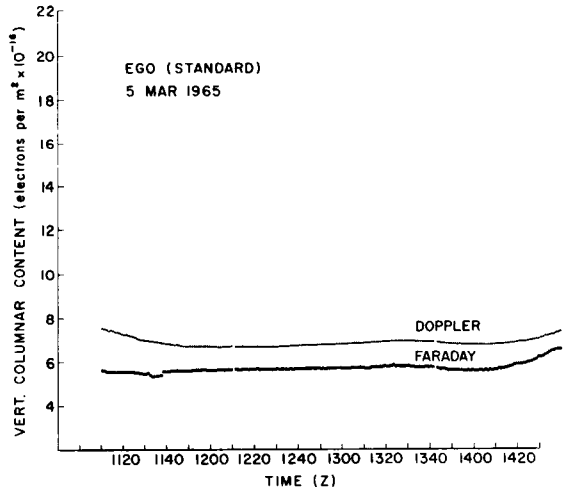
EGO (STANDARD)
5 MAR 1965
DOPPLER
FARADAY
VERT. COLUMNAR CONTENT (electrons per m² x 10⁻¹⁶)
TIME (Z)

(b)

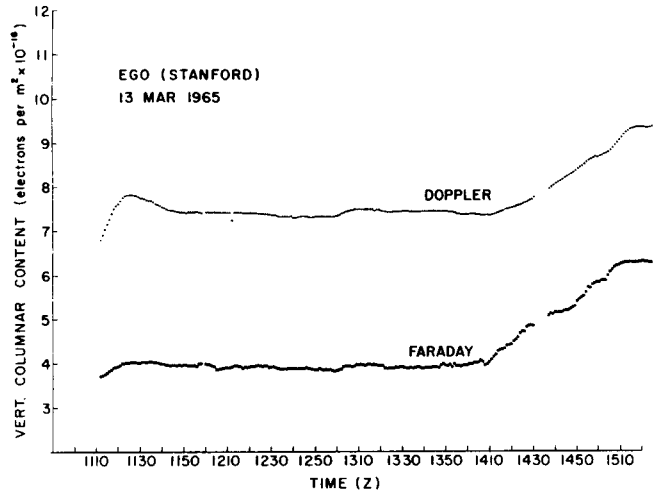
EGO (STANFORD)
13 MAR 1965
DOPPLER
FARADAY
VERT. COLUMNAR CONTENT (electrons per m² x 10⁻¹⁶)
TIME (Z)

(c)

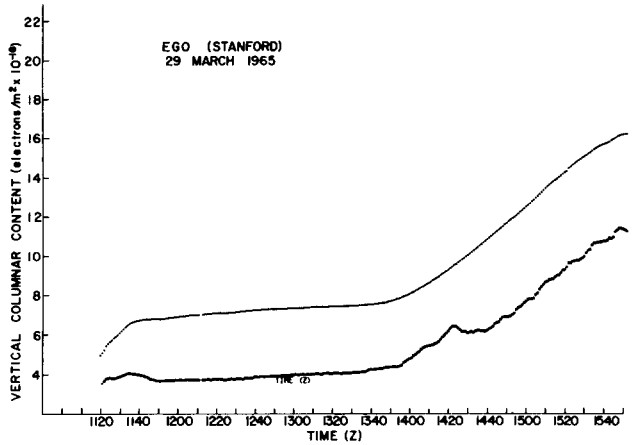
EGO (STANFORD)
29 MARCH 1965
VERTICAL COLUMNAR CONTENT (electrons/m² x 10⁻¹⁶)
TIME (Z)

(d)

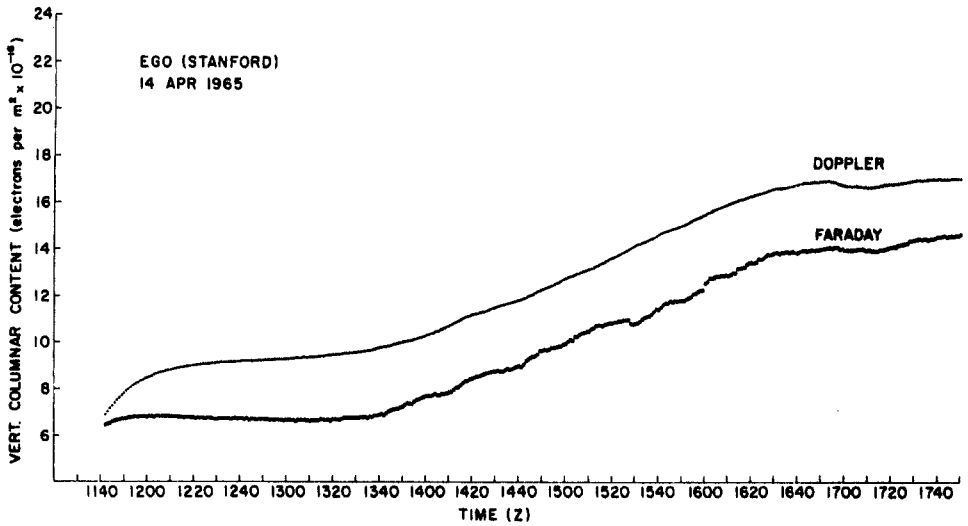

(e)

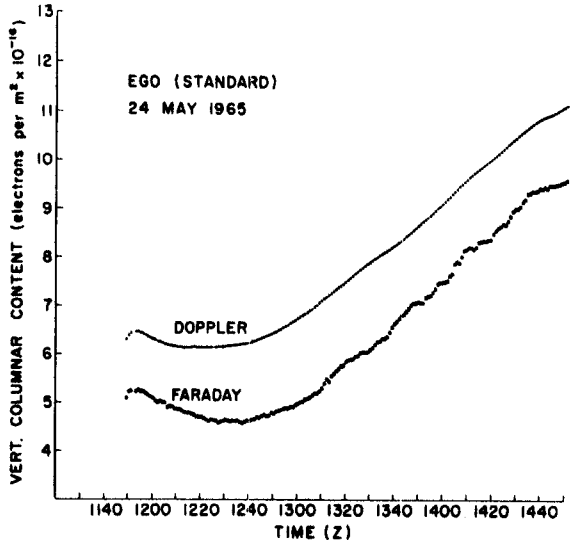

(f)

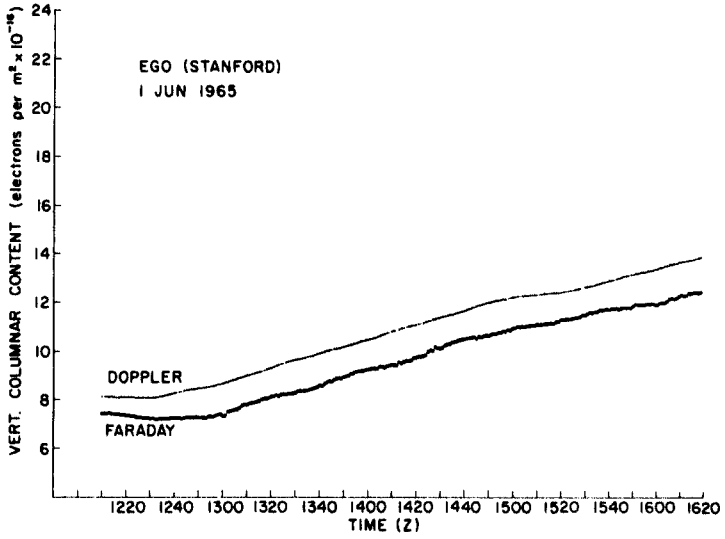

(g)

FIG. 14. THE COLUMNAR ELECTRON CONTENT DURING LATE NIGHT AND EARLY MORNING OBSERVED AT STANFORD USING THE DOPPLER AND THE FARADAY TECHNIQUES. The EGO radio beacon was used to obtain the data.

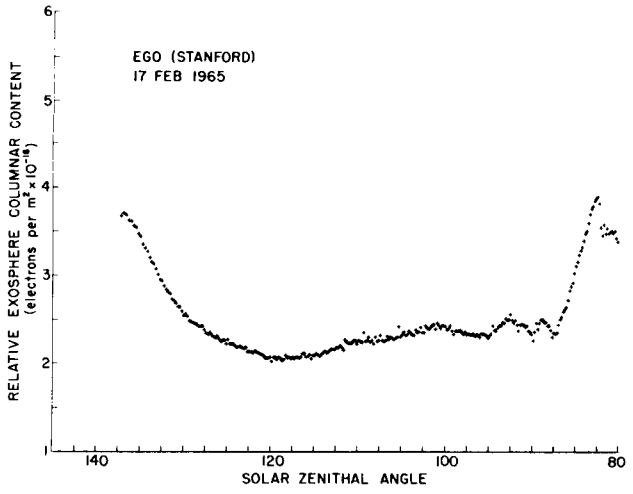
EGO (STANFORD)
17 FEB 1965
RELATIVE EXOSPHERE COLUMNAR CONTENT
(electrons per m² x 10⁻¹⁶)
SOLAR ZENITHAL ANGLE
140
120
100
80

(a)

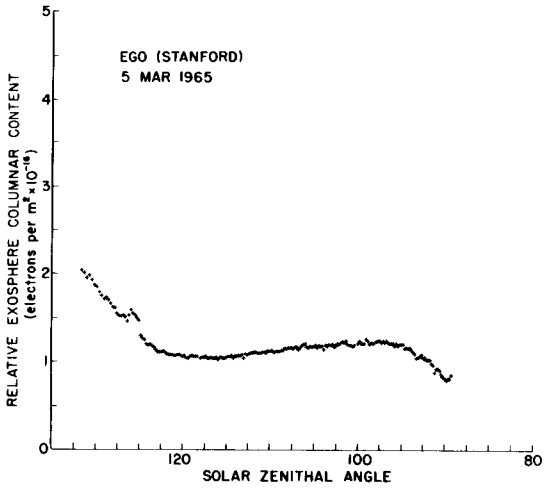
EGO (STANFORD)
5 MAR 1965
RELATIVE EXOSPHERE COLUMNAR CONTENT
(electrons per m² x 10⁻¹⁶)
SOLAR ZENITHAL ANGLE
120
100
80

(b)

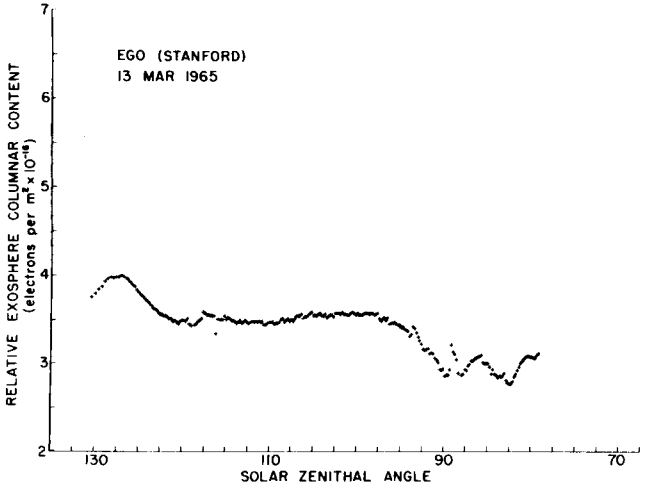
EGO (STANFORD)
13 MAR 1965
RELATIVE EXOSPHERE COLUMNAR CONTENT
(electrons per m² x 10⁻¹⁶)
SOLAR ZENITHAL ANGLE
130
110
90
70

(c)

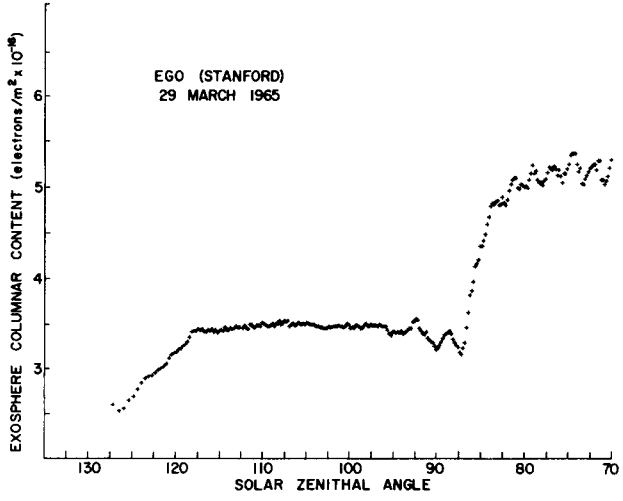
EGO (STANFORD)
29 MARCH 1965
EXOSPHERE COLUMNAR CONTENT (electrons/m² x 10⁻¹⁶)
SOLAR ZENITHAL ANGLE
130
120
110
100
90
80
70

(d)

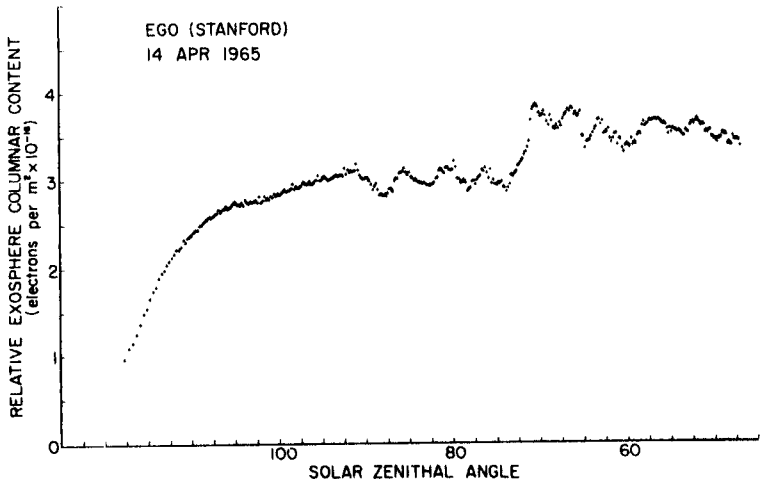

(e)

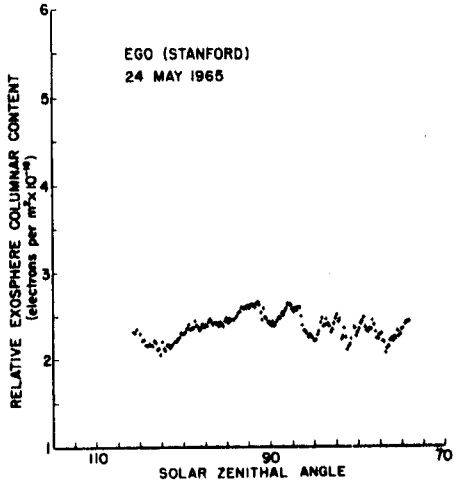

(f)

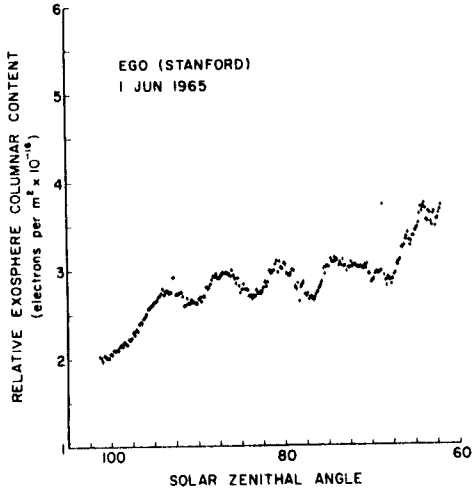

(g)

FIG. 15. THE DIFFERENCE BETWEEN THE COLUMNAR CONTENTS OBSERVED BY THE DOPPLER AND FARADAY TECHNIQUES IS CALLED HERE "RELATIVE EXOSPHERIC CONTENT," AND IS PLOTTED FOR THE RUNS DEPICTED IN FIG. 14.

The seven runs, the results of which appear in the figures above, constitute the sum total of the available dawn data at the time of this writing. The reasons for this scarcity are the relatively infrequent EGO passes (eight days between consecutive passes at the same local time) and the fact that early morning runs that, seen from Stanford, had sufficient elevation to be useful, occurred only during the period from beginning of January 1965 to the end of May 1965. In addition, the first six weeks of this time interval were lost owing to the intermittent power shortage that periodically beset the satellite when the solar paddles - sun angle becomes unfavorable. Of the 13 remaining possible passes, six were lost due to equipment difficulties or inability to track the satellite long enough to observe the sunrise. The 24 May and 1 June runs were made at small elevation angles (the last one at less than 25°), under less favorable conditions.

As a consequence of this small amount of data, it is impossible to generalize the observations and draw statistically valid conclusions. Nevertheless, one can, from the inspection of these data, note the occurrence of phenomena not previously reported and gain some insight into some of the complex machanisms that control the dawn ionosphere.

To be used as a reference, a "sunrise" can be arbitrarily defined as the solar zenithal angle corresponding to the time determined by the intersection of two straight lines, one being the extrapolation of the nighttime content and the other that of the linear part of the early morning build-up. Figure 16 shows, schematically, an idealized dawn content-vs-time curve, displaying the main features observed and showing the two sunrise times, one derived from the Doppler and the other from the Faraday results. These two times, which are recorded in Table 3, do not in general coincide due to the errors made in extending the lines,

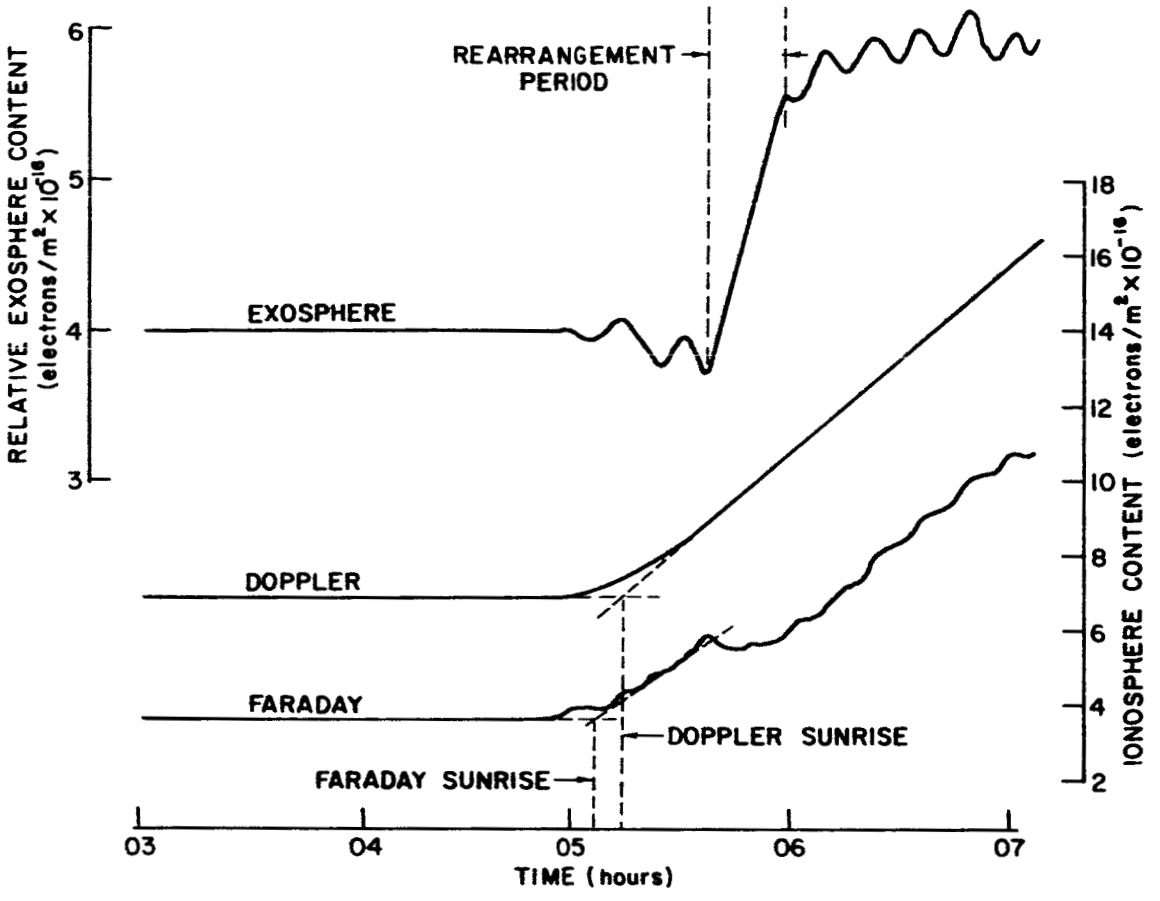

FIG. 16. IDEALIZED REPRESENTATION OF THE EXOSPHERIC AND IONOSPHERIC COLUMNAR-CONTENT CURVES PLOTTED VS TIME

especially on days when the plots are not smooth. The means are, however, close enough, indicating that these times really coincide as expected in view of the negligible production at levels high enough to affect the Doppler measurements substantially more than the ones from Faraday.

Although the nighttime value of the exospheric columnar content in Fig. 16 is represented by a steady, unchanging value, the number of actual measurements is insufficient to permit generalization of this behavior. On 29 March 1965 the content was constant throughout the latter part of the night; on the three earlier runs a small increase occurred

during the pre-dawn period. The three runs after 29 March started too close to sunrise to permit observation of the late night exosphere. For the moment, apparently strong changes in exosphere content that seem to take place near the beginning of each run, should be disregarded; in Section F an explanation of these changes will be given. When much more data is available, it may well turn out that the behavior of the pre-dawn exosphere content can be linked to that of the ionosphere, studied in Chapter V, and that there will be nights when the exosphere content decreases and others when it increases.

TABLE 3. SOLAR ZENITHAL ANGLE AT "SUNRISE"

DATE	SUNRISE SOLAR ZENITHAL ANGLE (deg)	
	DOPPLER	FARADAY
7 FEB	94.0	93.1
5 MAR	93.9	95.2
13 MAR	88.0	90.1
29 MAR	91.9	93.1
14 APR	90.3	93.0
24 MAY	95.5	93.8
1 JUN	96.4	95.0
MEAN	92.9	93.3

Figure 16 shows a feature common to all the experimental curves: at sunrise the exosphere content becomes irregular and oscillations in its value appear. These oscillations have periods of about 20 minutes and peak-to-peak amplitude of 0.3×10^{16} electrons m^{-2}. The 1 June run is an exception having both longer period and higher amplitude (47 minutes and 0.5×10^{16} electrons m^{-2}, respectively). These oscillations seem to be a real effect; efforts to find

periodic errors in the data reduction that could explain these fluctuations were unsuccessful. Examination of the ionospheric content curves of Fig. 14 shows that the Doppler curves are, in general, smooth compared with the Faraday ones which seem to be responsible for the exosphere fluctuations, indicating that their cause must be rearrangements of the lower ionosphere and, as such, might be detectable in ionosonde records. Unfortunately, the available ionograms were taken at 15-minute intervals and have, thus, inadequate time resolution.

The next feature of Fig. 16 in chronological order is, certainly, the most striking: a rapid increase in the exosphere content that occurs some time after sunrise indicating profound rearrangements in the shape of the layer. This increase is clearly seen in the runs depicted in Figs. 15a, 15d, and 15e and, perhaps, in 15g. The phenomenon may be a daily, regular occurrence and the reason that it was not seen on three of the seven runs may be due to the fact that these runs did not extend long enough into the morning.

Table 4 summarizes some of the characteristics of this rearrangement period.

It is clearly impossible to obtain reliable statistics based on only four samples and for this reason the two observations below are made with considerable reservations:

a) It can be seen that the time interval between sunrise ($\chi = 93^{o}$) and the inception of the rearrangement period is highly variable, ranging from half an hour to well over two hours. It seems that the longer delays are associated with smaller changes in the exosphere content.

b) The rate of content increase may be related to the value of predawn electron content in the ionosphere. Figure 17 indicates such a trend. It was shown in the previous chapter that the plasma temperature is very sensitive to the electron concentration; on the other hand the temperature

TABLE 4. CHARACTERISTICS OF THE REARRANGEMENT PERIOD.

Date	Beginning		Duration	Content Increase	Content Increase Rate	Predawn Faraday Content
	χ Deg.	Time from sunrise minutes	Minutes	Electron m^{-2} $x10^{-16}$	Electron cm^{-2} sec^{-1} $x10^{-8}$	Electr. m^{-2} $x10^{-16}$
17 FEB	87.8	28	30	1.52	8.5	3.70
5 MAR	<89.5	-	-	-	-	2.56
13 MAR	<79.2	-	-	-	-	2.61
29 MAR	87.3	30	17	1.58	15.5	2.75
14 APR	75.1	94	24	0.70	4.9	5.00
24 MAY	<74.2	-	-	-	-	3.78
1 JUN	67.8	156	27	0.92	5.7	4.26

may be one of the factors that influence the increase rate. It is, therefore, not unreasonable to expect correlation between this rate and the electron content.

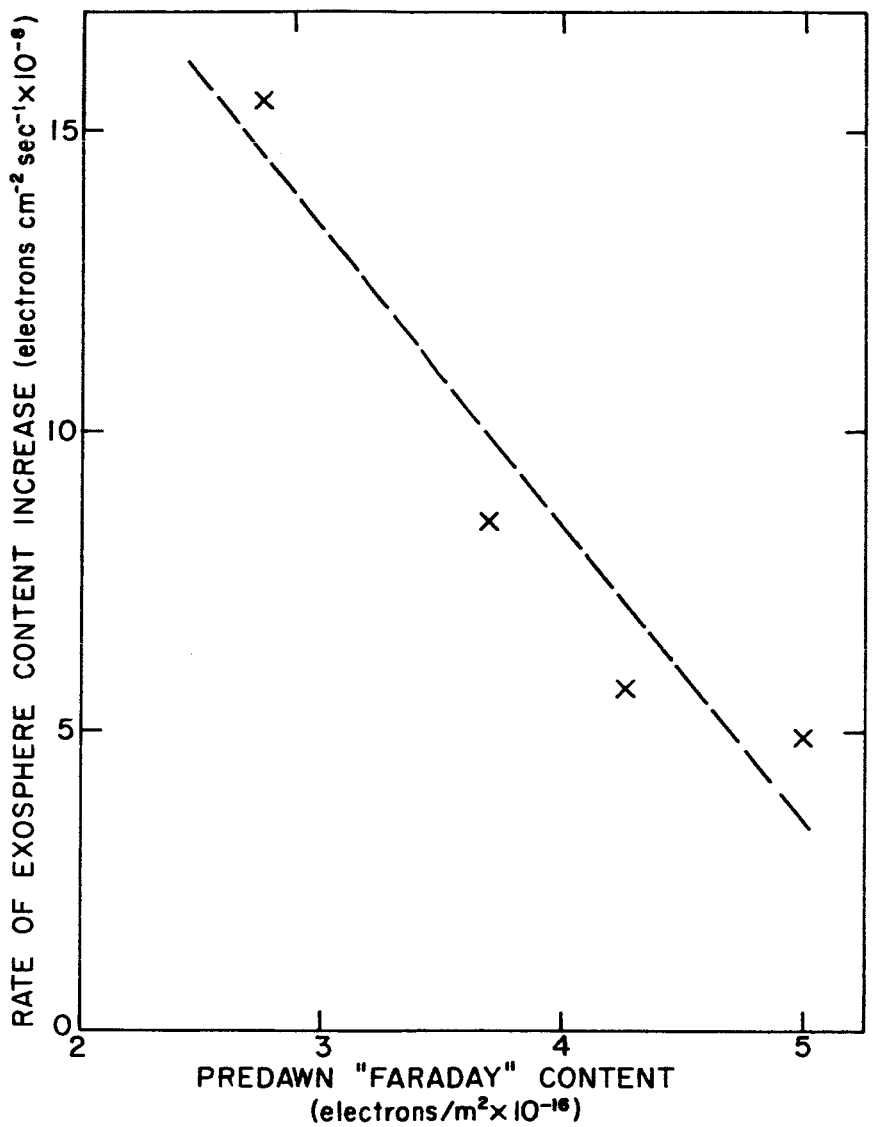

FIG. 17. SCATTER DIAGRAM SHOWING A POSSIBLE CORRELATION BETWEEN THE PREDAWN COLUMNAR CONTENT AND THE RATE OF EXOSPHERIC CONTENT INCREASE. The insufficient number of samples casts doubts about the validity of this correlation.

Referring to Fig. 14 it can be seen that during the rearrangement period there is no noticeable change in the smooth increase of the Doppler content and that all the perturbation observed in the exosphere content comes from the behavior of the Faraday curve.

In the post-rearrangement period the oscillations seem to persist with some evidence of damping in the 14 April case. Only two runs extend far enough into the morning hours to permit an examination of this period and, on one occasion, the mean value of the exosphere content continued growing slowly (Fig. 15d) while in the other (Fig. 15e) the value held steady.

C. POSSIBLE EXPLANATION OF SOME OF THE OBSERVATIONS

In Chapter III it was shown that substantial heating of the ionospheric electron gas can be expected at solar zenithal angles as high as 110 degrees. The observations described in the present chapter, on the other hand, indicate that detectable production of ionization will start at a zenithal angle of about 95° and the "sunrise" was defined as the moment when $\chi = 93^{\circ}$. Heating of the plasma precedes, therefore, the beginning of noticeable electron production by a considerable time. It is interesting to investigate the consequences of this situation.

If a very simple model were adopted in which the nighttime ionization had a Chapman-α distribution, the heating of the plasma would cause an increase in scale height and ionization would flow upward with a resulting reduction of the concentration at the F2-peak. At a certain height above this peak, one would find a level at which the concentration remained unchanged, i.e., an isopycnic level.

The above model is too simple to be realistic since the ionization at great heights departs markedly from the Chapman-α distribution. Nevertheless, the heating before production must cause considerable changes in the concentration profile.

Figure 18 displays the columnar contents of the ionosphere measured by the two techniques described and also shows the values of $N_{max}F2$ from ionograms obtained at Stanford. All data were taken on 17 February 1965. Since the satellite was seen at elevation angles of more than 70 degrees during

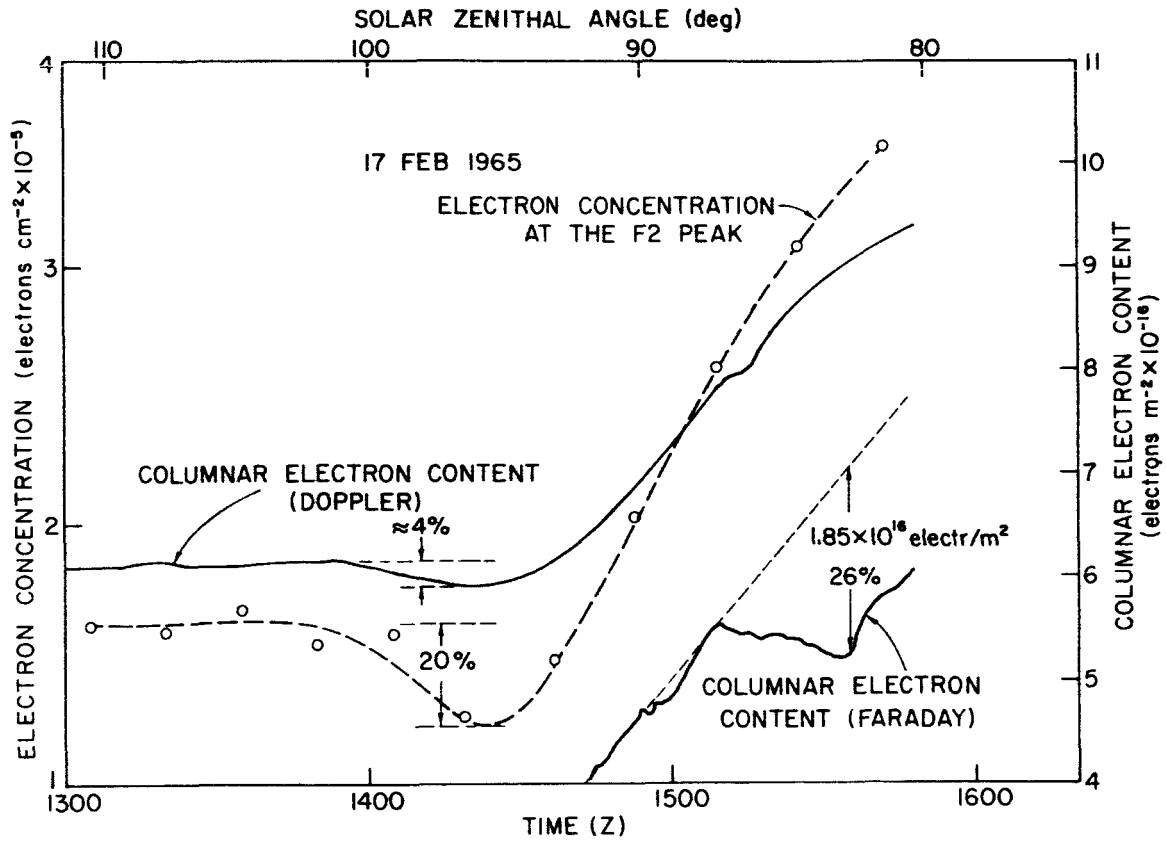

FIG. 18. DETAILED PLOT OF THE COLUMNAR-CONTENT AND THE F2-PEAK ELECTRON CONCENTRATION FOR THE DAWN OF 17 FEBRUARY 1965.

all of the time covered by the illustration, the distance between the location of the ionosonde and the subionospheric point of the EGO measurements never exceeded 200 km. All data were converted to the same local time. It can be seen from the figure that, when the solar zenithal angle was 95 degrees, the value of the F2-peak concentration was depressed by 20% compared with the nighttime level. The columnar

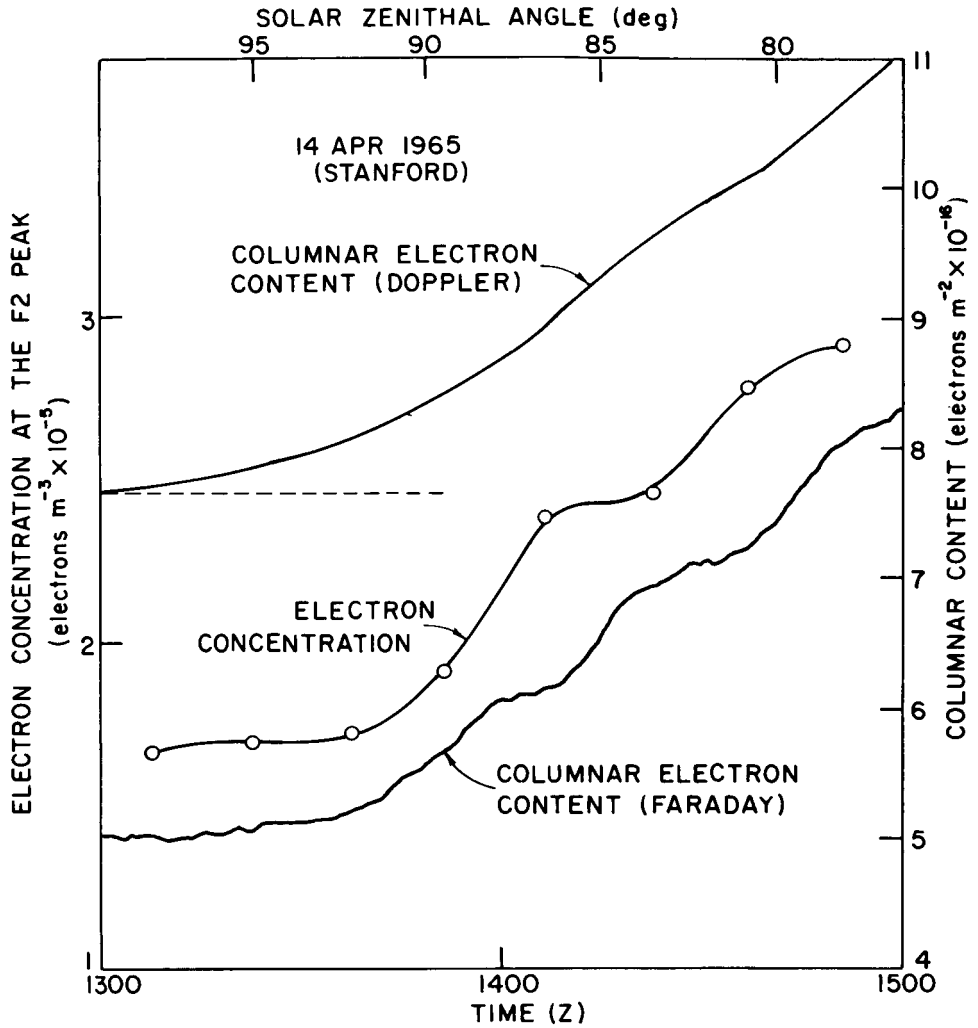

FIG. 19. DETAILED PLOT OF THE COLUMNAR-CONTENT AND THE F2-PEAK ELECTRON CONCENTRATION FOR THE DAWN OF 14 APRIL 1965.

content, on the other hand, showed only a small dip, indicating that the cause of decrease in the peak concentration was a reshaping of the layer and not an increase in losses. On the other days the predawn dip in the F2-peak concentration is absent and the mechanism described above does not seem to be applicable.

In Chapter III it was also shown that either a large solar euv flux, as found during high solar activity periods, or a small electron concentration, or both, will result in

high electron gas temperatures in the ionosphere. In particular, the numerical examples worked out indicate a great sensitivity of this temperature to the value of the concentration, so that in view of the well known day-to-day variation in the electron content of the ionosphere it is reasonable to expect a corresponding variation in plasma temperature. Rishbeth and Setty [1960] proposed as an explanation for the electron content changes the variability in the ratio of atomic oxygen to molecular nitrogen. Since both gases absorb ultraviolet but only the former is likely to generate observable ionization, it is clear that the electron content will depend on their ratio but the heat energy input will not. A positive feedback mechanism may exist which will tend to accentuate the high temperatures. If the n(O) to $n(N_2)$ ratio is smaller than the usual one, according to Rishbeth and Setty, the electron content will tend to be below the mean value for the occasion giving rise to higher plasma temperatures and consequently larger scale heights. The available ionization is now spread over a larger altitude range and smaller concentrations will result at the lower levels tending to raise even further the temperature there. This effect will be compounded if the loss coefficient has a positive temperature dependence so as to further diminish the concentration. Also, higher plasma temperatures will reduce the efficiency of the cooling of electrons by ions and again contribute to a temperature raise. These processes will eventually be limited by the increasing electron heat conductivity, which has a strong positive temperature dependence.

Doupnik and Nisbet [1965] have proposed as an explanation for the correlated fluctuations of electron temperature and concentrations in the daytime ionosphere observed by incoherent scatter measurements at Arecibo, a mechanism by which an increase of electron concentration near the F2-peak will

increase the cooling by ions causing, under certain circumstances, the heat output from the electron gas to exceed the input and resulting in a decrease in temperature which in turn, by reducing the scale heights, will bring the ionization to lower levels further increasing the heat loss and augmenting the losses of ionization through greater recombination. This process may be oscillatory, it is said. This author has made no quantitative test of this theory and has no information on whether Doupnik and Nisbet have done so. Since many factors have opposing influences on the behavior of the plasma, it is difficult to assess without a much more exhaustive evaluation, if the proposed scheme is realistic or not. It may even turn out that the explanation of the oscillation in the exosphere content is related to the scheme described above.

The explanation of the early morning rearrangement in ionization mentioned in Section B is, at present, very tentative and, probably, only after considerably more data has been acquired, can the theory be established on firmer basis. An inspection of Fig. 18 shows that the Faraday columnar content abandoned its relatively smooth growth at 1509Z, and actually began to decrease at that time while the Doppler curve was only very slightly affected. In Section E of this chapter it is argued that these changes in the Faraday content are too large to be accounted for by a mere vertical displacement of the profile; an actual change of shape of the layer, at relatively low levels, must take place without appreciably changing the smooth increase in the rate of the total columnar content. An exchange in ionization from the lower levels to the upper ones would have such an effect and would constitute an upward electron flux of considerable magnitude. It would, in fact, exceed the maximum possible steady-state flux from the ionosphere to the protonosphere, estimated by Hanson and Patterson [1964]. These authors have

found that upward fluxes larger than about 10^7 (electrons cm^{-2} sec^{-1}) cannot be maintained under steady-state conditions. The fluxes measured here have values, indicated in Table 4 under the heading "Content Increase Rate," and are one or two orders of magnitude larger than the Hanson and Patterson limit. They must be the result of a transient situation which might be brought about as follows:

As the sun begins to illuminate the ionosphere, the concentration of oxygen ions increases but there is little direct effect on the hydrogen ion population which originates almost exclusively from the charge exchange between oxygen ions and hydrogen atoms. Assume now that a mechanism exists that inhibits or delays this exchange for a while. The O^+ to H^+ ratio in the general area where both H^+ and O^+ exist in comparable amounts will exceed substantially the steady state value; the profile is "bottom heavy." If now the reaction is triggered or accelerated, the excess concentration of O^+ will be transformed into H^+ and diffuse rapidly upward. The sink for O^+ that is thus established will cause a flux of this species of particle to rush up modifying the shape of the profile by depleting the O^+ supply at higher altitude. The columnar electron content will not be altered but the Faraday measurements will show a decrease due to the migration of the ions to higher levels. The situation existing just prior and just after this rearrangement is depicted, schematically, in Fig. 20. Since the rearrangement is not instantaneous--it was observed to take around 20 minutes--the continuing production causes the columnar content to grow steadily during this time interval. This fact was omitted in the figure so as to facilitate the comparison of shapes.

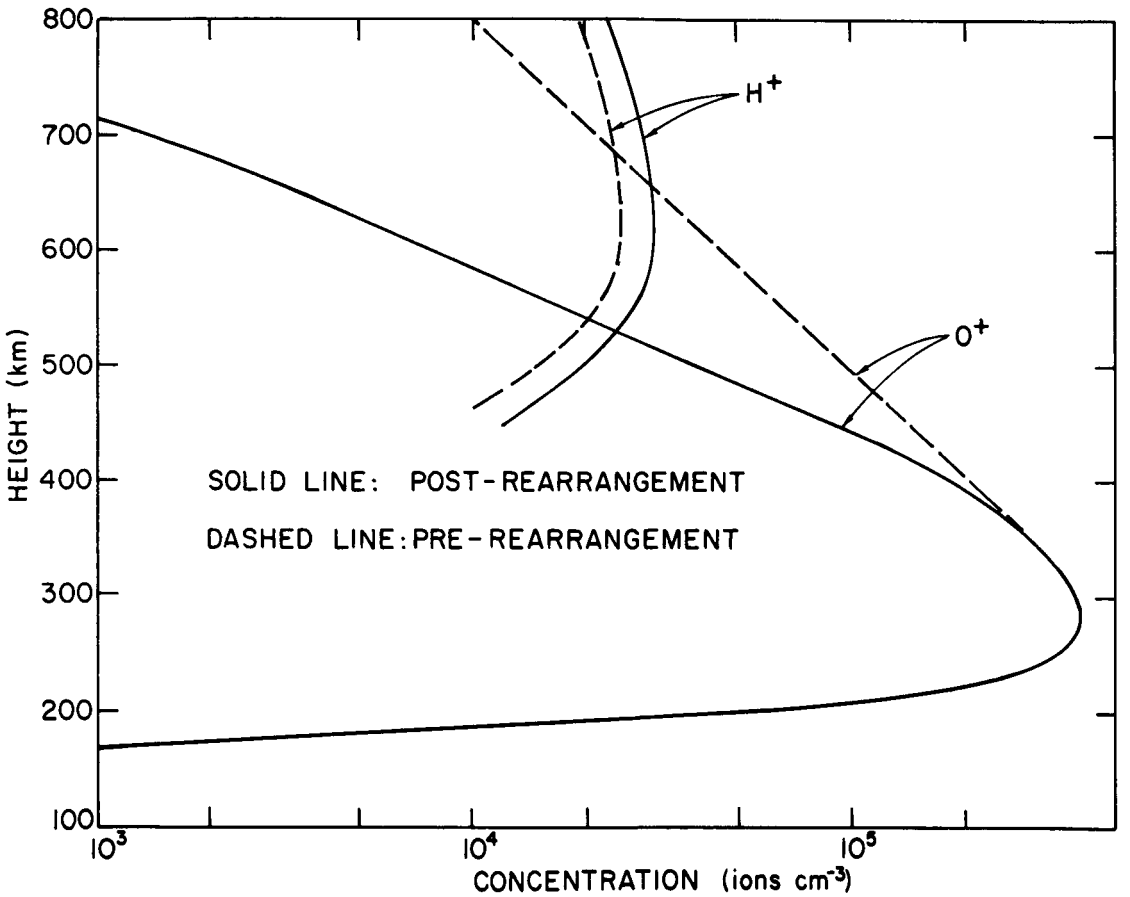

FIG. 20. SCHEMATIC REPRESENTATION OF THE SHAPES OF THE O^+ AND H^+ LAYERS JUST PRIOR AND JUST AFTER THE EARLY MORNING REARRANGEMENT OF IONIZATION.

D. DELAY IN THE OXYGEN ION TO HYDROGEN ATOM CHARGE EXCHANGE REACTION

In this section a suggestion is made as to one possible cause for a delay in the oxygen ion to hydrogen atom charge exchange reaction. The model developed is not realistic in that diffucion is disregarded; it is meant only as an indication that a delay mechanism must exist. A further contribution to a "triggering" of the reaction after a dormant interval would be a strong temperature dependence of the reaction rate coefficient.

At any point in the ionosphere the concentration of hydrogen ions must obey the continuity equation:

$$\frac{\partial}{\partial t} n(H^+) = P - L - \frac{\partial}{\partial z} \Phi_{H^+}$$

where P is the production, L is the loss term and Φ_{H^+} is the flux of H^+.

The assumption is made that $\frac{\partial}{\partial z} \Phi_{H^+} << P - L$, i.e., that we are examining a region where the chemical processes are dominant in determining the proton concentration.

The production of protons can be due to direct photoionization of hydrogen atoms or due to a charge exchange between these atoms and oxygen ions. The loss process for protons is the above chemical reaction in reverse -- radiative recombination is negligible. Photoionization of hydrogen will be disregarded. Attention will be focused on the reaction

$$H + O^+ \rightleftarrows H^+ + O$$

The continuity equation, under the stated assumptions, becomes

$$\frac{d}{dt}\, n(H^+) = K_1\, n(H)\, n(O^+) - K_2\, n(H^+)\, n(O)$$

or, by virtue of the fact that $K_2/K_1 = 8/9$

$$\frac{d}{dt}\, n(H^+) = K_1\, n(H)\, n(O^+) - \frac{8}{9}\, n(H^+)\, n(O) \qquad (1)$$

The steady-state solution of equation (1) leads to

$$n(H^+)_{ss} = \frac{9}{8}\, \frac{n(H)}{n(O)}\, n(O^+) \qquad (2)$$

If, at a given level, $n(O^+)$ is changing with time, but $n(H)$ and $n(O)$ are not, then equation (1) is of the form

$$\frac{d}{dt}\, n(H^+) = A\, f(t) - \frac{1}{\tau}\, n(H^+) \qquad (3)$$

where $A \equiv K_1\, n(H)$
$f(t) \equiv n(O^+)$
$\tau^{-1} \equiv \frac{8}{9}\, K_1\, n(O)$

Equation (3) is linear in $n(H^+)$ and can be integrated by using the integration factor $\exp(t/\tau)$

$$e^{\frac{t}{\tau}}\, d[n(H^+)] + \frac{e^{\frac{t}{\tau}}}{\tau}\, n(H^+)\, dt = d[n(H^+)\, e^{\frac{t}{\tau}}] = A\, f(t)\, e^{\frac{t}{\tau}}\, dt$$

whence

$$n(H^+) = A\, e^{-\frac{t}{\tau}} \int f(t)\, e^{\frac{t}{\tau}}\, dt + C\, e^{-\frac{t}{\tau}}$$

Assume now that the oxygen ion concentration, at a given level, is increasing linearly with time, as might well happen in the early post sunrise period. Then

$$f(t) = n(O^+) = n(O^+)_o + \alpha\, t$$

$$\alpha \equiv \frac{d}{dt}\, n(O^+) = \text{constant}$$

$$n(H^+) = A\, e^{-\frac{t}{\tau}} \int [n(O^+)_o + \alpha\, t]\, e^{\frac{t}{\tau}}\, dt + C\, e^{-\frac{t}{\tau}} =$$

$$= A\, \tau\, n(O^+)_o - A\, \tau^2 \alpha + A\, \alpha\, \tau\, t + C\, e^{-\frac{t}{\tau}}$$

Define $n(H^+)_{sso}$ as the steady-state proton concentration that would exist at $t = 0$.

$$n(H^+)_{sso} \equiv \frac{9}{8} \frac{n(H)}{n(O)}\, n(O^+)_o = A\, \tau\, n(O^+)_o$$

$$A\, \tau^2 \alpha = \frac{9}{8} \frac{n(H)}{n(O)} \times \frac{9}{8} \frac{\alpha}{K_1\, n(O)} = n(H^+)_{sso} \times \frac{9}{8} \frac{\alpha}{K_1\, n(O)\, n(O^+)_o}$$

Hence

$$n(H^+) = n(H^+)_{sso} \left[1 - \frac{9}{8} \frac{\alpha}{K_1\, n(O)\, n(O^+)_o} + \frac{\alpha\, t}{n(O^+)_o}\right] + C\, e^{-\frac{t}{\tau}}$$

When $t = 0$ then $n(H^+) \equiv n(H^+)_o$, hence

$$C = n(H^+)_o - n(H^+)_{sso} \left[1 - \frac{9}{8} \frac{\alpha}{K_1\, n(O)\, n(O^+)_o}\right]$$

so that

$$n(H^+) = n(H^+)_{sso} \left\{1 + \frac{\alpha\, t}{n(O^+)_o} - \frac{9}{8} \frac{\alpha}{K_1\, n(O)\, n(O^+)_o} + \right.$$

$$\left. + \left[\frac{n(H^+)_o}{n(H^+)_{sso}} - 1 + \frac{9}{8} \frac{\alpha}{K_1\, n(O)\, n(O^+)_o}\right] e^{-\frac{t}{\tau}}\right\} \qquad (4)$$

If chemical equilibrium conditions prevailed at t = 0

$$n(H^+)_o = n(H^+)_{sso}$$

and

$$n(H^+) = n(H^+)_o\left[1 + \frac{\alpha}{n(O+)_o}t - \frac{9}{8}\frac{\alpha}{K_1\, n(O)\, n(O+)_o}(1 - e^{-\frac{t}{\tau}})\right] \tag{5}$$

The rate at which the proton concentration builds up is

$$\frac{d(H^+)}{dt} = n(H^+)_o\left[\frac{\alpha}{n(O+)_o} - \frac{9}{8}\frac{\alpha}{\tau\, K_1\, n(O)\, n(O+)_o}e^{-\frac{t}{\tau}}\right] =$$

$$= \alpha\frac{n(H^+)_o}{n(O+)_o}(1 - e^{-\frac{t}{\tau}}) = \alpha\frac{9}{8}\frac{n(H)}{n(O)}(1 - e^{-\frac{t}{\tau}})$$

Thus the concentration increases slowly at the beginning; as time goes on, the rate approaches the value $\alpha\frac{9n(H)}{8n(O)}$ which is the rate of buildup that would exist if chemical equilibrium were maintained.

We next inquire what the proton concentration is, expressed as a fraction of the chemical equilibrium concentration.

Let $n(H^+)_{ss}$ be the chemical equilibrium concentration at any moment

$$n(H^+)_{ss} = n(H^+)_o\,(1 + \frac{\alpha}{n(O+)_o}t)$$

$$n(H^+) = n(H^+)_{ss} - \frac{9}{8}\frac{\alpha\, n(H^+)_o}{K_1 n(O)\, n(O+)}(1 - e^{-\frac{t}{\tau}})$$

$$\eta \equiv \frac{n(H^+)}{n(H^+)_{ss}} = 1 - \frac{9}{8}\frac{\alpha}{K_1 n(O)} \times \frac{1 - e^{-\frac{t}{\tau}}}{n(O+)_o + \alpha\, t}$$

For $t = 0$ and $t \to \infty$, $\eta = 1$, but for any time between these limits, $\eta < 1$ and the proton concentration may lag considerably behind its chemical equilibrium value.

As an example, consider the situation that would exist, under the assumptions of this problem at an altitude of 600 km in the ionosphere, during solar cycle minimum conditions, if the O^+ concentration were increasing at a rate of 12 ions $cm^{-3}sec^{-1}$ and no diffusion were present. (The rate indicated above would correspond to an increase rate of 45 ions cm^{-3} sec^{-1} at the F2 peak, in the winter model of ionosphere, used in Chapter III). In this example, using the neutral concentrations given by the Harris and Priester model for 0600 LMT and the value of K_1 (4×10^{-10} cm^3sec^{-1}) given by Hanson, Patterson and Degaonkar [1963], the time constant for the reaction comes out a surprisingly long 40000 seconds. At lower altitudes the concentration of atomic oxygen increases and a corresponding reduction in τ occurs. Thus under the above conditions the time constant becomes 3900 seconds at 500 km and 320 seconds at 400 km. Since the hydrogen ion production derives contributions from a large range of altitudes where O^+ and H exist in substantial amounts, the time constant for the integrated production depends in a complicated way on the time constant for each altitude. All that is intended by the examination of the model described here is an indication that a mechanism capable of considerably delaying the appearance of hydrogen ions may exist.

In Fig. 21 the H^+ concentration is plotted versus time for two cases: one is the hypothetical case of instantaneous reaction and is labelled "chemical equilibrium"; the other is the actual concentration which is seen to lag initially very much behind the steady-state value; as time goes on, however, the "transient concentration" builds up faster and faster until eventually it reaches the same rate as that of the instantaneous case.

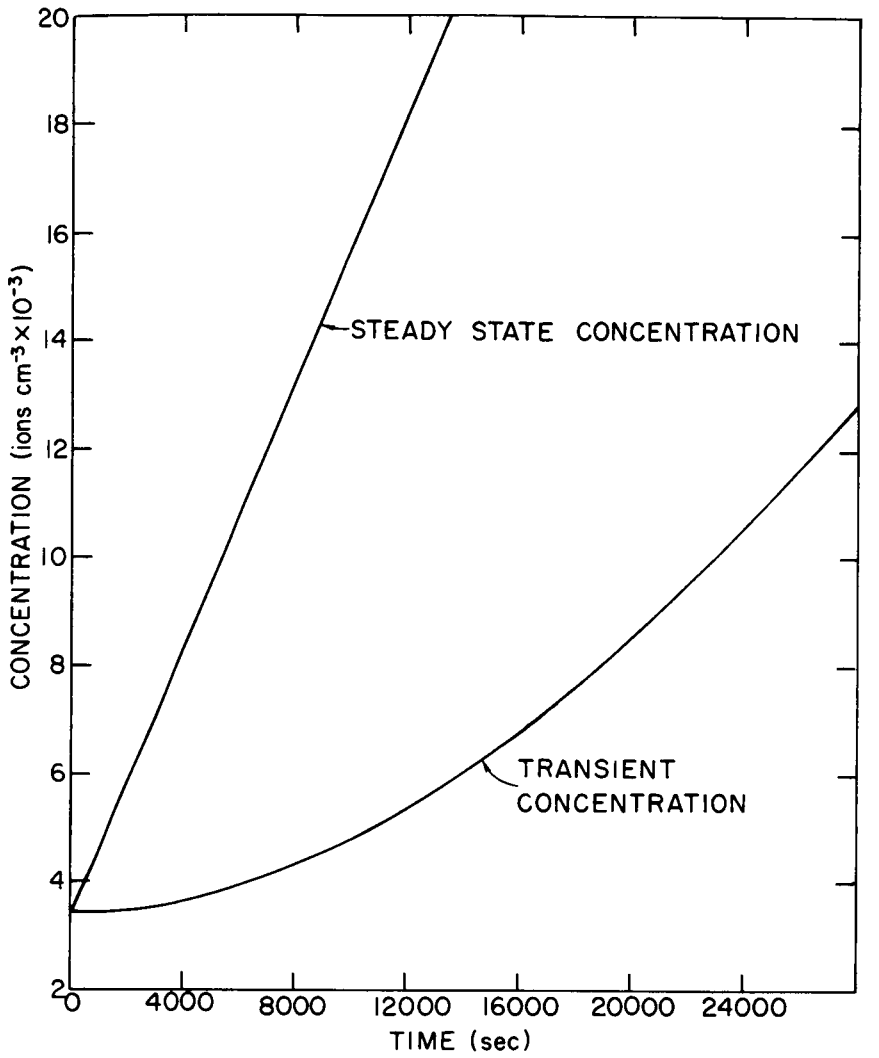

FIG. 21. HYDROGEN ION CONCENTRATION PLOTTED VERSUS TIME, RESULTING FROM THE CHARGE EXCHANGE BETWEEN O^+ AND H. The O^+ concentration is assumed to grow at the rate of 12 ions cm^{-3} sec^{-1}. Neutral concentration (atomic oxygen and hydrogen) is that that would exist at 600 km altitude during the solar cycle minimum at 6 hours LMT. The straight line is the concentration that would exist if the charge exchange reaction were instantaneous. Diffusion was disregarded.

As the hydrogen ion flux into the protonosphere results from the contribution of each height level, every one with a different time constant and it appears plausible that the full rate of flow will be established after a fairly appreciable time delay.

The physical reason for this somewhat unexpected behavior is that, due to the reversible character of the reaction, the rate of H^+ production can reach its full value only after the O^+ ion concentration has had time to establish an adequate excess of the value that would result in an equilibrium H^+ population.

E. DISCUSSION OF THE RELATIVE EXOSPHERIC COLUMNAR CONTENT

Sections B and C of this chapter dealt, in part, with the difference between the columnar contents derived from the Doppler and the Faraday measurements. In this section the significance of this difference, called "relative exospheric columnar content," is examined.

The differential Doppler beat frequency f_D is related directly to the time change of the slant columnar electron content

$$f_D = Q_D \frac{d}{dt} \int_0^R n \, ds \, ,$$

where Q_D is a constant that in the case of the EGO experiment is equal to 3.31×10^{-15} (mks),

n is the electron concentration,

ds is a length element along the ray path of length R.

If the value of the integral at $t = 0$ is known and is equal to I_{D_0} then the slant columnar content, I_D at any time t is

$$I_D \equiv \int_0^R n \, ds = \frac{1}{Q_D} \int_0^t f_D \, dt + I_{D_0}$$

Thus the Doppler data can, in a straight forward manner, be interpreted in terms of the total columnar content between satellite and observer.

In the Faraday rotation angle measurement, one has

$$\Omega = Q_F \int_0^R H\, n\, ds$$

where Ω is the angle of rotation between transmitter and receiver of the polarization plane of the wave, H is the component of the geomagnetic field intensity along the ray path, and Q_F is a constant.

Since Ω can be measured and Q_F is known, the value of the integral can be found and from it a value of columnar electron content, I_F, can be obtained through the relation

$$I_F \equiv \frac{1}{H_a} \int_0^R H\, n\, ds = \frac{\Omega}{Q_F H_a}$$

where the value of H_a is chosen in such a way that, if the satellite were at 1000 km or other preselected height, the columnar contents derived from Doppler and from Faraday would be the same, i.e., so that $I_F = I_D$. H is a variable that can be expressed in terms of the geocentric distance, r, to the point of integration on the ray path; since H_a is an "average" geomagnetic field, it is possible to associate it with a geocentric distance r_a and since $H \propto r^{-3}$ one obtains

$$I_F = r_a^3 \int_0^R \frac{n}{r^3}\, ds$$

The $1/r^3$ weighting factor causes the ionization at high altitudes to have only a small influence in the determination of I_F, hence, compared to the Doppler method, the Faraday method is rather insensitive to exospheric changes. Advantage is taken of this fact to observe the exospheric ionization by means of a satellite that is much higher than the altitude

at which $I_F = I_D$ because under such circumstances, $I_D > I_F$ and $I_E \equiv I_D - I_F$, where I_E is the "exospheric columnar electron content." To illustrate this point, consider a model consisting of a Chapman-α layer of O^+ ions topped by an H^+ layer in diffusive equilibrium. Let the temperature be uniform and equal to 1000 degrees K, the peak concentration be 5×10^{11} electrons m^{-3} at a height of 220 km and the O^+ to H^+ transition be at 1000 km. The vertical columnar content up to 1000 km is $I_D = 10.95 \times 10^{16}$ electrons m^{-2} and the Faraday rotation angle is 2920 degrees. An adequate choice of r_0 (about 6770 km or 400 km above sea level) results in $I_F = I_D$. If now, without altering r_0 one investigates what values of I_D and I_F would be obtained if the beacon transmitter were not at 1000 km but at 8000 km, one would find $I_D = 11.05 \times 10^{16}$ electrons m^{-2} and $I_F = 10.99 \times 10^{16}$ electrons m^{-2} resulting in an "exosphere content" of 0.06×10^{16} electrons m^{-2}, a very low value that reflects the meager ionization that exists in this model at high altitudes. If now, still keeping the value of r_0 unaltered we double the temperature above 1000 km then the values of I_D and I_F up to 8000 km become respectively 16.84×10^{16} and 13.28×10^{16} electrons m^{-2} showing a very much increased value of I_E, which now is equal to 3.56×10^{16} electrons m^{-2}.

The foregoing example illustrates the sensitivity of this method of observation of the changes in high altitude ionization. An <u>apparent</u> change in exospheric content will, however, result if the whole profile is shifted up or down vertically, changing the centroid of the distribution but altering very little the true content of the exosphere. Thus if a layer, without changing shape, moves to lower altitudes so that the centroid descends from 400 to 300 km, then if a corresponding change in r_a is not made, there will be an overestimate in I_F of

$$\frac{6370 + 400}{6370 + 300}^{3} = 1.043 \text{ or } 4.3\%$$

The dawn rearrangement described in Section B results from a decrease in Faraday content which, were it to be explained in terms of a simple vertical shift would require an upward motion of the ionosphere, a very unlikely event at this period of the day. In addition, the changes observed in the Faraday content are much too large to be due to any reasonable vertical motion. Referring to Fig. 18, one can see that on 17 February 1965 the Faraday content reached a minimum (at about 1540Z) which corresponds to a value 26% below that that would exist if the linear increase in content had continued without interruption. On 29 March the minimum was more than 50% below the corresponding extrapolated value. One must therefore conclude that the cause of the phenomenon observed is a major rearrangement in the shape of the layer.

F. ABOUT THE STRUCTURE OF THE EXOSPHERE

The observed changes in columnar electron content in the exosphere, as seen from EGO data, may be due to one of the following causes:

a. The radial motion of the satellite which results in in a varying amount of ionization being included in the ray path. From this effect local electron concentrations can be derived.

b. The "tangential" motion of the satellite, i.e., the motion perpendicular to the ray path, which reveals horizontal gradients in the exosphere.

c. Temporal changes in the exosphere.

Changes in the height of the ionization can result in apparent modifications in the exospheric content, as discussed in Section E. Fluctuations in the contents of the lower ionosphere should not cause any changes in the observed

exosphere content because of the cancellation that results from the subtraction of the Faraday from the Doppler values.

In Section B, temporal changes in the exosphere were examined and the implicit assumption was made that effects a and b were negligible. Justification for this lies in part in the small radial motion of the satellite when it is sufficiently far from perigee, coupled with the very small ion concentration that seems to exist beyond the plasmapause or "knee." For this reason, to examine temporal changes, advantage should be taken of those runs in which the sunrise occurs when the satellite is at considerable distance away from the earth. In particular, observations near apogee, which cannot be carried out with EGO in view of the reduced signal strength resulting from the unfavorable antenna orientation due to the spinning of the spacecraft, are valuable for this kind of investigation. The influence of effect b cannot be so simply dismissed; it may, however, be noted that during a substantial time interval in the outbound part of the run, the tangential velocity is very small resulting in a minimization of this effect, which, in any case, can cause only a slow change in the content and not the abrupt ones described.

In this section, parts of the runs near perigee will be examined and local electron concentration profiles will be derived. The assumptions here are that effects b and c are negligible. In fact, effect b is probably unimportant as long as the totality of the ray path remains inside the plasmapause. Once the satellite is beyond this boundary, the sharp concentration gradients may cause the apparent exosphere content to change and, to interpret the results, careful attention must be paid to the individual geometry of each run. Temporal changes--effect c--will, if present, alter the numerical values of exospheric concentration. When a much larger number of runs is available, it may be possible

to gain statistical support for disregarding this effect at some hours of the day. The results obtained here are arbitrarily based on the assumptions that there were no temporal changes and that, inside the plasmapause, there exist horizontal stratification.

Figures 15d, 15e, and 22 show runs in which conditions were favorable for local concentration measurements. A well defined rise in exosphere content can be seen at the beginning of each pass; a smooth curve was drawn by inspection through the points and the slope was read off at two-minute intervals. This slope was converted to local concentration and displayed in Fig. 23. The error bars indicate the uncertainty due to the spin-period error and the inaccuracy in the reference value of columnar electron content for the Faraday measurement. (See da Rosa [1965]). It was assumed that the spin period used was correct within 1 millisecond and that the reference value derived from the differential Faraday measurements was within 10% of the true value. Errors due to temporal changes and horizontal gradients as well as scaling errors were not included.

In two of the runs the effect of the knee can be seen. On 18 November 1964 the knee was at $L \cong 3.5$ while on 12 December 1964 it was further out, at $L \cong 5$. The geomagnetic index, K_p, was respectively 2- and 0 during the time of measurement and 1.4 and 0.5 when averaged over the previous 48 hours. Carpenter and Angerami [1965] have found that at higher K_p values the knee moves inward, as observed here. It is not clear why no pronounced knee was seen in the other two runs. A much larger number of days have to be examined before this point can be understood.

To date, the most reliable exosphere concentration measurements are those obtained from whistler observations. In order to compare the present result with the whistler data, it is convenient to convert the former to equatorial concentrations.

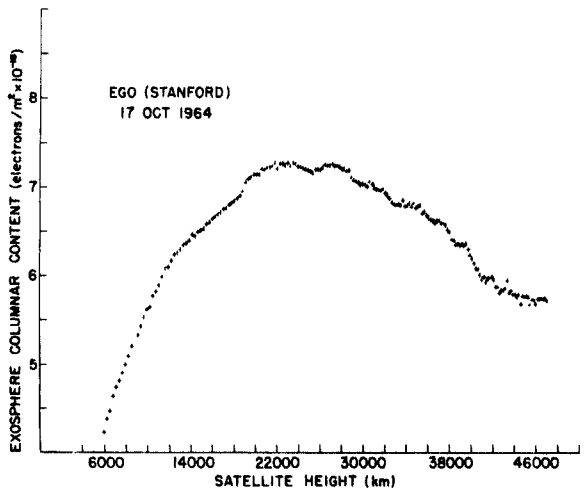

(a)

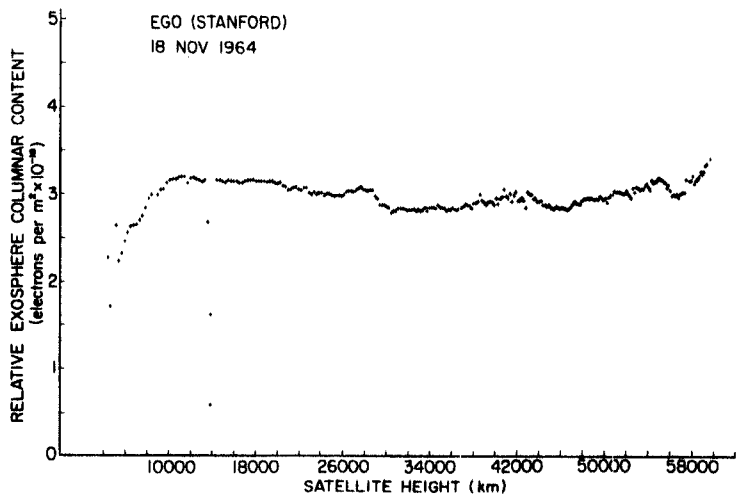

(b)

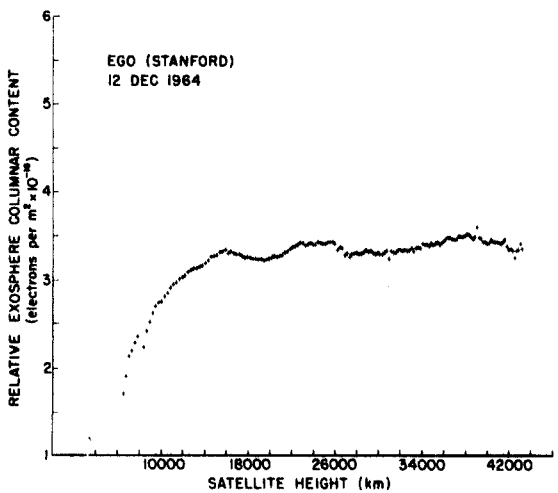

(c)

FIG. 22. THE RELATIVE EXOSPHERIC COLUMNAR CONTENT IS PLOTTED VS SATELLITE HEIGHT FOR THREE RUNS IN WHICH CONDITIONS WERE FAVORABLE FOR THE DETERMINATION OF LOCAL ELECTRON CONCENTRATION.

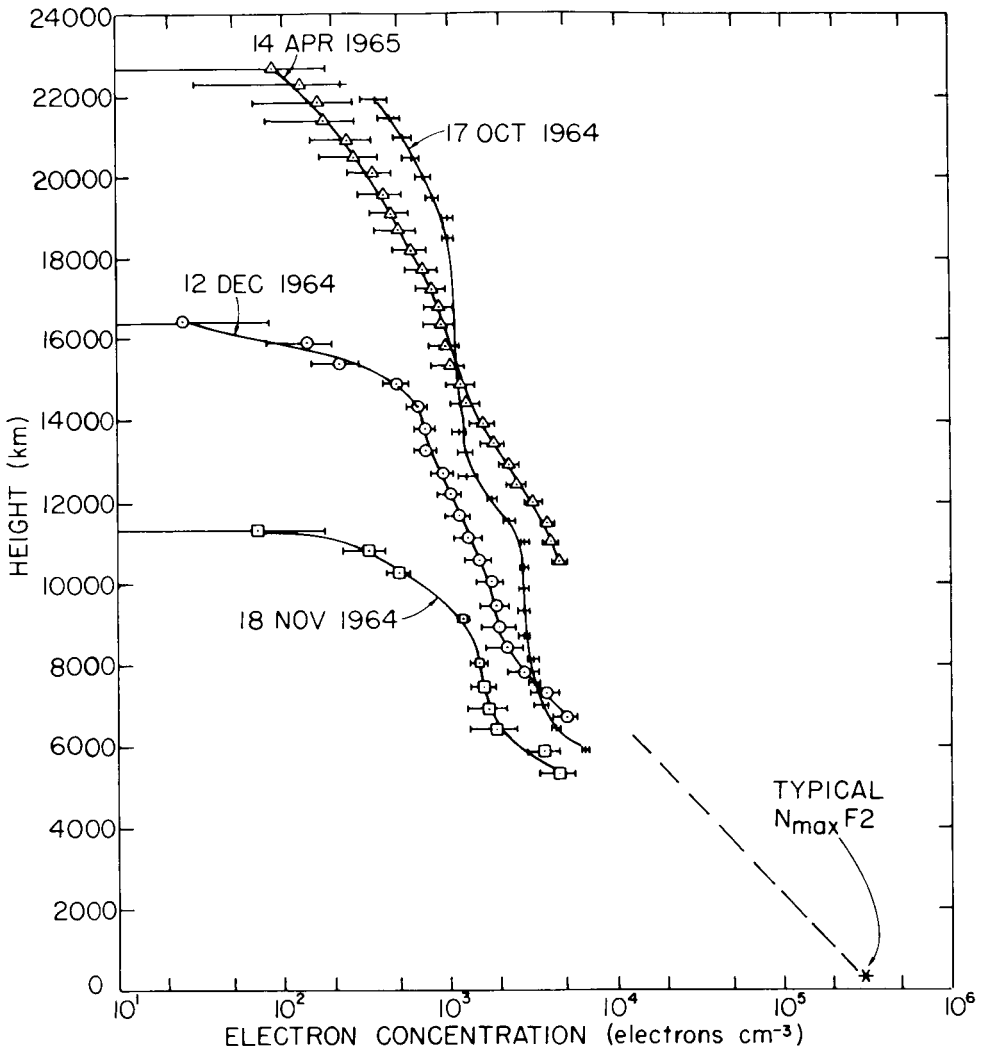

FIG. 23. PROFILES OF ELECTRON CONCENTRATION IN THE EXOSPHERE DERIVED FROM COLUMNAR-ELECTRON-CONTENT MEASUREMENTS: Error bars represent only the errors due to the spin period and reference level uncertainties. Scaling errors and the effect of horizontal gradients and temporal variations have not been taken into account.

This was done with the 12 December 1964 run and the results are plotted in Fig. 24. The conversion was made by assuming that hydrostatic equilibrium conditions prevailed and that the temperature of the H^+ and electron plasma was 1500 degrees K. The dashed line represents values obtained

by Angerami and Carpenter [1965] (6 June 1963, 0150 LMT). The EGO data seems to be higher by a factor of two. Since both EGO and whistler data were obtained under very quiet geomagnetic conditions, one cannot invoke differences in K_p to explain the difference. It should also be noted that the EGO results for 17 October 1964 and 14 April 1965 are even higher than the one shown in Fig. 24. The whistler data was for nighttime while the radio beacon result was for mid-day. This may account for some of the difference, although the one nighttime result for EGO showed high electron concentration. However, in view of the uncertainties involved in both the EGO and the whistler measurements, the agreement between these results may be considered satisfactory.

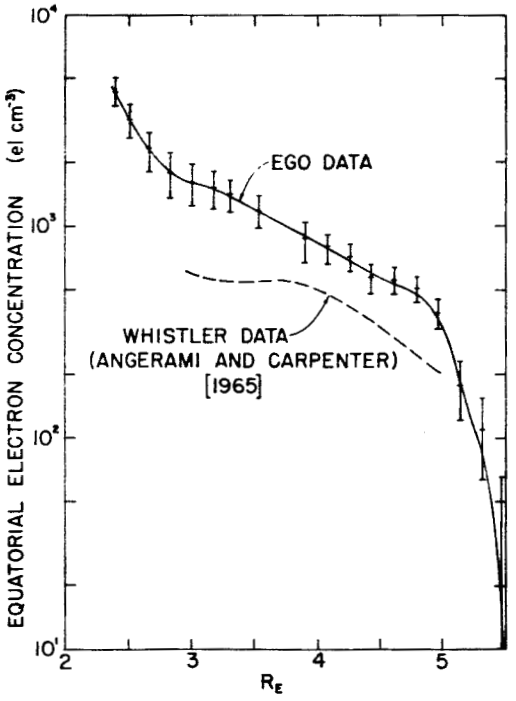

FIG. 24. COMPARISON BETWEEN THE EXOSPHERIC CONCENTRATIONS OBSERVED BY MEANS OF WHISTLER AND RADIO-BEACON TECHNIQUES.

As pointed out previously, the individual geometry of each pass must be taken into account when interpreting the EGO data. The reason for this is that different passes have different relationship with the volume of high electron

concentration within the plasmapause, partly due to the changes in dimensions of the latter and partly due to the variations in the geomagnetic position of the satellite, which are caused by the changes in longitude from pass to pass. Figure 25 shows how, for each successive pass in a sequence of runs at the same local time, the geomagnetic latitude decreases continuously. Thus, for the sequence of early morning runs in the beginning of 1965, the satellite initially (February) went out to almost 50 degrees N, geomagnetic latitude, while at the end of the sequence, in June, it barely reached 30 degrees.

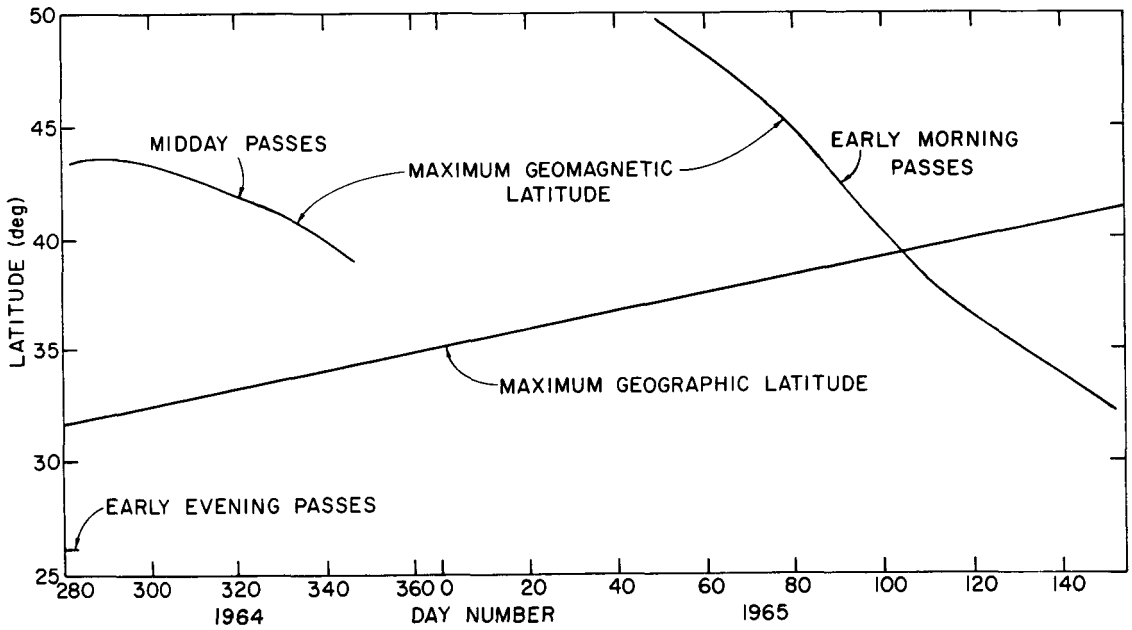

FIG. 25. THE HIGHEST GEOGRAPHIC LATITUDE ATTAINED BY EGO IN EACH PASS INCREASES AS TIME GOES ON. For each sequence of passes at the same time of day the highest geomagnetic latitude decreases continually as plotted above.

In Chapter II it was indicated that there is a secular increase in the inclination of the S-49 orbit, due probably to the strong lunar perturbation. For this reason the highest

geographic latitude attained in each pass increases as time goes on, as can be seen from the plot in Fig. 25. This results in a steady increase of geomagnetic latitude from sequence to sequence. Fig. 26 is a plot of the geomagnetic latitude of the satellite versus radial distance. It may aid in the visualization of what happens but one must remember

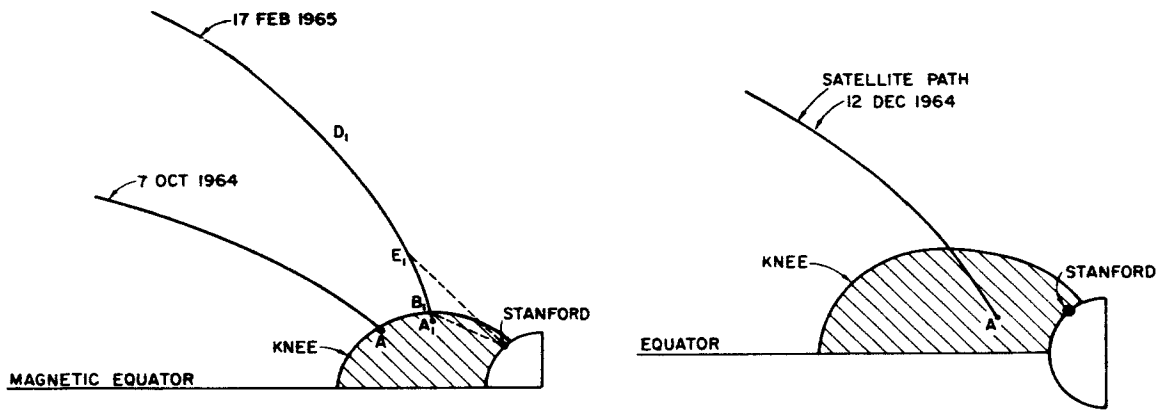

FIG. 26. PLOTS OF ALTITUDE-VS-GEOMAGNETIC LATITUDE ALONG THE PATH OF EGO. The hatched area represents a section through the high electron concentration volume bounded by the plasmapause.

that the situation is more complicated than indicated in the figure due to the three dimensional nature of the problem. The hatched area represents a section through the volume inside the plasmapause outside which the electron concentration is very small. The plasmapause was considered to be at $L = 3.5$. The 17 February, 1965 run started at point A_1 (Fig. 26a) and the ray path from Stanford was entirely inside the plasmapause. As the satellite moved from A_1 to B_1, the columnar content increased as indicated by the first two points in Fig. 15a; from there on, in spite of the fact that the distance from ground station to spacecraft increased steadily, the columnar content decreased because the tangential motion caused the ray path to intercept less and less of the high concentration volume inside the knee. As the satellite

reached the neighborhood of point D_1, some 30,000 km out, the tangential velocity became so small that the sharp gradient of electron concentration at the knee had no longer any effect on the changes of electron content. On later runs, as the path of the spacecraft came to lower latitudes, this effect became progressively less important until it no longer showed up. This can be seen in the sequence of figures from 15a through 15e where the decay of content in the beginning of the run gets smaller the later in the year the data were taken. In Fig. 15h and 15g the sunrise effect started too early in the run so that the different phenomena were mixed together.

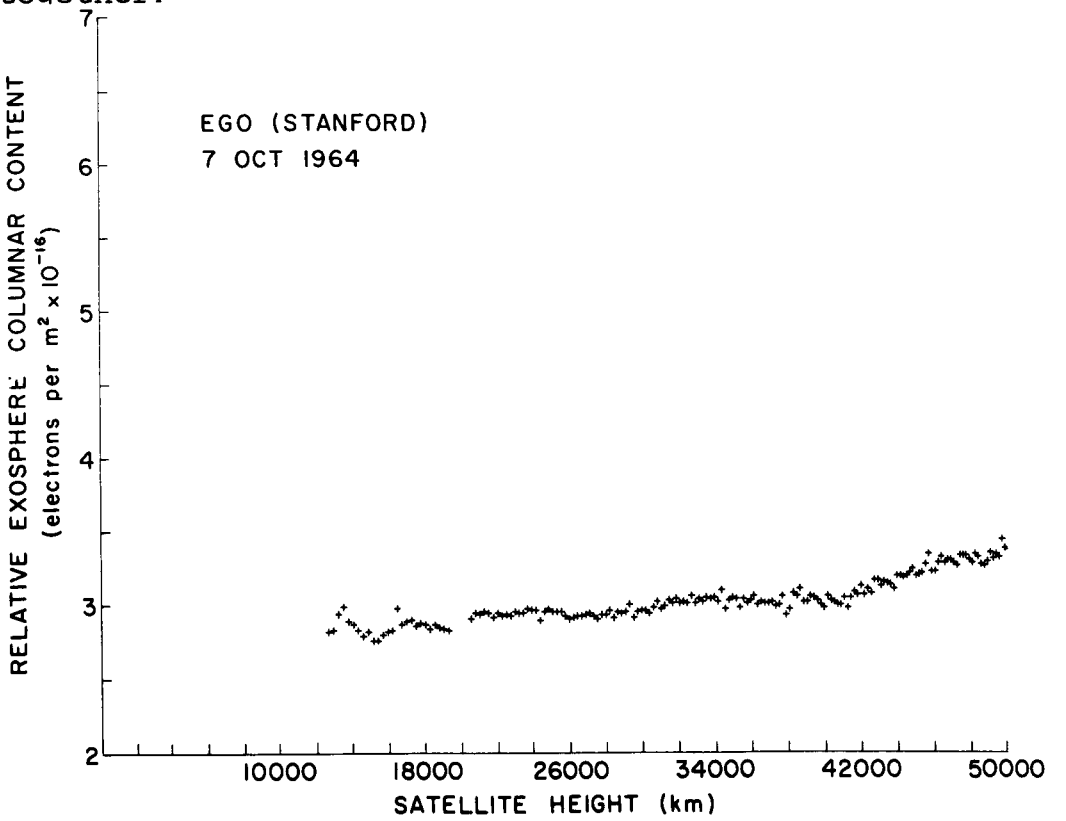

FIG. 27. THE EXOSPHERIC COLUMNAR CONTENT IN THE RUN ABOVE DOES NOT SHOW ANY APPRECIABLE INCREASE BECAUSE THE SATELLITE WAS ALREADY BEYOND THE PLASMAPAUSE WHEN THE DATA BEGAN TO BE TAKEN.

The 7 October, 1964 path is also plotted in Fig. 26a. It represents the extreme case of a low geomagnetic latitude pass. The run started when the satellite was very near or beyond the plasmapause, and this explains the flatness of the exospheric content-vs-height curve shown in Fig. 27.

Fig. 26b portrays a situation that is favorable for the measurement of local electron concentrations. The 12 December, 1964 path of EGO is plotted as described above. The plasmapause is out at L = 5.6. It can be seen that, observed from Stanford, the ray path remains for a considerable length of time, entirely within the plasmapause. Clearly the most favorable condition to observe the knee is when, just at the moment when the satellite crosses this boundary, its motion is entirely along the line of sight, so that the tangential velocity is zero.

V. THE BEHAVIOR OF THE NIGHTTIME IONOSPHERE

The nighttime coupling between the ionosphere and the exosphere is studied in this chapter by examining the behavior of the total electron content of the nocturnal ionosphere. The results support the theory of an ionosphere fed by the exosphere, at night.

An examination of Fig. 14 which shows the columnar contents for seven early morning EGO passes, confirms the unpredictability of the ionosphere. In some nights (24 May, 1965, Fig. 14f) there is a pronounced decay in columnar content, while in others (29 March, 1965, Fig. 14d) the content grows steadily and smoothly although the sun is very much below the horizon. On other occasions (13 March, 1965, Fig. 14c) the ionization was remarkably steady and unaffected by the time.

The EGO curves provide a very good time resolution and show very little scatter. Unfortunately, these data exist for a limited number of runs because the satellite repeats a pass at the same local time only every eight days and dawn runs could only be taken between the middle of February and the beginning of June. Prior to February the beacon was not turned on in view of the power shortage resulting from unfavorable angle between the solar paddles and the sun. After June, the early morning passes occurred at too small an elevation angle and the data lost the necessary accuracy. It became imperative to look for statistical support for the EGO information in the very extensive catalogue of the diurnal variation of columnar electron content of the ionosphere prepared by Fred L. Smith, III, of Stanford University and Paul C. Yuen of the University of Hawaii. The catalogue, as yet unpublished, contains observations of the columnar content measured by the Faraday rotation-angle technique using the 136-Mc transmission of the geostationary satellite, Syncom III positioned over the international date line in the Pacific

Ocean. The technique was described by Garriott, Smith and Yuen [1965]. The measurements were made every five minutes, 24 hours per day and refer to the ionosphere near Stanford and near Hawaii. With a few exceptions -- due to periods when the satellite did not transmit or the ground equipment was being adjusted or repaired -- there is a continuous coverage since the middle of September, 1964, to the present (September , 1965). These data were kindly loaned to the author by F. L. Smith, III.

The subionosphere points were located as indicated in Table 5.

TABLE 5. COORDINATES OF THE OBSERVING STATIONS

Observing Station	Sub-Ionosphere Point				L-Shell Ionos. Pt. (400 km)
	Geographic Latitude	Geographic Longitude	Dip Angle	Dip Lat.	
Hawaii	19.7°N	159.8°W	36°	26°	1.20
Stanford	33.8°N	132.3°W	57°	37°	1.66

The data were examined with the hope of establishing an average behavior of the nighttime ionosphere and any correlation of deviations from the average with some geophysical index.

Attention was focused on the time interval between local midnight and just prior to sun rise. All available runs were classified in four categories:

FLAT - Those runs in which there is no perceptible change in columnar content during the period of interest.

DECLINING - Those runs in which the columnar content decayed monotonically during the night.

RISING - Those runs in which the columnar content increased monotonically during the night.

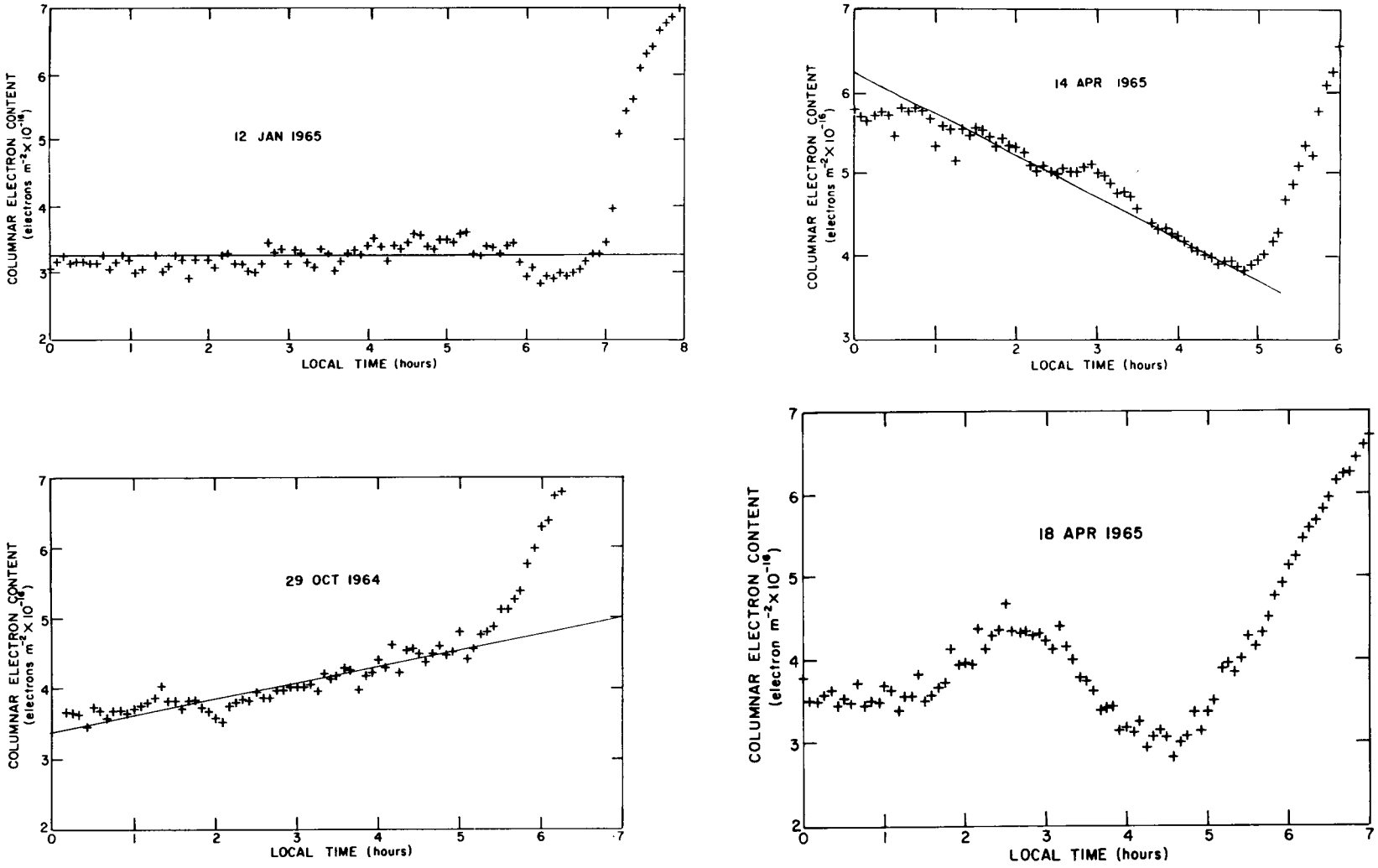

FIG. 28. EXAMPLE OF COLUMNAR CONTENT-VS-TIME CURVES OBTAINED FROM THE SYMCOM III SATELLITE. Data were furnished by F. L. Smith, III.

IRREGULAR - Those runs that could not be classified in any of the above categories. In general this included runs in which the columnar content-vs-time curves exhibited humps and troughs.

Fig. 28 shows the columnar content variations for days representing each of the above categories.

Garriott, Smith and Yuen [1965] point out that the nighttime total ionospheric content in Hawaii quite generally exhibits a small but clear decrease as time goes on, while at Stanford it is, most of the time, remarkably constant. This is confirmed by the somewhat more extensive statistical study presented below. Table 6 shows the probability of occurrence of each category at the two different stations.

TABLE 6. BEHAVIOR OF THE NIGHTTIME IONOSPHERE

Category	Stanford	Hawaii
FLAT	53.0%	14.9%
DECLINING	18.1%	48.0%
RISING	7.2%	0.7%
IRREGULAR	21.7%	36.4%

This table is based on 83 runs for Stanford and 154 runs for Hawaii. It is immediately clear that during the period considered, a steady nighttime ionosphere was the rule at Stanford, while, farther south, at Hawaii, the progressive decay of ionization was the most common condition encountered.

The average value of the K_p index for 2 six-hour periods was listed for every day. For Stanford these periods were from 1600 to 2200 and from 2200 to 0400 local mean time. For Hawaii the periods were from 1700 to 2300 and from 2300 to 0500, local mean time. These values of K_p correspond to periods just preceeding or coinciding with the time of interest.

From the tabulation so obtained the average value of K_p for FLAT and DECLINING nights was derived. The results appear in table 7.

TABLE 7. GEOMAGNETIC INDEX CORRELATION WITH NIGHTTIME BEHAVIOR OF THE IONOSPHERE

	STANFORD	
	Average value of the K_p index	
	1600 to 2200 local time	2200 to 0400 local time
FLAT	1.21	1.01
DECLINING	2.81	2.09
Average K_p	1.66	1.24
	HAWAII	
	Average value of the K_p index	
	1700 to 2300 local time	2300 to 0500 local time
FLAT	1.67	1.51
DECLINING	1.50	1.36
Average K_p	1.60	1.45

It appears that at Stanford under low K_p conditions there is a tendency to have a steady nighttime ionosphere, while the decaying ionosphere seems to be associated with higher values of the index. We may also note that at Stanford the correlation is stronger with the K_p of the six hours period preceding the period of interest rather than with the index for the period itself.

In Hawaii the K_p corresponding to both FLAT and DECLINING nights was nearly equal to the average K_p for the whole period, leading to the conclusion that no correlation exists between geomagnetic activities and the nighttime behavior of the ionosphere at the Hawaiian latitude.

In order to interpret these results, it may be helpful to examine briefly some of the ideas advanced to explain the existence of a relatively large nighttime ionosphere, although none of the several theories proposed has, as yet, been entirely successful.

One suggestion is that the rate coefficient of the reaction that destroys oxygen ions is temperature dependent; little, however, is known about this topic. In a private communication, L. Thomas has mentioned that there are indications, both from laboratory experiments and on theoretical grounds, that this coefficient is in fact temperature sensitive in a way that could account for the diminished loss of nighttime ionization.

Another popular explanation invokes the appearance of electric forces that impart an upward velocity to the plasma, carrying the F-layer to greater heights where the recombination is slower. Duncan [1956] derived a theorem showing that a Chapman-α layer perturbed by a vertical drift velocity (independent of height) will move with the drift to a different height where it will maintain itself stationary, keeping its Chapman-α shape and decaying with an effective attachment coefficient equal to the coefficient corresponding to the height of the new peak in concentration. Since the loss process assumed is linear, many different Chapman-α layers can be superposed to generate layers of almost any, reasonable, arbitrary shape. When the drift is upward, the ionization may be lifted high enough so as to have a negligible decay during the hours of the night. Hanson and Patterson [1964] have examined this process in greater detail

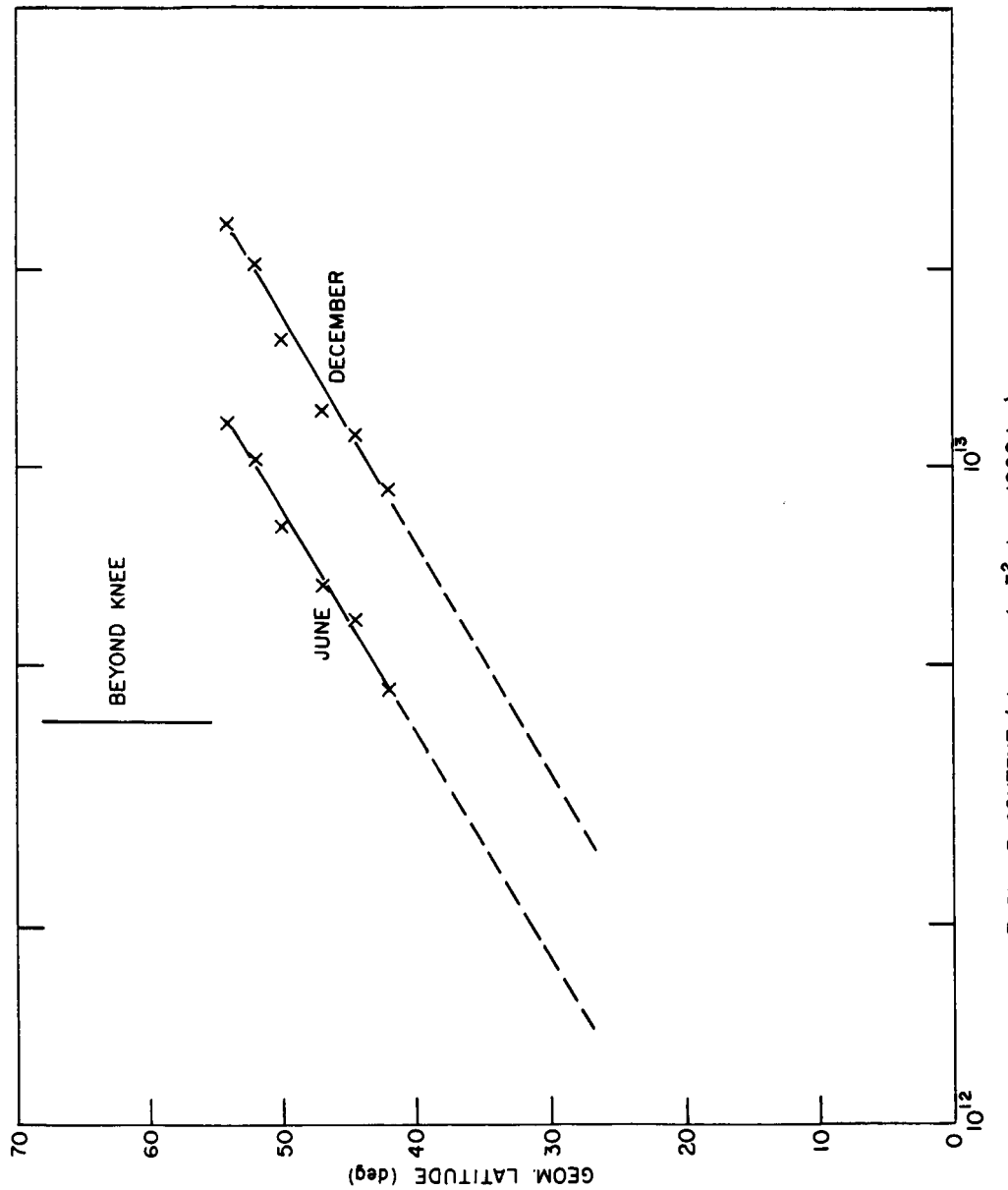

FIG. 29. THE TUBULAR ELECTRON CONTENT OF THE EXOSPHERE, ABOVE 1000 KM.

and found it to be a plausible explanation of the nighttime permanence of the F-layer. Since the existence of electric fields in that region of the atmosphere cannot, as yet, be verified experimentally there can be no final assesment of the role that the mechanism described plays. It cannot, however, account for the frequently observed increase in ionization during the night. For this a nocturnal ionization source is needed. Such a source is readily available in the store of protons in the magnetosphere.

A great deal of attention has been paid to the possibility that the nocturnal ionosphere is maintained by the downward flux of ions from the protonosphere. Hanson and Patterson [1964] showed that a flux of the order of 10^8 electrons cm^{-2} sec^{-1} is necessary to sustain an ionosphere with a peak concentration of 10^5 ions cm^{-3}. In view of the uncertainties in the experimental value of the recombination coefficient β, it is important to point out that the flux is rather insensitive to the value of β used. In examples worked out by Hanson, a change of 10:1 in the coefficient causes only a change of about 1.6:1 in the flux. The difficulty in this theory resides in the fact that under steady state conditions the maximum upward flux that can be forced into the protonosphere is insufficient to replenish the supply, making up for the losses at night. The subject does not seem to be entirely closed, however. YOH [1965] observes in his Doppler - Faraday moon echo experiment, rather large upward fluxes in the morning hours. The radio-beacon data from EGO also can be interpreted as indicating fluxes considerably in excess of the maximum computed by Hanson, some time after sunrise.

The amount of available ionization in the protonosphere can be estimated by means of whistler data. Fig. 29 shows the geomagnetic latitude variation of the "tubular electron content", i.e., the number of electrons contained in a tube of force having a cross-section of 1 cm^2 at a height of 1000

km and extending all the way to the equator. J.J. Angerami calculated the information displayed in the figure using in part data from Smith [1961].

It must be remembered here whistlers do not measure equatorial concentrations directly; what is measured is, essentially

$$\int \frac{f_p}{f_g^{1/2}} \, ds$$

the integral of the plasma frequency, f_p, weighted by the inverse of the square root of the gyro frequency, f_g. To obtain the equatorial concentration, a model for the dependence of plasma frequency on distance along the field line must be adopted. Smith [1961] used what he calls the gyro frequency model which sets n proportional to r^{-3}, approximately.

In calculating the tubular content, it is advisable to employ the same model as the one used for the derivation of equatorial concentrations. This was done by Angerami and accounts for the difference between the values in Fig. 29 and those presented by Hanson and Patterson [1964] who applied to the Smith data a diffusive equilibrium expression due to Johnson [1960]. For values of content beyond the knee, Angerami and Carpenter [1965] justified the use of a r^{-4} law.

The main feature that can be discerned in Fig. 29 is the growth of the protonospheric electron supply as the latitude increases (mainly due to the increasing size of the tube), and the abrupt drop in content at the knee, the position of which depends on the magnetic activity of the day (Carpenter and Angerami [1966]). Making a rather extended extrapolation it appears that at 20 degrees of geomagnetic latitude, which corresponds to the situation in Hawaii, there are less than 10^{12} electrons cm^{-2} available in the summer and less than twice this amount in the winter. The required flux of 10^8 electrons cm^{-2} sec^{-1} can last no more than 3 hours. Conse-

quently, the ionosphere will, as a rule, decay during the night, as it is observed to do in the Syncom data. On the other hand, at latitudes near 50 degrees the supply of hydrogen ions and electrons is more than one order of magnitude larger and is, therefore capable of maintaining a constant ionospheric columnar content at night. At still higher latitudes it is possible that the decay conditions are again satisfied due to the depletion of the protonosphere beyond the knee.

When the ionosphere point lies on L-shells between about 2.5 and 7, the columnar content behavior should show a strong dependence on the geomagnetic activity index which is known to influence the position of the knee. In disturbed nights the knee would be pushed towards lower latitudes and the content would decay, while during quiet nights it would remain steady. At present the author has no data from stations situated far enough north to corroborate this point.

The latitude of the ionosphere point of the Stanford measurements -- 37 degrees, geomagnetic -- is high enough so that, in general an adequate supply of protonospheric electrons exists and, as the experiment confirms, the nights show mostly a constant content. Under high K_p conditions the protonospheric content, even inside the knee, appears substantially depressed, (Carpenter and Angerami [1966]). This may be enough to cause the ionosphere to decay under increased K_p conditions, as the observations show.

As was mentioned earlier, Smith [1961] found that the equatorial concentration of exospheric electrons was larger around December than around June. One would expect that, if the protonosphere is the source of the nighttime ionosphere then such annual variation would affect the relative number of FLAT and DECLINING nights. In Table 8 the year was divided into two halves -- one from October to March, inclusive, labeled "year end", and one consisting of September, April, May and June, labeled "midyear". No data is at present avail-

able for July and August. It can be seen from this table that there is some indication of the predicted annual variation of probability of occurrence of FLAT or RISING nights.

TABLE 8. ANNUAL EFFECT ON THE NIGHTTIME IONOSPHERE

	Number of FLAT or RISING nights	Total number of nights	Percentage of FLAT or RISING nights
STANFORD			
Year end	48	80	60.0%
Midyear	21	51	41.2%
HAWAII			
Year end	20	140	14.3%
Midyear	6	95	6.3%

It is also clear that if the mechanism described here really takes place, then the total tubular content in the protonosphere should show an appreciable depletion during the night at low latitudes and also beyond the knee, and a relatively small change at high latitudes within the knee. That this appears to be so is the opinion of Carpenter who, in a private communication states that he as observed this effect. Recent whistler measurements made at lower latitudes, especially those taken aboard the research ship "Eltanin" may help to confirm this point.

VI. SUMMARY AND CONCLUSIONS

The present work covers three distinct topics, one of a theoretical and two of an experimental nature.

The considerable theoretical work done on the thermal behavior of the ionospheric plasma by Hanson, Dalgarno, Geisler and Bowhill, and other authors is extended here from the steady-state solutions found by them to a time-dependent solution that allows the examination of the temperature changes in the ionosphere at dawn. Physical consideration of this problem leads to models that can be mathematically represented by a second order, non-linear, partial differential equation, the numerical integration of which presents serious stability difficulties. An unconditionally stable form of the equivalent difference equation is developed. Numerical examples are worked out for models that attempt to represent the dawn ionosphere at summer and winter for both solar cycle maximum and minimum conditions, and the following conclusions are drawn:

1. Very substantial heating occurs in the ionosphere before any perceptible increase in ionization. Experimental evidence shows that a measurable increase in ionization begins at a solar zenithal angle of about 95 degrees while considerable heating starts at angles larger than 110 degrees.
2. As the sun begins to shine on the high atmosphere, the competing effects of increasing heat production and growing heat capacity of the electron gas result in an electron gas temperature that initially rises very fast, reaches a peak, and then declines. This peak is more pronounced the higher the altitude and predominates in the winter when the electron concentration buildup is faster.
3. Due to smaller electron concentrations in the summer, the temperatures during this season are higher than in the winter.
4. The much slower rate of increase of electron concentration during the solar cycle minimum period results in a tendency for the temperature in this period to be higher than during the solar cycle

maximum.

5. In most models it is observed that up to the time when the temperature reaches its peak, it is practically height independent at levels above the altitude of maximum heat production. Later on a "bulge" is formed at the altitude of maximum heat production and a negative gradient of temperature exists in the higher levels resulting in an upward heat flow.

The second topic treated deals with experimental results obtained from the radio-beacon experiment aboard the EGO satellite. The difference between the columnar electron contents obtained by the differential-Doppler-frequency and the Faraday-rotation-angle techniques is defined as the "exospheric columnar electron content" and yields some interesting information.

Strong horizontal gradients are shown to exist. This is in general agreement with the whistler observations of the equatorial "knee" in ion concentration.

Profiles of electron concentration in the exosphere are deduced from the data. The values found show fair agreement with the results of the whistler studies.

Perhaps the most interesting phenomenon revealed by the experiment is the rearrangement in the ionized layers that occurs between one half and one and one half hours after sunrise. This rearrangement can be interpreted as an upward flux of ionization from the ionosphere into the exosphere, and lasts about 20 minutes, in the passages observed. The flux attained the value of 1.5×10^{9} electrons cm^{-2} sec^{-1} on one of the days measured. A tentative explanation is presented for this phenomenon; it requires a mechanism that would delay the oxygen ion to hydrogen atom charge exchange reaction. It is shown that, in an extremely simplified model of the ionosphere, a delay in the oxygen ion to hydrogen atom exchange reaction exists permitting speculations that the same mechanism will cause the required delays in a more

complete model. A mathematical treatment of the problem is undertaken and yields quantitative values for the delay. It is shown that under conditions prevalent at solar cycle minimum at heights between 400 and 600 km the time constant of the exchange reaction varies from some 300 seconds at the lower altitute to more than 40,000 seconds at the higher.

The final topic consists of a statistical investigation of the behavior of the nighttime columnar electron content of the ionosphere and is based on data obtained from Faraday-rotation-angle measurements using the 136 Mc telemetry carrier of the Syncom III satellite. It is observed that the majority of nights during the winter, at Stanford, showed no perceptible decay in content after midnight, while those observed at Hawaii showed such a decay very often. In addition, it was found that the average K_p associated with non-decaying nights at Stanford was much lower than that associated with decaying ones. No such effect was observed at Hawaii. These and similar results are interpreted as supporting the theory of the maintenance of nighttime F-layer by a downward flux of electrons from the pronosphere.

It is suggested that the investigation of the exosphere by means of radio-beacon experiments be continued not only by further observations of EGO and its successor, OGO-B, but also by the use of geostationary satellites (capable of revealing only the temporal changes of the exosphere) and by the use of highly eccentric vehicles placed in low inclination orbits (appropriate for the measurement of exospheric electron concentration). The geostationary experiment would help shed light on the problem of exchange of ionization between the ionosphere and the protonosphere, a subject not fully understood at present. The concentration profiles obtained from the OGOs and from other satellites in eccentric orbits can complement the results obtained with whistlers.

BIBLIOGRAPHY

1. Angerami, J. J. and D. L. Carpenter, "Whistler Studies of the Plasmapause in the Magnetosphere - 1; Equatorial Density and Total Tube Electron Content near the Knee in Magnetospheric Ionization", submitted to J. Geophys. Res., 1965.

2. Bourdeau, R. E., S. Chandra and W. M. Neupert, "Time Correlation of Extreme Ultraviolet Radiation and Thermospheric Temperature", J. Geophys. Res., 69, p. 4531, 1964.

3. Carlson, H. C., Jr., "Evidence for a Magnetic Conjugate-Point Origin of Ionospheric Heating", preprint, 1965.

4. Carpenter, D. L. and J. J. Angerami, "Whistler Studies of the Plasmapause in the Magnetosphere - 2; Temporal Variations in the L Value of the Knee and Some Evidence on Plasma Motions near the Knee", submitted to J. Geophys. Res., 1966.

5. Crank, J. and P. Nicholson, "A Practical Method for Numerical Integration of Solutions of Partial Differential Equations of the Heat-Conduction Type", Proc. Cambr. Phil. Soc., 43, p. 50, 1947.

6. da Rosa, A. V., "Eccentric Geophysical-Observatory Satellite S-49. Interpretation of the Radio-Beacon Experiment", Tech. Report No. 1, NASA Contract NASr-136, Stanford University, Radioscience Laboratory, 1965.

7. Dalgarno, A., M. B. McElroy and R. J. Moffett, "Electron Temperatures in the Ionosphere", Planet. and Space Sci., 11, p. 463, 1963.

8. Dalgarno, A. and R. J. Moffett, "Electron Cooling in the D-Region", Planet. and Space Sci., 9, p. 939, 1962.

9. Doupnik, J. and J.S. Nisbet, "Electron Temperature and Density Fluctuations in the Daytime Ionosphere", paper presented at the AGU Meeting, Washington, D. C., April 1965.

10. Duncan, R. A., "The Behavior of a Chapman Layer in the Night F2 Region of the Ionosphere, under Influence of Gravity, Diffusion and Attachment", Aust. J. Phys., 9, p. 436, 1956.

11. Evans, J. V., "Cause of the Midlatitude Evening Increase in F_0F_2", J. Geophys. Res., 70, p. 1175, 1965.

12. Evans, J. V. and Loewenthal, M., "Ionospheric Backscatter Observations", Planet. Space Sci., 12, p. 915, 1964.

13. Ferguson, E. E., F. C. Fehsenfeld, P. D. Goldan, A. L. Schmeltekopf and H. I. Schiff, "Laboratory Measurements of the Rate of the Reaction $N_2^+ + O \quad NO^+ + N$ at Thermal Energy," Planet. Space Sci., 13, p. 823, 1965.

14. Garriott, O. K., and C. G. Little, "The Use of Geostationary Satellites for the Study of Ionospheric Electron Content and Ionospheric Radio-Wave Propagation," J. Geophys. Res., 65, p. 2025, 1960.

15. Garriott, O. K., F. L. Smith, III, and P. C. Yuen, "Observations of Ionospheric Electron Content Using a Geostationary Satellite," Planet. Space Sci., 13, p. 829, 1965.

16. Geisler, J. E., and S. A. Bowhill, "Ionospheric Temperatures at Sunspot Minimum," J. Atmos. and Terr. Phys., 27, p. 457, 1965.

17. Hanson, W. B., "Electron Temperatures in the Upper Atmosphere," Space Research, Proc. Int. Space Sci. Symp. 3rd, Washington, p. 282, 1962.

18. Hanson, W. B., and F. S. Johnson, "Electron Temperatures in the Ionosphere," Memoires Soc. R. Liege, IV, p. 390, 1961.

19. Hanson, W. B., and T. N. L. Patterson, "The Maintenance of the Night-Time F-Layer," Planet. Space Sci., 12, p. 979, 1964.

20. Hanson, W. B., T. N. L. Patterson and S. S. Degaonkar, "Some Deductions from a Measurement of the Hydrogen Ion Distribution in the High Atmosphere," J. Geophys. Res., 68, p. 6203, 1963.

21. Harris, I., and W. Priester, "Time-Dependent Structure of the Upper Atmosphere, J. Atmos. Sci., 19, p. 286, 1962.

22. Jacchia, L. G., and J. Slowey, "An Analysis of the Atmospheric Drag of the Explorer 9 Satellite from Precisely Reduced Photographic Observations," Smithsonian Astrophys. Obs. Spec. Rept. 125, 1963.

23. Jacchia, L. G., and J. Slowey, "Atmospheric Heating in Auroral Zones: A Preliminary Analysis of the Atmospheric Drag of the Injun 3 Satellite," J. Geophys. Res., 69, p. 905, 1964.

24. Johnson, F. S., "The Ion Distribution Above the F_2 Maximum," J. Geophys. Res., 65, p. 577, 1960.

25. Kamke, E., "Differentialgleichungen, Losungsmethoden und Losungen," Band 1, Chelsea, 1959.

26. Laasonen, P., "Uber eine Methode zur Losung der Warmeleitungsgleichung," Acta Math., 31, p. 309, 1949.

27. Lowan, A. N., "On the Cooling of the Upper Atmosphere after Sunset," J. Geophys. Res., 60, p. 421, 1955.

28. Mariani, F., "Distribution of the Photoelectrons and Origin of the Geomagnetic Anomaly in the F2-Layer," J. Geophys. Res., 69, p. 556, 1964.

29. Martin, H. A., W. Neveling, W. Priester and M. Roemer, "Model of the Upper Atmosphere from 130 through 1600 km. Derived from Satellite Orbits," Mitt. Sternwarte Bonn, No. 35, 1961.

30. Rishbeth, H., "Diffusion of Ionization in the Sunrise F-Layer," J. Atmos. and Terr. Phys., 20, p. 277, 1961.

31. Rishbeth, H., and D. W. Barron, "Equilibrium Electron Distribution in the Ionospheric F2-Layer," J. Atmos. and Terr. Phys., 18, p. 234, 1960.

32. Rishbeth, H., and C. S. G. K. Setty, "The F-Layer at Sunrise," J. Atmos. and Terr. Phys., 20, p. 263, 1961.

33. Smith, R. L., "Properties of the Outer Ionosphere Deduced from Nose Whistlers," J. Geophys. Res., 66, p. 3709, 1961.

34. Snyder, C. W., M. Neugebauer and U. R. Rad, "The Solar Wind Velocity and Its Correlation with Cosmic-Ray Variations and with Solar and Geomagnetic Activity," J. Geophys. Res., 68, p. 6361, 1963.

35. Spencer, N. W., G. P. Newton, C. A. Reber, L. H. Brace and R. Horowitz, "Results from the Aeronomy Satellite, Explorer XVII," Trans. Am. Geoph. U., 45, p. 729, 1964.

36. Spitzer, L., Jr., Physics of Fully Ionized Gases, Interscience, 1962.

37. Yoh, P., "Radar Studies of the Cislunar Medium," Sci. Report No. 12, NASA Grant NS-G-377, Stanford University, Radioscience Lab., 1965.